Modelling of the Pressure Distributions in Twin-Wire Blade Formers

by

Claes Holmqvist

September 2002
Technical Reports from
Royal Institute of Technology
Department of Mechanics
FaxénLaboratoriet
S-100 44 Stockholm, Sweden

Akademisk avhandling som med tillstånd av Kungliga Tekniska Högskolan i Stockholm framlägges till offentlig granskning för avläggande av teknologie licentiatexamen onsdagen den 16:e oktober 2002 kl 10.00 i seminarierum 40, Teknikringen 8, KTH, Valhallavägen 79, Stockholm.

Universitetsservice US AB, Stockholm 2002

C. Holmqvist 2002 Modelling of the Pressure Distributions in Twin-Wire Blade Formers.

Department of Mechanics, FaxénLaboratoriet, Royal Institute of Technology
S-100 44 Stockholm, Sweden

Abstract

During papermaking, the internal structure of the fibre network constituting the paper is to a dominating extent determined in the forming zone of the paper machine. This thesis is aimed at studying the pressure distribution in blade forming sections, which is commonly considered to be a key quantity of the process.

Previous work has provided insight into the physics of different devices employed in blade forming. However, there has been a lack of models enabling studies of the effects of the interaction between different components on the pressure distribution. In the thesis, a model is presented for a generic blade forming section consisting of three blades. The positions of two of the blades are fix, and in between them is located a suction box. The third blade is applied by a prescribed force to the opposing wire, in a position facing the suction box. The model admits the study of the interaction between the pulses from the different blades in the blade/counterblade configuration, and between the pulses and one-sided suction.

The wires are modelled as tensioned and perfectly flexible Euler-Bernoulli beams of negligible mass. The suspension is treated like an inviscid fluid. Consideration is taken to the influence of fibre deposition on the permeability of the fabrics. By assuming the ratio between the length scales in the thickness direction and the machine direction to be small, a quasi one-dimensional model is obtained.

For maximum flexibility, the model domain is divided into modules. Each module is solved individually using a finite difference based discretisation. The solutions for the different modules are matched with each other iteratively.

A comparison with published results for a single blade indicates that the model can be used to obtain qualitatively correct predictions of the pressure distribution. New results include a series of calculations showing the non-trivial interaction between the pressure pulses when the blades are positioned successively closer together, the effects of suction on the pressure pulse generated by a blade applied to the opposing wire, and how blades of modest curvature do not necessarily stay in contact with the fabric along their full width and the implication of this on the pressure gradient.

Descriptors: fluid mechanics, blade forming, pressure distribution, suction, interaction, permeable fabric, modules

Contents

CHAPTER 1

Introduction

1.1. Papermaking and forming

1.1.1. *Outline of the process from tree to product*

There is no precise definition of paper. Common to all products referred to by that name is however that they are a nested structure of slender particles, fibres, that are held together without the requirement of other components than the fibres themselves. In most cases these have a biological origin, but synthetic fibres are sometimes used as well.

After first having been developed in China in the 2$^{\text{nd}}$ century AD, papermaking has evolved to the interdisciplinary high technology process it is today. The large majority of paper products are wood based, and their production can be divided into three significantly different parts, each of which corresponds to an increased degree of refinement of the raw material:

- Forestry.
- Pulp production.
- Paper production.

During the pulp production, the fibres in the wood are freed through either mechanical or chemical treatment. They are delivered to the paper mill either as a concentrated suspension, or in dry sheets. At the mill, the pulp is transformed into a dilute suspension and is then processed. Although the techniques employed to produce different paper qualities (called grades) is more or less the same, the characteristics of the final products differ a lot in terms of mechanical and other properties. The dry mass per unit area, i.e. the 'grammage', of board is e.g. about 200–400 g/m^2, whereas that of tissue is only 14-25 g/m^2. The different stages of the paper production are in order:

- Stock preparation.
  Dissolving the pulp, Refining, Adding additives, Screening.
- Forming.
  Dilution, Deaeration, Ejection onto the forming fabrics, Dewatering.
- Wet pressing.
- Drying.
- Possibly calandering and/or coating.
- Rolling.

1.1.2. *The forming section*

The internal structure of the fibre network constituting the paper is to a dominating extent determined in the forming zone of the paper machine. In the remaining parts of the process only the structure in the thickness direction (referred to as the 'z-direction') can be influenced. Consequently, the forming zone has a critical influence on many, but not all, of the important properties of the final product. These include the grammage distribution, called formation, and the strength of the paper. As a result, it is of paramount importance to a papermaker to understand the forming part of the process.

The fibre mass concentration of the thick stock entering the forming section is 3–4%. It is then diluted with water that has been drained at positions further downstream in the forming process, so called 'white water', to a concentration of 0.1–1% depending on which grade is being produced. This diluted suspension passes several cleaning/screening devices that removes contaminants before it is fed into a nozzle that ejects it upon the fabric(s), where the dewatering will take place.

The nozzle is called 'headbox', and plays an important role in the forming process. A schematic illustration of its design is given in figure 1.1. The downstream end is a narrow slit, typically about 10 mm high and 10 m wide. It is important to have a uniform flow across the exit, and the upstream part of the headbox is therefore usually a tapered header whose purpose is to create a uniform pressure across the machine width (the 'Cross Direction'). Whatever non-uniformities remain after the tapered header is further reduced by the pressure drop created across the tube package by the stepwise enlargement of the channels between the header and the contraction. This part of the headbox also has a positive influence on the distribution of the fibres in the suspension. Although the concentration is usually low in the headbox the fibres still have a tendency to form clusters, called flocs, which will result in bad formation in the paper sheet (i.e. uneven local grammage distribution). The strong gradients in the flow caused by the tube bank disrupts these flocs. Finally the suspension is accelerated to the required speed in the contraction . The acceleration dampens the relative turbulence levels in the flow, which is necessary to obtain a jet of good quality. In addition, velocity non-uniformities in the Cross Direction is

further reduced. A disadvantage of the headbox is that the elongational flow causes anisotropy in the fibre orientation. The fibres are aligned in the direction of flow (the 'Machine Direction'), which for some products has a negative effect on product quality. A recent study of the flow in the headbox was carried out by Parsheh (2001).

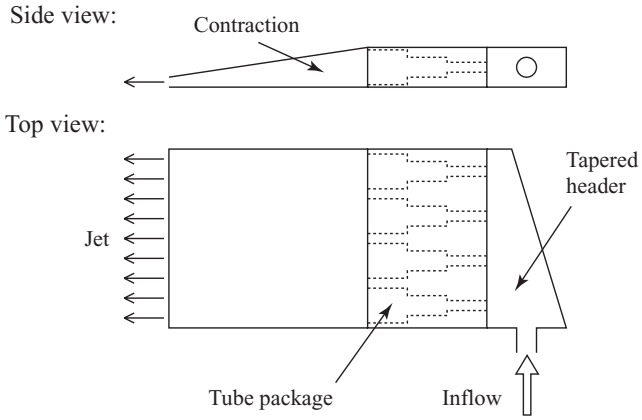

FIGURE 1.1. A schematic illustration of a headbox and its different parts: The tapered header, the tube bank and the contraction.

The jet from the headbox impinges on a permeable fabric moving with a speed of up to 30 m/s, depending on the capacity of the machine and which grade is being produced. As instabilities in the jet might impair the homogeneity of the paper sheet (Söderberg 1999), the distance travelled by the jet is kept to a minimum. When the jet hits the fabric, which is called 'wire', the drainage starts. The water passes through the wire while the fibres are left on top resulting in the build up of a fibre mat. In the rest of the forming section, the dewatering of the suspension continues till a fibre network of a concentration of about 4 % occupies the region between the wires. Thereafter, a thickening process takes place in which the concentration rises till a sheet of about 20 % fibre mass concentration has been formed. After this the sheet is passed on to the press section.

The easiest way to achieve drainage is to move the wire horizontally and let gravity force the water in the suspension through the fibre mat and the wire (possibly increasing the pressure difference across the wire by applying suction to the outside of the fabric). This method, called Fourdrinier forming, was the one first used to produce paper in a continuous process. Fourdrinier forming sections are still in use, also in combination with other techniques. The machine speeds obtainable in this way are however limited by the instability of the free surface of the suspension residing on top of the wire. To overcome

this problem, twin-wire forming was introduced in the 1950's and is now used predominately. An overview of the history of forming and different machine designs have recently been given by Malashenko & Karlsson (2000). Norman (1989) gave a detailed overview of forming as it was undertaken and understood at that time. In the latter reference, details of Fourdrinier forming are discussed.

1.1.3. *Twin-wire forming*

The basic principle of twin-wire forming is that both sides of the suspension is in contact with a wire at all times. This was not a new idea when practical designs first showed up. However, early attempts had not been successful due to the lack of insight that one must always (in any given position in the machine direction) allow at least one of the wires to automatically adjust its lateral position as a function of the current operating conditions. Drainage is achieved by creating a positive pressure difference between the region between the wires and the surroundings. Compared to Fourdrinier forming, twin-wire forming yields considerably higher dewatering rates. This is due to the fibre mats building up on both of the wires simultaneously. In addition, the flow resistance through the mat and wire on either side is significantly less than that of a single wire and mat after the same amount of total drainage. Another advantage is that carefully performed twin-wire forming gives a paper whose two sides have a more equal structure than does Fourdrinier forming.

The wires are pre-stressed and have an inner tension T which is typically 5–10 kN per metre width. As long as drainage takes place, the resistance to flow through the fibre mat and the wire generates a pressure drop across these layers, resulting in a local curvature $1/R$ of the wire. Assuming that the bending stiffness of the fibre web and the fabric is neglected, this implies that the pressure difference is T/R across the mat and the wire.

1.1.4. *Roll forming*

During roll forming, the wires are deflected over a cylindrical roll, as illustrated in figure 1.2, and hence a dewatering pressure is generated. Early twin-wire formers achieved drainage in this way. By using a roll with permeable surface, two-sided dewatering can be obtained. Roll forming is a quite gentle method in the sense that the amplitude of the dewatering pressure is rather low, of the order 10 kPa, and in that the pressure gradients in the machine direction are not severe. This yields a good retention of the fibres and the additives in the suspension, which at higher pressure levels to a larger extent would follow the water through the wires. However, as pressure gradients play an important role in breaking up fibre flocs, their absence yields flocculation and a final paper with bad formation. For quite some time it was generally accepted that the local radius of curvature of the wires were well described by the radius of the

forming roll. This is however too simplistic. The dynamics of roll forming is a complicated problem. A recent study is the one by Holm (2002).

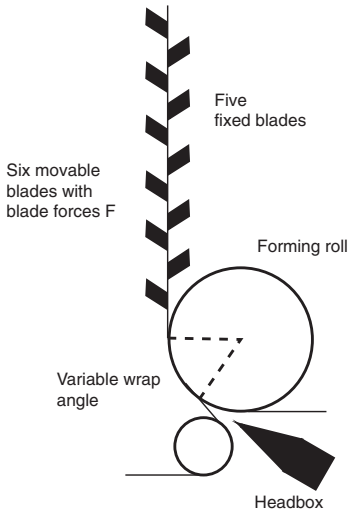

FIGURE 1.2. The layout of a former with roll dewatering followed by blade dewatering with adjustable blades. This design was first applied for the STFI-former on the FEX pilot machine in Stockholm.

1.1.5. *Blade forming*

During blade forming the wires follow an overall straight path. They are however locally deflected by ceramic blades, which are applied across the full width of the wires (i.e. perpendicular to the machine direction). The principle of blade application is illustrated in figure 1.3(c). In the figure, two wires pass a series of three blades of which two are applied to the top fabric and one to the bottom fabric. The deflection of the wires causes a pressure to be built up in the region between them. The underlying mechanism is readily explained: Assume first that the fabrics and the suspension in between them move linearly past the blades, on the verge of touching them but without actually doing so (figure 1.3(a)). Hence the pressure in the suspension will be the same as outside the wires. If – hypothetically – the bottom blade could be used to push the lower wire upwards without affecting the upper wire, a situation like the one in figure 1.3(b) would occur. It is evident that the available cross section for the flow of suspension has shrunk at the position of the middle blade. In order to cope with this situation the suspension must either pass through the wires, so that less of it has to pass the middle blade, or it must push the upper fabric

outwards to create a larger cross section. In reality, both of these things happen simultaneously as illustrated in figure 1.3(c). The deflection of the flow results in a local increase of the pressure which, at the same time, forces liquid through the fibre mats and the wires and displaces the opposing wire. The fabrics, of course, oppose displacement due to their internal tension. One might think that another option would be for the suspension to increase its velocity, thus allowing it to pass the constriction imposed by the blade. Why this does not happen is not a trivial issue. Without entering into the details we note, however, that if the wires are initially parallel (as is the case if the pressure in the gap between the fabrics equals the ambient pressure), the lower wire must at some point curve towards the upper fabric. This implies that the pressure in the gap at that point is higher than outside the fabrics. Consequently, the velocity at that point is lower than far upstream of the blades, which means that a deceleration takes place as opposed to the proposed acceleration.

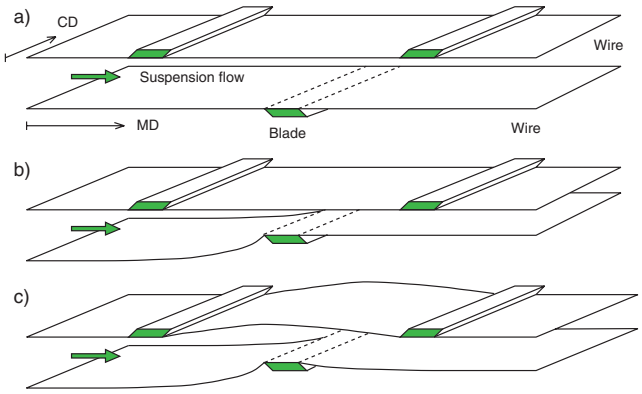

FIGURE 1.3. The principle of blade dewatering. Note that the proportions of the distances in the z-direction are not correctly reproduced. MD – Machine Direction, CD – Cross Direction. The different figures a–c are explained in section 1.1.5.

If expelled water adheres to the outer surface of the wires, it will remain till it is removed by centrifugal effects, or it is deflected away by the next blade or some other slicing device. This redirection, which is called 'doctoring', results in a pressure build-up close to the tip of the blade. It will influence the pressure difference across the wire and hence also the local drainage.

Figure 1.3 focuses on the situation in the region around the middle blade. Naturally, the positions of the fabrics at the different blades are not independent of each other. Moving the middle blade upwards will create restrictions on the flow at the upstream and the downstream blades as well, and, due to the same mechanism as explained above, regions of locally high pressure will be generated

at these blades. However, this has not been properly illustrated in the figure. Further, one should keep in mind that, unlike in the figure, blade dewatering is a slender problem. The distance between the wires is typically in the range 1–10 mm while the distance between the blades is an order of magnitude larger. The extension of the blades in the machine direction is normally 10–50 mm. All of this should also be put in relation to the width of the machine in the cross direction, which on a large production unit can be up to 10 m.

When a volume of suspension travels past a series of blades, it will repeatedly be exposed to regions of high pressure resulting in dewatering. From the point of view of the suspension volume, these regions will be experienced as pulses in time, although they are a result of translation in the machine direction. This has led to the use of the term 'pressure pulse' for the region of increased pressure in connection with a blade. The pressure pulses are of a quite different nature than the dewatering pressure achieved during roll forming. Measurements by e.g. Zahrai *et al.* (1997) and Zhao & Kerekes (1995) have shown that the magnitude of these pulses can be as high as 25 kPa or more, hence significantly higher than what has been reported for roll forming. Because of this, pure blade forming results in poor retention, since fibres and additives have a tendency to pass through the fibre mat and the wire. In addition, the pressure pulses are generally quite localised, and will therefore yield large pressure gradients in the machine direction. It is believed that this causes disruption of fibre flocs in the suspension, and that it explains the good formation of the final paper sheet that can be obtained by using blades for dewatering (Nordström 1995). The underlying mechanism is not yet properly understood. One theory is that the elongational flow resulting from the pressure gradients in the downstream region of a blade will stretch the flocs and possibly tear them apart. An additional theory is that the wire-side part of fibre flocs might get entangled in the fibre mat during the drainage, and subsequently torn apart since the outer part of the flocs are exposed to the suspension which moves with a different speed than the wire and the mat. These are current topics of research within the Faxén Laboratory at KTH. Because the blades are not permeable, one might suspect that the drainage through the two wires is assymetrical. This is true to a certain extent, but as a dominating part of the pressure pulse is found in front of the blade this is not normally a problem. The asymmetry is of course further reduced if the blades are applied alternately to the two wires as in figure 1.3, and, if such measures are taken, blade dewatering usually yields a sheet with acceptable two-sidedness.

In order to get a process with high retention in the forming section and a good formation of the final sheet, it is now common to combine roll forming with blade forming. Such a forming section might look as in figure 1.2. The idea is that fibre mats should be built up on the wires during the roll forming in order to generate sufficiently thick webs to prevent low retention in the subsequent blade section. Only partial dewatering should take place over the

roll though, as the purpose of the following blade section is to break up fibre flocs in the remaining suspension. This would not be possible if the drainage has gone too far.

According to Norman (1989) twin-wire blade formers were first developed by Beloit and Black Clawson at the end of the 1960's. At that time it was not understood that the blades generated pressure pulses. In the Beloit Bel Baie design the blades were arranged not in a straight configuration as is often done today, but instead mounted so that they described a circular arc with the tips lying on the circumference. The arc had a radius an order of magnitude larger than that of a conventional forming roll. Indeed, the wires were wrapped over the blades in order to mimic roll forming with a very large roll. The good formation that was achieved was attributed to a dewatering pressure that was thought to be of low amplitude and long duration, hence rather the opposite of what is actually the case. Norman (1979) was the first to give a reasonably accurate description of the physics of pulsating blade forming.

In the early designs incorporating deflection of the wires by blades, these were mounted in fixed positions. Whenever blades were applied to both wires, or blades were positioned on one side and other dewatering devices on the opposite side, the process got very sensitive to changes in the operating conditions. To understand this, one can e.g. look at the blade/counterblade arrangement illustrated in figure 1.3. It is evident that no drainage pressure is generated in the situation described by figure 1.3(a), where the blades are not acting on the wires. However, if the operating conditions were changed so that the distance between the incoming wires increased, while the blades remained in their positions, the blades would impose an obstruction to the flow and pressure pulses would be generated as in figure 1.3(c). To reduce the sensitivity, adjustable blades should be used, as suggested by Norman (1979). Baumann (1989) described a forming section with fixed blades applied to one of the wires, and flexible blades applied to the other side. These were pneumatically pushed against the wire, and hence the forces by which the blades were applied could be controlled. The forming section in figure 1.2 features such loadable blades. An important detail of this former is that the fixed blades (instead of the loadable ones) are applied to the wire in contact with the roll. As the position of this wire is more or less determined by the roll anyway, this reduces the necessity for adjustments.

1.1.6. *Suction shoes*

Drainage can also be achieved by lowering the pressure outside one of the wires compared to the pressure on the opposite side (usually the atmospheric pressure) . This is the case with e.g. a 'suction shoe' in the forming zone. By creating a low pressure inside the shoe, water is sucked out through the adjacent fibre mat and wire. To increase the control of the process, the shoe is usually divided into several compartments ('boxes'), with the possibility to set

different pressures in each one of them. An illustration of this is given in figure 1.4. The edges of the boxes can generate pressure pulses in the same way as blades do.

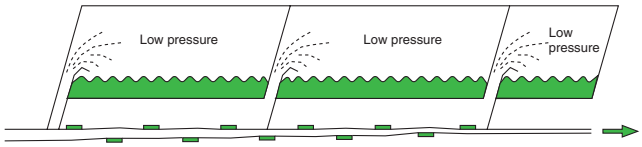

FIGURE 1.4. Vacuum boxes combined with blade-counterblade dewatering.

1.2. Research on blade forming and suction shoes

1.2.1. *Establishing the pressure pulses*

Although pressure pulses were predicted by Norman (1979), it was not until the work by Sims (1985) that experimental evidence (for a Beloit Bel Baie blade former) was published. A trailing pressure transducer was inserted through the headbox into the region between the wires, where an increased pressure was detected at each blade. The same technique was also used by Brauns (1986). The amplitude of the pulses were found to increase when the wire speed or the tension in the wire opposing the blades was increased. Amplitudes of up to 7.5 kPa were detected for some operating conditions. Brauns' work is also interesting because it investigates the effect of applying suction in between the blades. Yet another experimental study using a trailing pressure probe is the one by Bando *et al.* (1994). This technique is one of few available to measure the pressure during blade forming due to the difficulty in accessing the region between the wires. It has a drawback in that the position of the probe in the thickness direction of the gap between the wires can be neither controlled nor determined. The transducer might be embedded in the fibre mat or be located in the middle of the free suspension, or anywhere in between these two extremes. It is also unclear to what extent the presence of the probe influences the flow of suspension, and thus the measured pressure, at narrow gap sizes.

1.2.2. *Analytical results*

Zhao & Kerekes (1995) performed the first rigorous theoretical analysis of blade dewatering. A quasi one-dimensional model was developed for an isolated blade of infinitesimal extension in the machine direction. The wires extend an infinite distance in the upstream and downstream directions, and approach and leave the blade parallel at prescribed angles. The problem was treated like that of an inviscid fluid moving between thin, perfectly flexible, moving walls of constant permeability. No effects of the fibre deposition on the drainage resistance

were included. An important condition for the validity of the model is that the characteristic length scale in the machine direction is much larger than the distance between the wires. The equations were linearised and solved analytically, yielding pressure pulses located in front of the blade. It was noted that certain parameter combinations yield oscillatory solutions in this region. Behind the blade, the analysis gave zero pressure difference across the fabrics and, consequently, straight wires. A comparison with experimental data showed good agreement. It is worth mentioning that the pressure measurements by Zhao & Kerekes (1995) were not conducted with the trailing probe technique. Instead, pressure holes drilled trough a blade allowed the pressure distribution over the blade, due to the deflection of the wires at the downstream edge, to be measured.

Moch (1995) constructed a one-dimensional model for the flow around a single thin blade, including a variable permeability of the wires in order to simulate the effect of fibre deposition. The pressure pulses were found to become of larger amplitude and to extend for a shorter distance in the upstream direction than when no fibres were deposited (as would be the case if the suspension was replaced by pure water). Zhao & Kerekes (1996) performed a study of the influence of suspension concentration on the pressure pulses by using the model developed earlier (Zhao & Kerekes 1995), inserting different values for the (constant) drainage resistance. They also concluded that increased resistance gave pulses of larger magnitude. An attempt was made to relate the calculated integrated velocity difference between the suspension and the wires with experimental measurements of the formation, and a (weak) correlation was reported.

Zahrai & Bark (1995) presented a two-dimensional analysis of the application of a thin blade. The combined wire/fibre mat structure was considered to be inertialess and of negligible thickness, with constant permeability. The suspension was modelled as an inviscid fluid. A regular perturbation analysis, using the angle of deflection of the wires as the perturbation parameter, resulted in a linear analytical solution. In front of the blade, they found only small gradients in the z-direction, and the solution agreed well with the one-dimensional analysis by Zhao & Kerekes (1995). The main difference was that the one-dimensional model predicted a slightly higher pressure amplitude. However, downstream of the blade, the two-dimensional analysis yielded quite large gradients in the z-direction. Notably, there was a small region close to the blade tip where the pressure was lower than that outside the wires. This is due to the acceleration of the flow around the corner formed by the wire when the thin blade is applied to it. A comparison between the one-dimensional and the two-dimensional theory is reproduced in figure 1.5. In their study, Zahrai & Bark (1995) made no assumption on the magnitude of the ratio between the length scales in the machine direction and the z-direction. As a consequence, they were able to include the bending stiffness of the wires in their analysis. It

was found that it had no influence outside a very small region close to the blade tip, and can hence be neglected. A more accurate criterion for the appearance of oscillations in the dependent variables than that derived by Zhao & Kerekes (1995) was given as well. Among the first two dimensional models of blade dewatering should also be mentioned the study by Nigam & Bark (1997), where potential flow theory was used to study blade dewatering with a single flat or cylindrically curved blade. Linear analytical results were obtained through a perturbation analysis.

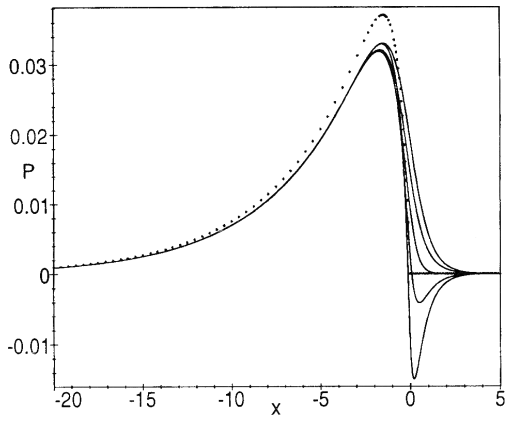

FIGURE 1.5. The pressure field around a thin blade (located at $x = 0$). Solid curves: Theory by Zahrai & Bark (1995), the different curves correspond to different positions in the z-direction. Dotted curve: Theory by Zhao & Kerekes (1995). The pressure P is non-dimensionalised by the dynamic pressure, the distance x with the initial distance between the wires.

1.2.3. *Numerical results*

Zahrai & Bark (1996) and Zahrai *et al.* (1997) developed a numerical method for solving the non-linear equations describing the two-dimensional flow over a blade of arbitrary shape. It was applied to a flat and to a triangular blade, and the results were compared with experimental data obtained using blades with pressure holes. Good and reasonable agreement was found for the triangular and the flat blade, respectively. During the numerical simulations, the drainage resistance was assumed to be constant.

Green & Kerekes (1998) numerically solved a one-dimensional non-linear model for a single thin blade incorporating a variable permeability for the wire/fibre mat. The same conclusions were drawn regarding the influence of fibre deposition as those made by Moch (1995). In the model, the wire/fibre mat was attributed a constant mass per unit area, giving only a small influence

on the calculated variables. The influence of wall shear stress was accounted for in a rudimental way. By testing viscosity values of different magnitudes, it was concluded that this parameter had a negligible influence on the pressures calculated with their model. An indication of the effects of doctoring of drained water was found by prescribing a pressure distribution on the outside of the wire in contact with the blade. It was concluded that the amplitude of the pressure pulse increased. Green *et al.* (1997) developed the model to deal with a blade of finite extension in the machine direction. Like Zahrai & Bark (1996) and Zahrai *et al.* (1997) they observed that, unless the blade is of short length, it produces two pressure pulses – one that is associated with wrap of the wires around the front edge and one with wrap around the back edge. The model was also used to study the effect of blade wear (Green & Roshanzamir 1997).

Roshanzamir *et al.* (1998) performed viscous two-dimensional simulations with a blade of finite extension in the machine direction. The wire/fibre mat was given a finite but constant thickness with constant flow resistance. This was the first time viscosity was included in a rigorous way, albeit under the assumption that the suspension behaves like a Newtonian fluid. Hence, an estimate of the shear in the suspension was obtained. The viscosity level did however not influence the calculated pressures. Roshanzamir *et al.* (1999) extended the model to include effects of doctoring of water drained upstream of the blade. Although the pressure building up on the outside of the wire due to the deflection of the approaching water was limited to a very short distance upstream of the blade, it was found that it can significantly affect the amplitude of the pressure pulse in between the wires, thus confirming what was indicated by Green & Kerekes (1998). More or less the same study can also be found in the reference Roshanzamir *et al.* (2001).

Green (1999, 2000) presented a one-dimensional model where suction was applied in between two thin blades. Roshanzamir *et al.* (2000*a*) presented a viscous 2D simulation of the same problem. Downstream of the first (upstream) blade, the pressure in the gap between the fabrics was found to rapidly decrease to a level half way between the pressure on the suction side and the pressure outside the opposing wire. This corresponded to the pressure in the gap being 3–5 kPa lower than the ambient pressure, which in the simulations resulted in an increased bending of the outer wire over the blades, and consequently pressure pulses of larger amplitude than if no suction was applied. It is, however, highly unlikely that such a pressure difference over the wire opposing the suction device could ever occur in a real forming section.

1.2.4. *Refined models*

Several studies have been undertaken in which models have been used that are more refined or complete, in regard to one or several aspects, than those mentioned so far. Roshanzamir *et al.* (2000*b*) investigated the effect of adding an inertial term to the permeability law of the wire. Zahrai *et al.* (1998)

included the physics governing the build-up of the fibre mat in their estimation of the drainage resistance, and then applied it to roll forming with good result[1]. Although no time-dependent analyses of blade forming has been carried out, such studies have been undertaken for roll forming by Turnbull *et al.* (1997) and Chen *et al.* (1998). In the cases where a comparison can be made, the more refined models yield no qualitative, and only modest quantitative, differences compared to the studies cited in sections 1.2.2 and 1.2.3.

1.3. The purpose of the current study

Previous work has given us insight into the physics of different devices employed in blade forming. Nevertheless, it is not possible to accurately predict the behaviour of important variables throughout the forming section for different device configurations and operating conditions. Hence, design of forming sections, trouble-shooting, or tuning of the controllable parameters after changes in the process, necessarily involves extensive use of trial and error techniques. Especially when developing new designs, it is advantageous if theoretical analysis could replace some experimental work, at least in the early stages. As it is prohibitively expensive to disrupt the production in a mill, one must today resort to using pilot paper machines for trials. Although less expensive, this is by no means a cheap solution.

A blade forming section does not consist of a single blade. Instead, as illustrated in figure 1.4, several blades are applied in series, and often to both of the wires and in combination with one-sided suction. Therefore, fine-tuning models in order to better describe what happens when a single component (such as e.g. a blade) is applied to a pair of wires, will not help us to better predict variables such as the pressure in a real forming section. If that is our ambition, we should focus on the interaction between different components, and try to clarify how the configuration of the devices influences the process. Previously, no research has been carried out that deals with fundamental questions like the following:

- When does the pressure pulses at two blades applied to a pair of fabrics start to interact?
- What is the result of their interaction?
- What are the implications of applying blades alternately to both wires?
- What are the effects of applying one-sided vacuum in combination with blades/counterblades?

In order to gain insight into the interaction effects, it was decided to develop a model of the kind illustrated in figure 1.6. It consists of three blades of arbitrary shape, two of which are fixed and a third which can be applied to the wire with a prescribed force. In between the fixed blades, there is vacuum application.

[1] A rigorous presentation of the sheet forming process can also be found in the review article by Meyer (1971).

The ambition was to obtain a model containing the relevant physics, but at the same time flexible and robust enough to allow easy changes (including major alterations of the geometry, such as e.g. applying additional blades) and a rather free choice of operation parameters.

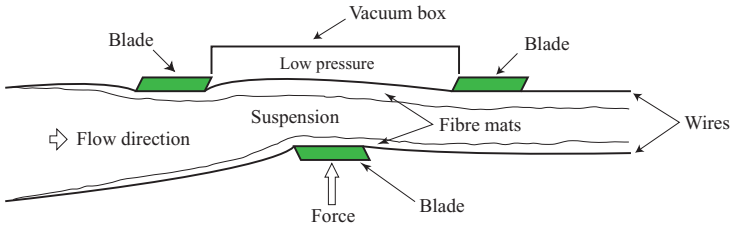

FIGURE 1.6. Illustration of the forming section considered in the thesis.

In chapter 2, a mathematical description of the model is derived. A numerical algorithm to solve the equations is presented in chapter 3. In that chapter, a comparison is also made with previous studies of blade forming in order to verify the algorithm and its implementation. Chapter 4 contains results from a number of simulations that both illustrate the capabilities of the model and give new insight into the forming process. Finally, in chapter 5, the limitations of the model, and possible means to neutralise them, are discussed.

CHAPTER 2

Mathematical model

2.1. The scope of the model

We start by giving a physical description of what we set out to model. A schematic illustration of the region close to one of the wires is given in figure 2.1. As can be seen there are essentially three different regions: The domain containing free fibre suspension, the mat of fibres deposited on top of the wire, and the wire itself. In addition, a complete model should deal with the drained water which has passed through the fibre webs and the wires and hence (at least temporarily) left the forming zone. Let us briefly elaborate on each of these regions to better understand the complications one encounters when modelling a twin-wire forming zone.

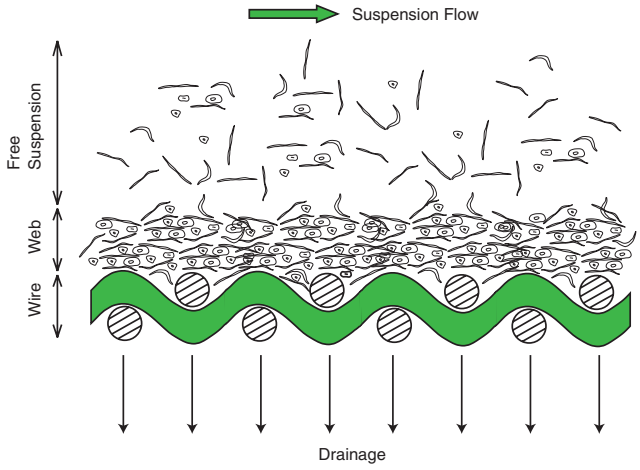

FIGURE 2.1. A schematic illustration of the different regions in the forming zone during sedimentation type drainage.

The fibre suspension has a number of constituents, the two most important being water and fibres. In addition, there are a number of additives, such as fillers and retention aid chemicals. The resulting mix has a very complicated rheology, that can either be treated as a single flowing medium, or as several

components that interact with each other. The reader interested in the mechanical properties of fibre suspensions and how to model them can find some useful references on the topic in the review article by Norman & Söderberg (2001).

The fibre mat is a structure consisting of fibres entangled in each other. Figure 2.2 shows a photograph of a fibre web starting to form on a wire. How is the mat built up? At early stages of the forming process, when there is still quite a lot of suspension between the wires, it is done through a sedimentation type process. Hence the concentration of fibres is fairly constant in the bulk of the suspension, and a rapid increase in concentration is found close to and in the mat. Late in the forming process, when most of the dewatering has already taken place, the fibre mat evolution is better described as a thickening process. In that situation, the entire distance between the wires is filled by a fibre web of varying (but high) concentration. It would no longer be meaningful to talk about a free suspension and a fibre mat. Instead the mat fills the available space between the wires and gradually thickens as the drainage continues.

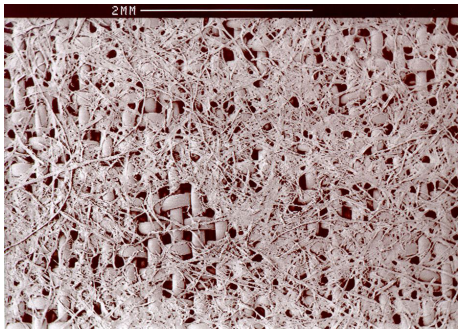

FIGURE 2.2. Photograph of a fibre web starting to form on a wire (by courtesy of Albany International AB).

The structure of the fibre mat plays a major role in determining the resistance to flow through the web which, of course, influences the rate of further drainage. The web is by no means isotropic, instead its characteristics depend on the direction considered. Further, the interaction between the liquid and the fibres when the former passes through the web results in compression and/or shearing of the mat, which in turn influences the flow. Apart from fibres, the suspension contain smaller particles, called 'fine material'. As noted by Mantar *et al.* (1995), these particles tend to get entrapped in the fibre mat once it reaches a certain thickness, hence reducing the pore size and altering the permeability.

The wires constitute the outer edges of the forming zone. Typically they have a thickness of 0.7-0.8 mm with pore sizes of about 0.1–0.2 mm, resulting

in a porosity of 30-40%. The distance between them changes as dewatering takes place, from an initial value which can be as large as 10 mm, down to a final distance of the order of the wire thickness. The liquid flowing through the wires also experience different resistances in different directions due to the anisotropic internal structure, the transversal direction typically yielding less resistance than the longitudinal one. At the interface between the fibre web and the wire, one should take into account that fibres might block the openings of the pores, which results in lower drainage rates than would be found if one considers the fibre mat and the wire separately. In figure 2.3 a close-up photograph of a modern triple-layered wire has been reproduced.

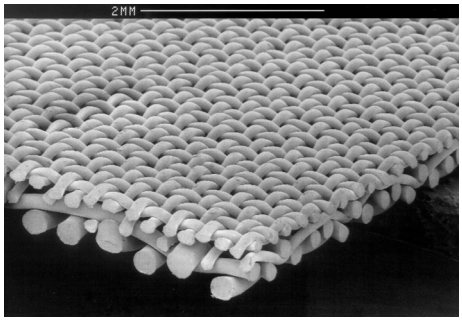

FIGURE 2.3. Close up of a triple-layered wire (by courtesy of Albany International AB).

At least part of the drained water adheres to the outside of the wire (unless wire curvature causes it to be removed by centrifugal effects). When a blade is encountered, this water has to either be deflected away from the wire, or pushed back into the wire and the fibre mat. This, of course, influences e.g. the fibre web structure and the pressure in between the wires.

From the outline above of the different regions in the forming zone, it is clear that it would be a formidable task to construct a model that encompass all details of the dewatering process.

2.2. Derivation of the governing equations

As stated in chapter 1, our ambition is to develop a simple but robust and flexible model for the interaction between different components in the forming section. However, the strategy will be to first derive rather complete equations, which will subsequently be greatly simplified. In this way, a better understanding of the physics involved is obtained, and it also clarifies what is being left out of the model as well as what assumptions have to be made to allow the simplifications.

For the time being we content ourselves with assuming that the problem is well described as two-dimensional. Given the large ratio between the cross directional dimension of the forming section and the distance between the wires, this is not likely to be a severe restriction.

Further, we will not pay any attention to the effect of doctoring of drained water. Since it is difficult to determine how much of the drained water that actually remains adjacent to the outside of the wires, the improvement of our model achieved if doctoring effects are included are judged too costly in relation to the extra effort. Although the work by Roshanzamir *et al.* (1999) indicates that doctoring is of importance when quantitatively predicting the pressure pulses, it is not likely to have a qualitative influence.

When deriving the equations, we shall consider only one of the wires. Naturally, analogous equations govern the other wire.

2.2.1. *The flow through the wires and fibre mats*

Assume that the wires, and the fibre mats they are supporting, can be treated as continuous media characterised by (macroscopic) permeabilities. Let Λ denote a representative macroscopic length scale of the geometry under consideration. In order for the assumption to be reasonable, it is necessary that there exist a representative volume, large enough to contain a great number of pores, but small compared to Λ^3. Let λ denote a typical pore size. For both the wire and the web, a good choice of Λ is their thickness, which for both is of the order 1 mm. For the wire, λ is of the order 0.1 mm. Hence it is questionable if a representative volume such as the one described above can be defined, and the continuum hypothesis is probably not adequate. On the other hand, considering the nature of the fibre sheet when it reaches the blade forming section, it is safe to say that a typical pore size in the deposited fibre web is at least ten times less than in the wire, i.e. 10^{-5} m. This leaves room to define a volume V_{ref} such that $\lambda \ll V_{ref}^{1/3} \ll \Lambda$, and hence a continuum description is justified. As the ambition is to construct a fairly simple model of the entire blade forming section, we shall ignore the shortcomings of the continuum assumption in the case of the wire. Furthermore, the wire and the web will be treated as a single medium, which means neglecting e.g. blockage effects at the interface between the wire and the web.

Let $\boldsymbol{u_p}$ be the volume average, over the volume V_{ref}, of the microscopic velocities in the material. The following macroscopic momentum equation will be used as model for the average velocity,

$$\rho \frac{\mathrm{D}\,\boldsymbol{u_p}}{\mathrm{D}\,t} = -\nabla p + \mu \mathbb{K}^{-1} \boldsymbol{u_p}\,. \tag{2.1}$$

Here, ρ and μ are the density and the dynamic viscosity of the fluid, respectively, $\mathrm{D}/\mathrm{D}\,t$ is the material time derivative, p is the volume averaged pressure and $\mathbb{K}$ is the permeability tensor. The equation expresses a balance between the

pressure gradient and viscous and inertial forces. We shall attempt to reduce it somewhat.

The microscopic flow in the pores, represented by the pore velocity $\boldsymbol{v_p}$, can be considered to follow the Navier-Stokes equation for the momentum,

$$\rho \frac{\mathrm{D}\,\boldsymbol{v_p}}{\mathrm{D}\,t} = -\nabla p_m + \mu \Delta \boldsymbol{v_p}\,, \tag{2.2}$$

where p_m is the microscopic pressure in the pores. It seems like a reasonable assumption to say that, if the inertial or the viscous terms are negligible in equation 2.2, they will be so in equation 2.1 as well. Let W be a measure of the volume averaged macroscopic velocity, and n the porosity of the material, defined as the ratio between the volume occupied by fluid and the total volume (note that the volume concentration of solid α_p is $1 - n$). The magnitude V of the pore velocity is then W/n. The magnitudes of the viscous and the inertial terms in equation 2.2 can be estimated to $\mu W/(n\lambda^2)$ and $\rho W^2/(n^2\lambda)$, respectively. Let us define a Reynolds number for the microscopic flow as $Re_\lambda = \rho V \lambda/\mu$. It is clear that the inertial term is negligible in comparison to the viscous one if $Re_\lambda \ll 1$.

How large is Re_λ in the wire and fibre mat during blade forming? The mass concentration of fibres right before the press section is typically 0.2 (see chapter 1). As dry cellulose has a density 1.5 times that of water, a naiv calculation gives a volume concentration of fibres of 0.14, and hence a porosity of 0.86. The effective porosity to be used when estimating the pore velocity is probably less than this due to the low flow through the hollow interior of the fibres[1]. Let us consider n to be 0.5. The magnitude of W can be found by considering the blade forming process. Assuming that dewatering causes the wires to approach each other 1 mm as they travel 1 m in the machine direction with a speed of 15 m/s, the drainage velocity W should be of the order 0.1 m/s. As the density and viscosity of water is 1000 kg/m^3 and 0.01 g/(cm s), respectively, we have a Re_λ of the order 1. Apparently the inertial term is as important as the viscous term in equation 2.2. We shall nevertheless chose to neglect inertia in equation 2.1 in order to gain simplicity in our model. To justify this, we refer to the results from studies that have included inertia in the description of the drainage, which showed that it had little effect on the calculated pressure pulses (see e.g. Roshanzamir *et al.* 2000*b*).

Without the inertial term, equation 2.1 turns into the well known Darcy's law,

$$\boldsymbol{u_p} = -\frac{1}{\mu}\mathbb{K}\nabla p\,. \tag{2.3}$$

[1] This cavity is called 'lumen'.

The equation appears to be linear, but the permeability tensor $\mathbb{K}$ may of course depend on the flow $\boldsymbol{u_p}$ due to effects such as e.g. compressibility and deformation due to shear. It is also influenced by the entrapment of fine material in the web. However, we will assume the tensor to be constant. For an isotropic material, the elements along the diagonal in $\mathbb{K}$ are equal, and the off-diagonal elements are zero, which means that the flow through the material is parallel to the direction of the pressure gradient. Introduce a co-ordinate system (ξ, ζ) with the origin on the outer surface of the wire, the ξ-direction pointing tangentially along the wire in the direction of movement, and the ζ-direction pointing along the normal to the wire surface, away from the fibre mat (see figure 2.4). In order to model the wires, we will assume $\mathbb{K}$ to be diagonal, with a finite permeability k_ζ in the ζ-direction, and zero permeability in the ξ-direction. In other words, we postulate that there is no flow of liquid inside the fibre mat or the wire parallel to the wire. In reality, this is most likely not true. However, this tangential flow is mainly interesting if a good description of the shear between the suspension and the fibre web is desired[2]. As our ambition is not to resolve such details, we can allow ourselves to focus on the flow in the other direction. What remains of equation 2.3 is consequently the following relation,

$$w_p = -\frac{k_\zeta}{\mu}\frac{\partial p}{\partial \zeta}\,, \tag{2.4}$$

where w_p is the ζ-component of $\boldsymbol{u_p}$. Further, assuming that the pressure varies linearly between the value p_w at the suspension side of the web, and p_e on the outer side of the wire, and denoting the combined thickness of the fibre mat and the wire d, equation 2.4 turns into

$$w_p = \frac{k_\zeta}{\mu\, d}(p_w - p_e)\,. \tag{2.5}$$

Note that, due to our assumptions of constant permeability and a constant pressure gradient, w_p does not vary in the ζ-direction.

Let us introduce a drainage resistance $R = \mu d/k_\zeta$. Even though we have assumed a constant permeability of the wire and the web, R will still vary during the drainage process due to the increase in mat thickness as new fibres are deposited. The rate of change of R in the ξ-direction can be related to the speed of the wire, U, and the volume fractions of fibres, α_p and α_s, in the fibre mat and the suspension, respectively. Assuming that α_p and α_s are constant, and that the fibre mat does not move in relation to the wire, conservation of fibres yield

$$\frac{\partial d}{\partial \xi} = \frac{\alpha_s}{\alpha_p}\frac{w_p}{U}\,. \tag{2.6}$$

[2]Interesting studies treating the flow over a porous wall are the ones by Taylor (1971) and James & Davis (2001).

Equation 2.6 can be derived by considering a control volume[3] consisting of a segment of wire and mat, as illustrated in figure 2.4. From the definition of R

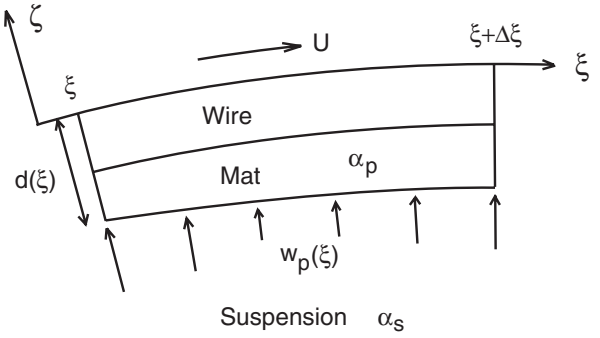

FIGURE 2.4. A segment, of length $\Delta\xi$, of the wire and the mat. Confer the text for an explanation of the notation.

and equations 2.5 and 2.6, we have that the evolution of the drainage resistance is described by

$$\frac{\partial R}{\partial \xi} = \frac{1}{U}\frac{\mu}{k_\zeta}\frac{\alpha_s}{\alpha_p}\frac{p_w - p_e}{R}\,. \tag{2.7}$$

For ease of notation, we introduce the 'drainage coefficient'

$$K = \frac{\mu\alpha_s}{k_\zeta\alpha_p} \tag{2.8}$$

for the group of constant parameters in equation 2.7. Due to the difficulty in predicting k_ζ, which is not likely to be constant during actual forming, it is hard to determine K. Zhao & Kerekes (1996) presented some experimental data, obtained by considering the water balance around a blade, relating the drainage resistance to the mass concentration of fibres in the web. Knowing the density of the wet fibres, the mass per unit area of the web, and the concentration of fibres in the suspension, these data can be used to estimate k_ζ. It should be noted that these measurements were performed on a pilot paper machine during operating conditions similar to those in the industrial process. Experimental data obtained with special drainage testing devices have been reported by Mantar *et al.* (1995), Wildfong *et al.* (2000) and Paradis *et al.* (2002). In the last study, the drainage measurements were done while the suspension and the mat was subject to shear.

Having derived equation 2.7, the thickness d of the wire and the mat will no longer be of any concern to us in our description of the drainage, and we

[3]For an example of such an analysis, see section 2.2.2 where an equation for the mass of the wire/fibre mat is derived.

shall think of the wire and the mat as being of infinitesimal thickness. Further, the relation between ξ and the co-ordinate x in the system introduced in figure 2.5 is

$$\xi(x,t) = \int^x \sqrt{1 + f_x(x',t)^2}\,\mathrm{d}x'\,, \tag{2.9}$$

where $f(x,t)$ gives the position of the wire as a function of the position in the machine direction and time. Note that the subscript x denote differentiation with respect to x. By combining equations 2.7 and 2.9 with the relation

$$\frac{\partial R}{\partial \xi} = \frac{\partial R}{\partial x}\left(\frac{\partial \xi}{\partial x}\right)^{-1}\,, \tag{2.10}$$

we obtain a time-dependent expression for the evolution of the drainage resistance,

$$R_x(x,t) = \frac{K}{U}\frac{p_w - p_e}{R(x,t)}\sqrt{1 + f_x(x,t)^2}\,. \tag{2.11}$$

Of course, the time dependency does not enter through $f(x,t)$ alone, we may have $w_p = w_p(\xi,t)$ as well.

We shall assume that a wire passing over a blade is in contact with the surface of the blade, thus excluding the possibility of a thin liquid film between the two of them. Consequently, over the blade there will be no flow through the wire and the fibre mat, yielding $p_w = p_e$, and hence

$$R_x(x,t) = 0\,. \tag{2.12}$$

2.2.2. *The mass of the wires and the fibre mats*

Although the combined wire and fibre mat is considered infinitely thin, we shall continue to assume that it has a mass m per unit of length along the wire and unit of width across the machine direction. Since the wire and the fibre mat is treated as a single permeable medium, in what follows the term 'wire' or 'fabric' will refer to both of the components together, unless we specify otherwise. Figure 2.5 illustrates a section of a wire in a Cartesian co-ordinate system (x,z) whose origin is located in the gap between the wires. The x-direction is parallel to the machine direction, and the z-direction is oriented across the gap. The position of the wire is given by $f(x,t)$, and its axial velocity (i.e. the 'wire speed') is U. By considering the wires as inelastic, it follows that U is constant. The velocity of a particular point on the wire is $\boldsymbol{u_w}$, and the velocity of the suspension immediately adjacent to the wire is $\boldsymbol{u_s}$. The components of $\boldsymbol{u_w}$ and $\boldsymbol{u_s}$ in the (x,z)-system are (u_w, w_w) and (u_s, w_s), respectively. The directions of the normal and the tangent to the wire are given by $\hat{\boldsymbol{n}}$ and $\hat{\boldsymbol{t}}$, respectively,

$$\hat{\boldsymbol{n}} = \frac{(-f_x, 1)}{\sqrt{1+f_x^2}} \quad \text{and} \quad \hat{\boldsymbol{t}} = \frac{(1, f_x)}{\sqrt{1+f_x^2}}\,. \tag{2.13}$$

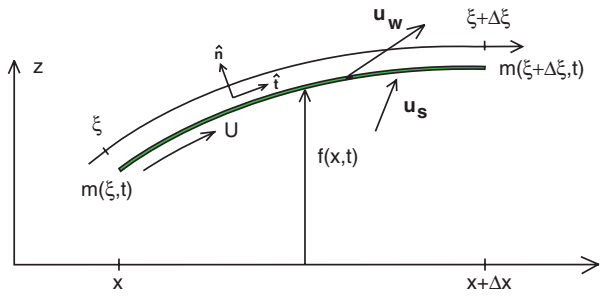

FIGURE 2.5. A segment of the upper wire. The mathematical model is expressed in the Cartesian system (x, z). Confer the text for an explanation of the notation.

An equation for the rate of change of the mass of a wire segment between x and $x + \Delta x$ is easily obtained by considering a control volume consisting of the volume occupied by the segment. The explicit rate of change equals the amount of mass entering the volume, minus the amount leaving,

$$\frac{\partial}{\partial t}\int_{\xi}^{\xi+\Delta\xi} m(\xi', t)\,\mathrm{d}\xi' = Um(x,t) - Um(x+\Delta x, t) + \int_{\xi}^{\xi+\Delta\xi} c\,(\boldsymbol{u_s} - \boldsymbol{u_w})\cdot\hat{\boldsymbol{n}}\,\mathrm{d}\xi' \,. \quad (2.14)$$

The parameter c relates the build-up of the mass of the fibre mat to the amount of drainage. An important issue is whether the mass of the water residing inside the wire and the fibre web should be included in the mass of the 'wire', or not. From the assumptions made in section 2.2.1 regarding the permeability of the wire in different directions, it follows that when the wire is accelerated in the axial direction, the water inside it will have to be accelerated at the same rate as well. In that case, it would be reasonable to include the mass of the water. However, when the wire is accelerated in the transversal direction, there can (and will) be a relative velocity between the wire and the water. As a result, the water does not have to be accelerated to the same extent as the wire, and its full mass should not be included. Consequently, the effective values of both m and c depend on the motion of the wire. For the sake of simplicity we choose not to consider such effects, and assume that c is some suitable constant. If no consideration at all was paid to the water in the pores between the fibres, we would have $c = \alpha_s \rho_f$, where ρ_f is the density of the (wet) fibres. Using the relation 2.9, the two integrals in equation 2.14 can be transformed so that the

variable of integration becomes x instead of ξ. Then, by employing the mean value theorem, the term on the left hand side turns into,

$$\frac{\partial}{\partial t}\left(m\sqrt{1+f_x^2}\right)|_{x=x_1}\Delta x\,, \tag{2.15}$$

and the integral on the right hand side into

$$c\Big((w_s-w_w)-f_x(u_s-u_w)\Big)|_{x=x_2}\Delta x\,, \tag{2.16}$$

where $x \le x_1, x_2 \le x+\Delta x$. Note that, although x_1 and x_2 will subsequently be used in other equations, they do not necessarily correspond to the same x-positions as in the equations above. They are introduced for notational convenience, and their values depend on the equation in which they appear. Taylor-expanding the second term on the right hand side of equation 2.14 yields

$$Um(x+\Delta x,t) = Um(x,t) + U\frac{\partial}{\partial x}m(x,t)\Delta x + \mathcal{O}(\Delta x^2)\,. \tag{2.17}$$

When inserting 2.15, 2.16 and 2.17 into equation 2.14, dividing by Δx, and letting $\Delta x \to 0$, the following equation governing the mass of the fabric is obtained,

$$\left[m\sqrt{1+f_x^2}\right]_t + Um_x = c\Big((w_s-w_w)-f_x(u_s-u_w)\Big)\,. \tag{2.18}$$

As there is no flow through the wires when they pass over a blade (see section 2.2.1), we have $(\boldsymbol{u_s}-\boldsymbol{u_w})\cdot\hat{\boldsymbol{n}}=0$ over the blade. In that case, equation 2.18 is reduced to

$$\left[m\sqrt{1+f_x^2}\right]_t + Um_x = 0\,. \tag{2.19}$$

The wire does not necessarily have to pass over the entire surface of the blade, although this is the case in most situations. At the positions where the wire is in contact with the blade, $f(x,t)$ is given by the position of the blade surface. The time-derivative in equation 2.19 has been kept since the position of a loadable blade is determined by a balance between the forces acting on the blade and its momentum, and may consequently vary in time. This effect is however likely to be insignificant under normal operating conditions. If it is included, the model has to be supplemented by an equation for the position of the blade.

It is possible to relate $\boldsymbol{u_w}$ to $f(x,t)$. Let $\boldsymbol{r_p}=(x_p(t),z_p(t))$ be the position of a certain part of the wire, whose velocity is $\boldsymbol{u_w}$. As $z_p(t)=f(x_p(t),t)$, we have that

$$u_w = \dot{x}_p(t) \quad \text{and} \quad w_w = \dot{z}_p(t) = \frac{\partial f}{\partial x}\dot{x}_p(t) + \frac{\partial f}{\partial t}\,, \tag{2.20}$$

where dots denote time differentiation. So far, we have put no constraints on $f(x,t)$. However, the motion of the wire is not completely free. The limited available length of the wire imposes a restriction on the possible movements, and this has to be incorporated in the model. In order to do this, we shall assume that there is a fix point $\boldsymbol{r_0}=(x_0,z_0)$ through which the wire always

passes, i.e. $f(x_0, t)$ is constant. In a paper machine, e.g. a roll supporting the wire can be considered as such a point. The distance along the wire from $\boldsymbol{r_0}$ to $\boldsymbol{r_p}$ is

$$\int_{x_0}^{x_p(t)} \sqrt{1 + f_x(x,t)^2}\,\mathrm{d}x = Ut + l_0\,, \tag{2.21}$$

where l_0 is the distance at $t = 0$. When differentiating equation 2.21 with respect to time, we obtain

$$\sqrt{1 + f_x(x_p(t),t)^2}\dot{x}_p(t) + \frac{\partial}{\partial t}\int_{x_0}^{x_p(t)} \sqrt{1 + f_x(x,t)^2}\,\mathrm{d}x = U\,. \tag{2.22}$$

The first term on the left hand side of equation 2.22 expresses the fact that, even if the position of the wire is stationary in space, the distance from the fix point $\boldsymbol{r_0}$ to a certain point $\boldsymbol{r_p}$ on the wire will increase as the wire is constantly moving with an axial velocity U. The second term on the left hand side tells us that, even if the point on the wire we are considering is not moving in space, the distance between $\boldsymbol{r_0}$ and that point will still increase due to more wire constantly passing by $\boldsymbol{r_0}$ with velocity U. By solving the kinematic expression 2.22 for $\dot{x}_p$ and inserting the result in equation 2.20 we obtain the components of $\boldsymbol{u_w}$,

$$u_w = \frac{1}{\sqrt{1 + f_x(x_p(t),t)^2}}\left(U - \frac{\partial}{\partial t}\int_{x_0}^{x_p(t)} \sqrt{1 + f_x(x,t)^2}\,\mathrm{d}x\right) \tag{2.23}$$

and

$$\begin{aligned} w_w = {} & f_t(x_p(t),t) + \\ & + \frac{f_x(x_p(t),t)}{\sqrt{1 + f_x(x_p(t),t)^2}}\left(U - \frac{\partial}{\partial t}\int_{x_0}^{x_p(t)} \sqrt{1 + f_x(x,t)^2}\,\mathrm{d}x\right)\,. \end{aligned} \tag{2.24}$$

As $\boldsymbol{r_p}$ is arbitrary, we can of course consider $\boldsymbol{r_p}$ to be the point whose x-position is currently x, and hence replace $x_p(t)$ with x in the equations. By doing this, and introducing the notation $l(x,t)$ for the distance along the wire from (x_0, z_0) to $(x, f(x,t))$, we can write the expressions 2.23 and 2.24 as

$$u_w = \frac{1}{\sqrt{1 + f_x^2}}\left(U - l_t\right) \tag{2.25}$$

and

$$w_w = f_t + \frac{f_x}{\sqrt{1 + f_x^2}}\left(U - l_t\right)\,. \tag{2.26}$$

The equations 2.25 and 2.26 may now, if desired, be inserted into equation 2.18.

2.2.3. *The momentum of the wires and the fibre mats*

Consider the fabric segment in figure 2.5. During the drainage, suspension is approaching the fabric with some velocity normal to the wire. If the wire is saturated, our assumption of zero permeability in the tangential direction and constant permeability across the wire implies that the water enters and leaves the wire with the same velocity. Hence, the water has no direct influence on the inertia of the wire (there is of course an indirect influence due to the pressure drop across the fabric caused by the drainage resistance). The fibres, on the other hand, remain on the surface of the fibre mat and will thus add their momentum to that of the wire. The time rate of change of the momentum in the z-direction of the wire segment between x and $x + \Delta x$ is

$$\frac{\partial}{\partial t}\int_{\xi}^{\xi+\Delta\xi} w_w m \,\mathrm{d}\xi' + (mUw_w)|_{x+\Delta x} - (mUw_w)|_x - \\ - \int_{\xi}^{\xi+\Delta\xi} \rho_f \alpha_s w_s (\boldsymbol{u_s} - \boldsymbol{u_w}) \cdot \hat{\boldsymbol{n}} \,\mathrm{d}\xi' \,. \tag{2.27}$$

In analogy with the analysis in section 2.2.2, Taylor-expansion and the mean value theorem can be used to turn the expression into

$$\frac{\partial}{\partial t}(w_w m\sqrt{1+f_x^2})|_{x=x_1}\Delta x + \frac{\partial}{\partial x}(mUw_w)|_x \Delta x + \\ -\rho_f \alpha_s w_s \Big((w_s - w_w) - f_x(u_s - u_w)\Big)|_{x=x_2} + \mathcal{O}(\Delta x^2)\,, \tag{2.28}$$

where $x \le x_1, x_2 \le x + \Delta x$. Expression 2.28 should, of course, be balanced by the forces acting on the wire. These are illustrated in figure 2.6, where T denotes the axial force in the wire per unit width, referred to as the 'wire tension', τ is the shear stress acting on the wire surface, and S and M are the transverse force and internal moment per unit width, respectively.

Let us start by considering the pressure. The z-component of the force due to the pressure drop across the wire is

$$\int_x^{x+\Delta x} (p_w - p_e)\,\mathrm{d}x' = \{\text{MeanValueTheorem}\} = (p_w - p_e)|_{x=x_1}\Delta x\,, \tag{2.29}$$

where $x \le x_1 \le x + \Delta x$.

The tension in the wire exerts a force in the z-direction that is found to be

$$\frac{\partial}{\partial x}\frac{T f_x}{\sqrt{1+f_x^2}}\Delta x + \mathcal{O}(\Delta x^2)\,. \tag{2.30}$$

A wire has very small bending stiffness, and it is normally safe to ignore it when studying blade forming, as was demonstrated by Zahrai & Bark (1995). However, it is instructive to re-demonstrate this result, and hence we shall include stiffness for the time being in our study of the momentum of the wires.

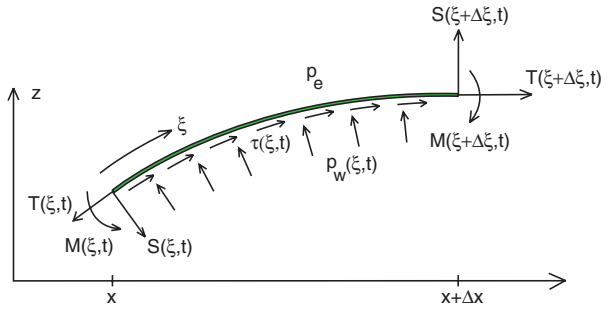

FIGURE 2.6. The different forces acting on the wire. T, S and M denote the wire tension, the transversal force and the bending moment, respectively. p_w and p_e are the pressure in the suspension adjacent to the wire and the external pressure, respectively. τ is the shear stress acting on the wire.

The resultant in the z-direction of the transversal forces on the segment is

$$\frac{\partial}{\partial x}\frac{S}{\sqrt{1+f_x^2}}\Delta x + \mathcal{O}(\Delta x^2)\,. \tag{2.31}$$

By assuming that the wire behaves like an Euler-Bernoulli beam, the following classical result holds,

$$S = \frac{\partial M}{\partial \xi}\,. \tag{2.32}$$

Employing expression 2.9, relating ξ to x, equation 2.32 is turned into

$$S = \frac{M_x}{\sqrt{1+f_x^2}}\,. \tag{2.33}$$

Further, let us introduce the parameter χ,

$$\chi = \frac{f_x}{\sqrt{1+f_x^2}}\,. \tag{2.34}$$

As χ_x is the curvature of the wire, beam theory tells us that

$$M = -B\chi_x\,, \tag{2.35}$$

where B is the bending stiffness of the wire. It will be assumed constant. By combining the equations 2.31, 2.33 and 2.35, the contribution to the vertical forces on the wire segment from transversal forces is found to be

$$-B\frac{\partial}{\partial x}\frac{\chi_{xx}}{1+f_x^2}\Delta x + \mathcal{O}(\Delta x^2)\,. \tag{2.36}$$

If the suspension next to the fabric is accelerated or decelerated by the wire in the $\hat{\boldsymbol{t}}$-direction, there will be a shear stress τ on the wire. For the segment in figure 2.6, the vertical force per unit width due to this stress is

$$\int_x^{x+\Delta x} f_x \tau \, \mathrm{d}x' = \{\text{MeanValueTheorem}\} = (f_x \tau)|_{x=x_1} \Delta x \,, \tag{2.37}$$

where we have $x \leq x_1 \leq x + \Delta x$. The value of τ at each position depends on the rheology of the suspension.

We now have all the pieces necessary to establish the momentum balance in the z-direction for the wire. The time rate of change of the momentum given by expression 2.28 equals the sum of all the forces in the z-direction. These are given by 2.29, 2.30, 2.36 and 2.37. Writing down the balance, dividing by Δx and letting $\Delta x \to 0$, one finds

$$\left[w_w m \sqrt{1+f_x^2}\right]_t + U\left[m w_w\right]_x - \rho_f \alpha_s w_s \Big((w_s - w_w) - f_x (u_s - u_w) \Big) = \\ p_w - p_e + \left[T\chi\right]_x - B\left[\frac{\chi_{xx}}{1+f_x^2}\right]_x + \tau f_x \,. \tag{2.38}$$

An analysis analogous to the one undertaken above can be performed for the momentum in the x-direction. The result would be

$$\left[u_w m \sqrt{1+f_x^2}\right]_t + U\left[m u_w\right]_x - \rho_f \alpha_s u_s \Big((w_s - w_w) - f_x (u_s - u_w) \Big) = \\ -(p_w - p_e) + \left[\frac{T}{\sqrt{1+f_x^2}}\right]_x - B\left[\frac{\chi \chi_{xx}}{\sqrt{1+f_x^2}}\right]_x + \tau \,. \tag{2.39}$$

In the equations 2.38 and 2.39, u_w and w_w are given by 2.25 and 2.26, respectively. To get u_s and w_s, the flow in the suspension has to be solved.

As the wire passes a blade, $(\boldsymbol{u_s} - \boldsymbol{u_w}) \cdot \hat{\boldsymbol{n}} = 0$, causing the last terms on the left hand sides in equations 2.38 and 2.39 to disappear. Also note that, in that case, $f(x,t)$ is given by the position of the blade surface. At a blade, the shear stress τ should include the friction between the wire surface and the blade. The magnitude of the friction is much larger than the viscous stress resulting from the acceleration/deceleration of the suspension, and might cause significant changes in the wire tension T.

2.2.4. *The flow of the suspension*

The flow of any continuous medium is governed by Cauchy's equation, which, if we neglect body forces such as e.g. gravity, has the form

$$\rho \frac{Du_i}{Dt} = \frac{\partial T_{ij}}{\partial x_j} \,. \tag{2.40}$$

Here, u_i and x_i denote the i-components of the velocity and the position, respectively, and T_{ij} are the elements of the stress tensor $\mathbb{T}$. As usual, when two indices in a term are equal, a summation over those indices is implied

unless otherwise stated. Although a fibre suspension has several constituents such as water, fibres, fillers and various chemicals, we will treat it as a single flowing medium. Consequently its motion is described by equation 2.40. It is well known that the fibre suspensions encountered in papermaking have a rheology different from a Newtonian fluid, and a natural question is how to chose $\mathbb{T}$ in equation 2.40 to model their behaviour. This is a complicated issue, and we shall make no attempt to address it. Here, like in the only study concerned with blade dewatering where viscous effects were included in a rigorous way (Roshanzamir *et al.* 1998), we shall assume that the suspension can be considered as Newtonian with a dynamic viscosity μ_s. For qualitative predictions this might be an adequate assumption in the blade forming section, although one should probably be careful when drawing qualitative conclusions about shear-related issues.

Let $\boldsymbol{u}$ be the velocity of the suspension, with the components (u, w) in our (x, z)-system. Given our assumption about the rheology, Cauchy's equation turns into the well known Navier-Stokes equations for the momentum,

$$\frac{\partial u}{\partial t} + u\frac{\partial u}{\partial x} + w\frac{\partial u}{\partial z} = -\frac{1}{\rho}\frac{\partial p}{\partial x} + \frac{\mu_s}{\rho}\left(\frac{\partial^2 u}{\partial x^2} + \frac{\partial^2 u}{\partial z^2}\right), \tag{2.41}$$

$$\frac{\partial w}{\partial t} + u\frac{\partial w}{\partial x} + w\frac{\partial w}{\partial z} = -\frac{1}{\rho}\frac{\partial p}{\partial z} + \frac{\mu_s}{\rho}\left(\frac{\partial^2 w}{\partial x^2} + \frac{\partial^2 w}{\partial z^2}\right), \tag{2.42}$$

which are supplemented by the continuity equation for an incompressible fluid,

$$\frac{\partial u}{\partial x} + \frac{\partial w}{\partial z} = 0\,. \tag{2.43}$$

The drainage will determine $\boldsymbol{u} \cdot \hat{\boldsymbol{n}}$ at the wire. As the fabric is a permeable medium, $\boldsymbol{u} \cdot \hat{\boldsymbol{t}}$ is not likely to be zero even if a viscous description of the fluid is adopted. We shall not try to investigate the relative velocity difference between the suspension and the wire, but refer the interested reader to e.g. Taylor (1971) or James & Davis (2001). These conditions, together with suitable conditions at the inlet and the outlet of the model domain, and equations 2.41, 2.42 and 2.43, could in theory be solved for the pressure and the velocity field in the suspension. From the assumption of a Newtonian rheology follows that the shear stress, by which the fluid acts on the wire, can be obtained by evaluating the following expression at the surface of the fabric (see e.g. Acheson, 1990),

$$\tau = -\mu_s\Big(2(\hat{\boldsymbol{n}} \cdot \nabla)\boldsymbol{u} + \hat{\boldsymbol{n}} \times (\nabla \times \boldsymbol{u})\Big)\,. \tag{2.44}$$

2.3. Simplifications

The dependent variables in our mathematical description are the drainage resistances of the wires (governed by equations of the form of equation 2.11), the mass per unit length and unit width of the wires (governed by equations of the form of equation 2.18), the positions of the two wires (given by equation

2.38 together with an analogous equation for the other wire), the tensions in the wires (given by equation 2.39 together with an analogous equation for the other wire), and the velocity field and the pressure in the suspension (given by the equations in section 2.2.4). The equations in their present form are rather complex, and we shall try to simplify them.

Our main aim is to predict the pressure distribution in a forming zone like the one in figure 1.6. As we have assumed that the suspension behaves like a Newtonian fluid, and the viscosity in that case has little influence on the pressure pulses (Roshanzamir *et al.* 1998), we shall start by neglecting viscous effects. This is further motivated by the fact that our final model will be quasi one-dimensional, which does not allow us to rigorously deal with shear phenomena anyway. We shall further assume that there is no friction between the wires and the blade surfaces. Consequently, the wire tensions will be constants, and we can omit the momentum balances in the x-direction for the wires from the model.

Green & Kerekes (1998) measured the dry mass of a certain twin-wire forming fabric to 415 g/m^2. As noted in chapter 1, the grammage of the final product varies from the order of 10 g/m^2 up to 400 g/m^2. Blade dewatering is not used to produce the most lightweight grades. However, the technique is employed for newsprint, with a grammage of 40–45 g/m^2. As we are employing twin-wire forming, and assuming we can neglect the water content in the wire and the fibre mat when considering their grammage, a mass of about 20 g/m^2 will be built up on each fabric. Normally, a blade forming section contains more than the three blades we are modelling. In addition, when the wires reach the blades, a sheet has usually already been formed on the fabrics. Let us however guess that roughly 10 % of the total drainage occurs as the wires pass through our model, which in the newsprint case means 2 g/m^2/wire. This increase in mass is clearly insignificant in comparison with the mass of the wire and the already formed fibre mat when they reach the blades. The mass of the 'fabrics' in our model can hence in this case be assumed constant. For a heavier grade, this is not as obvious, but 10 % of 400/2 g/m^2 is 20 g/m^2, which shall be compared to at least the mass of the wire. Hence, even in that case the combined mass of the wire and the fibre mat is not too ill described as constant. Although the analysis above is rather dubious, we shall assume m for each fabric to be constant, and hence not make use of equation 2.18 and its analogous counterpart for the other wire. By neglecting the mass of the fibres depositing onto the fibre mat, it follows that we should also neglect their influence on the momentum of the wire.

Let λ_x and λ_z denote typical length scales in the x- and z-directions, respectively. As the distance between the wires is generally an order of magnitude smaller than the distance between the blades, we expect that $\lambda_z < \lambda_x$. Based on this observation, we assume that $(\lambda_z/\lambda_x)^2 \ll 1$, and can consequently neglect f_x^2 in comparison with 1 in the equations. More physical, but less direct,

estimates of λ_x can be found by considering the linear analytical solution for a single thin blade derived by Zhao & Kerekes (1995). In the case of isolated blades, this would have been the only option. Equation 2.11 can now be simplified into

$$R_x(x) = \frac{K}{U}\frac{p_w - p_e}{R(x)}\,, \tag{2.45}$$

which is the form in which it will be used in the final model. Note that the time-dependency has been omitted. Equation 2.38 for the momentum in the z-direction becomes

$$mf_{tt} + 2mUf_{xt} + mU^2 f_{xx} = p_w - p_e + Tf_{xx} - Bf_{xxxx}\,, \tag{2.46}$$

where we have made use of the fact that now $w_w = f_t + Uf_x$. An estimate of the ratio between the term containing the wire tension T and the term containing the bending stiffness B in equation 2.46 is

$$\frac{B}{T}\frac{1}{\lambda_x^2}\,. \tag{2.47}$$

The wire tension is normally of the order of 10 kN/m. Zahrai & Bark (1995) mention the value 4.91×10^{-3} Nm as the bending stiffness of a typical two-layered wire. This suggests that we can take 10^{-2} Nm as an estimate of B. If λ_x is somewhere in the range 0.05-0.1 m, the ratio 2.47 is of the order 10^{-4}, and it is hence clear that the effects of bending stiffness can be neglected. However, if we consider a region very close to a blade edge (which is where the wire has its largest curvature), so that λ_x is very small, the influence of bending stiffness is as important as that of wire tension. This region cannot be studied using equation 2.46, since it is based on the assumption that $(\lambda_z/\lambda_x)^2 \ll 1$. As a consequence of this lack of resolution, the slope of the fabric might appear to change discontinuously at a blade edge. An order of magnitude analysis of the bending stiffness and wire tension terms in equation 2.38 indicates that the extent of the region where bending stiffness is important is of the order 1 mm, in which case λ_z/λ_x is of the order 1. This is in accordance with the results found by Zahrai & Bark (1995). Further, as m and U are of the order 1 kg/m^2 and 10 m/s, respectively, we see that mU^2 is negligible in comparison with T. If we finally assume that the problem is stationary, we find that equation 2.46 is reduced to

$$p_w - p_e + Tf_{xx} = 0\,. \tag{2.48}$$

From this we see that the excess pressure in the gap between the fabrics should be of the order $T\lambda_z/\lambda_x^2$, which, using the values above and $\lambda_z \sim 10^{-3}$mm, means about 1 kPa.

Now, consider the equations 2.41–2.43 governing the flow of the suspension. As for the wires, viscosity is neglected and steady flow is assumed. Hence we

have

$$u\frac{\partial u}{\partial x} + w\frac{\partial u}{\partial z} = -\frac{1}{\rho}\frac{\partial p}{\partial x}\,, \tag{2.49}$$

$$u\frac{\partial w}{\partial x} + w\frac{\partial w}{\partial z} = -\frac{1}{\rho}\frac{\partial p}{\partial z}\,, \tag{2.50}$$

$$\frac{\partial u}{\partial x} + \frac{\partial w}{\partial z} = 0\,. \tag{2.51}$$

Assume for a moment that the left hand side of equation 2.50 is negligibly small (we shall verify this a posteriori). Then $\partial p/\partial z$ is essentially zero, and p is a function of the x-position alone. From equation 2.49 now follows that the rate of change of u when following a fluid particle is a function of only x, and independent of z. Far upstream of the blades, the velocity in the u-direction is independent of z (it equals the wire speed for all fluid particles). Due to the material time-derivative of u being a function of the sole variable x, this independence of z will be maintained throughout the blade forming section, and hence u is also a function of x alone. Equation 2.49 turns into

$$u\frac{\mathrm{d}u}{\mathrm{d}x} = -\frac{1}{\rho}\frac{\mathrm{d}p}{\mathrm{d}x}\,. \tag{2.52}$$

We will now verify the initial assumption about equation 2.50. Let Δu and Δw denote typical changes in the x-direction of the u-component and the w-component of the velocity, respectively. Note that, since the fabrics are parallel and no drainage takes place far upstream of the blades, Δw is also a measure of the magnitude of w itself, and not only of a typical change. The magnitude of the terms in equation 2.51 are as below.

Equation:	$\dfrac{\partial u}{\partial x}$	$+$	$\dfrac{\partial w}{\partial z}$	$= 0$
Magnitude:	$\frac{\Delta u}{\lambda_x}$		$\frac{\Delta w}{\lambda_z}$	

From this we conclude that $\Delta w \sim \Delta u \lambda_z/\lambda_x$. We now make use of this when considering equation 2.50, which describes changes in w. As drainage occurs through both of the wires, there should be some position in the gap where w is zero. Hence, Δw is also a measure of the change of w in the z-direction. The magnitudes of the terms in the left hand side of equation 2.50 are consequently as follows.

Equation:	$u\dfrac{\partial w}{\partial x}$	$+$	$w\dfrac{\partial w}{\partial z}$	$= -\frac{1}{\rho}\dfrac{\partial p}{\partial z}$
Magnitude:	$U\frac{\Delta u}{\lambda_x}\left(\frac{\lambda_z}{\lambda_x}\right)$		$\Delta w\frac{\Delta u}{\lambda_x}$	

Clearly, if we assume that $\lambda_z/\lambda_x \ll 1$, the first term on the left hand side is of a much smaller magnitude than the pressure term in equation 2.49, which is of the order $U\Delta u/\lambda_x$. This assumption is a more severe restriction than the earlier

assumption that $(\lambda_z/\lambda_x)^2 \ll 1$, but it is reasonable due to the slenderness of the problem. The assumption also yields that $\Delta w \ll \Delta u$. Earlier in this section, the pressure pulses were predicted to be of the order 1 kPa. If $u \sim U$, the pulses would be of the same order as the dynamic pressure of the suspension. This is clearly not the case, and it is safe to conclude that $\Delta u < U$ and hence that $\Delta w \ll U$. It follows that the second term on the left hand side of equation 2.50 is of much smaller magnitude than the pressure term in equation 2.49 as well. Hence, in comparison with changes in the x-direction, the pressure variations in the z-direction are insignificant, which justifies that they are neglected.

Equation 2.52 is a one-dimensional equation relating the pressure and the velocity in the x-direction. As the velocity in the z-direction is of such small magnitude, we shall neglect it altogether and not make use of equation 2.50. The continuity equation 2.51 cannot be used in its present form either. By integrating it in the positive z-direction across the distance between the wires, one gets

$$w\Big(x, f(x)\Big) - w\Big(x, g(x)\Big) = -\frac{\partial}{\partial x}\int_{z=g(x)}^{z=f(x)} u(x)\,\mathrm{d}z = \\ = -\frac{\mathrm{d}}{\mathrm{d}x}\Big(u(x)\big(f(x) - g(x)\big)\Big)\,, \tag{2.53}$$

where $f(x)$ and $g(x)$ give the position of the two wires, and we have made use of the fact that u is independent of z. Henceforth, we shall refer to the fabric whose position corresponds to the largest z-value as the 'upper wire', and to the other as the 'lower wire'. Due to our assumptions of stationary flow and $(\lambda_z/\lambda_x)^2 \ll 1$, the velocity of the suspension in the z-direction at the upper wire equals the drainage velocity, given by equation 2.5. Hence

$$w(x, f) = \frac{p(x) - p_{e1}(x)}{R_1(x)}\,, \tag{2.54}$$

where the subscript 1 refer to the upper wire. Note that p_w in equation 2.5 have been replaced by p, since the pressure is independent of position in the z-direction. At the bottom wire (denoted by the subscript 2), the drainage is directed in the negative z-direction, and thus

$$w(x, g) = -\frac{p(x) - p_{e2}(x)}{R_2(x)}\,. \tag{2.55}$$

Combining the equations 2.53, 2.54 and 2.55, we obtain the following equation to replace 2.51,

$$\big[u(f-g)\big]_x = -p\left(\frac{1}{R_1} + \frac{1}{R_2}\right) + \frac{p_{e1}}{R_1} + \frac{p_{e2}}{R_2}\,. \tag{2.56}$$

2.4. The model

In section 2.2 we derived equations governing one of the wires and the flow of the suspension between the fabrics. They were subsequently simplified in section 2.3. We are now ready to write down a complete set of equations that describe the blade forming section. At x-positions where no blade is present, they are as follows, where the subscripts 1 and 2 refer to the upper and the lower wire, respectively.

$$R_{1x} = \frac{K}{U}\frac{p - p_{e1}}{R_1} \tag{2.57}$$

$$R_{2x} = \frac{K}{U}\frac{p - p_{e2}}{R_2} \tag{2.58}$$

$$[u(f-g)]_x = -p\left(\frac{1}{R_1} + \frac{1}{R_2}\right) + \frac{p_{e1}}{R_1} + \frac{p_{e2}}{R_2} \tag{2.59}$$

$$uu_x + \frac{1}{\rho}p_x = 0 \tag{2.60}$$

$$p - p_{e1} + T_1 f_{xx} = 0 \tag{2.61}$$

$$p - p_{e2} - T_2 g_{xx} = 0 \tag{2.62}$$

Equations 2.58 and 2.62 are related to the lower fabric. The first one is exactly analogous to equation 2.57, whereas equation 2.62 differs from 2.61 in that the sign of the pressure term is reversed, which is due to the pressure acting in the opposite direction on the lower wire. The functions p_{e1} and p_{e2} are the pressures prevailing on the exterior of the upper and lower fabric, respectively. Suction boxes are accounted for by specifying a low pressure outside of the wire passing the box.

At a blade, a slightly different system of equations is used. As there is no drainage through a fabric passing over a blade, $p_{ei} = p$ in the equations corresponding to that wire. Over the blade we must also drop the equation for the position of the contacting wire (i.e. equation 2.61 or 2.62). Instead, the position of the fabric is given by the blade surface.

The equations above are in dimensional form. We shall introduce non-dimensional quantities (denoted by $*$) as below.

$$\begin{array}{ll} p = \rho U^2 p^* & p_{ei} = \rho U^2 p_{ei}^* \quad i = 1,2 \\ u = U u^* & R_i = \frac{\rho U D}{h_0} R_i^* \quad i = 1,2 \\ f = h_0 f^* & g = h_0 g^* \\ x = D x^* & \end{array}$$

Here, h_0 is the distance between the wires far upstream of the blades, and D is some convenient length which, unless otherwise specified, will be taken as the length along the x-axis of the first blade. This is often a good indication of the reach in the machine direction of the pressure pulse generated by the blade. When the new variables are inserted into the equations 2.57 – 2.62 the result is as below. Note that the superscripted stars have been left out. For ease of notation we shall continue to do so, and adopt the convention that we always refer to dimensionless quantities unless we specify otherwise.

$$R_{1x} = \kappa \frac{p - p_{e1}}{R_1} \tag{2.63}$$

$$R_{2x} = \kappa \frac{p - p_{e2}}{R_2} \tag{2.64}$$

$$[u(f-g)]_x = -p\left(\frac{1}{R_1} + \frac{1}{R_2}\right) + \frac{p_{e1}}{R_1} + \frac{p_{e2}}{R_2} \tag{2.65}$$

$$uu_x + p_x = 0 \tag{2.66}$$

$$p - p_{e1} + \varepsilon_1 f_{xx} = 0 \tag{2.67}$$

$$p - p_{e2} - \varepsilon_2 g_{xx} = 0 \tag{2.68}$$

The following dimensionless groups have appeared,

$$\kappa = \frac{Kh_0^2}{\rho U D}\,, \tag{2.69}$$

$$\varepsilon_1 = \frac{T_1 h_0}{\rho U^2 D^2}\,, \tag{2.70}$$

$$\varepsilon_2 = \frac{T_2 h_0}{\rho U^2 D^2}\,. \tag{2.71}$$

As $\rho U^2 h_0$ is a measure of the inertial force of the suspension approaching the blades, and Th_0/D is a measure of the force exerted on the suspension as a result of the tension in the fabrics, we can define a Weber number for each wire as

$$We_i = \frac{\rho U^2 D}{T_i} \quad i = 1, 2\,. \tag{2.72}$$

The parameters ε_1 and ε_2 can consequently be regarded as the product of the inverse Weber number and a slenderness ratio for the problem,

$$\varepsilon_i = \frac{1}{We_i}\left(\frac{h_0}{D}\right) \quad i = 1, 2\,. \tag{2.73}$$

In order to solve the equations 2.63–2.68, conditions must be imposed on the solution. As we have some liberty of choice regarding which conditions to

specify, we shall defer this issue to chapter 3, where we discuss the details of the solution algorithm.

CHAPTER 3

Numerical algorithm

3.1. A module strategy

Before the full problem (as illustrated in figure 1.6) was solved, a test-problem of less complexity was considered. It consisted of two tensioned fabrics between which a liquid flows, like in figure 3.3(a). A robust numerical solver was developed for a partly integrated system of the governing equations (confer section 3.2.1 below). In order to obtain maximum flexibility, the model for the full problem was then made up of elementary modules resembling the initial test-problem. Each module acts like a black box with respect to its environment. Given certain parameters as input, it gives as output the evolution of the dependent variables of the model throughout its interior, as well as other key information. By adopting such an approach, structural changes of the full model, such as e.g. adding another blade, is easily undertaken.

Let us consider an assembly of n modules that together constitute a model of a certain blade forming section. Each module can be represented as in figure 3.1. The superscript i will subsequently be used to refer to the i^{th} module. Out

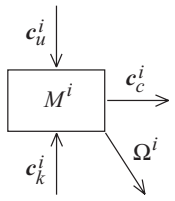

FIGURE 3.1. The i^{th} module (arbitrary type). $\boldsymbol{c}_k^i$ and $\boldsymbol{c}_u^i$ are vectors containing input parameters. $\boldsymbol{c}_c^i$ is a vector of parameters passed on to the next module. Ω^i is the evolution of the dependent variables throughout the module.

of the parameters necessary to solve the governing equations for the module M^i, certain are known from the full model and are grouped together in the vector $\boldsymbol{c}_k^i$. Others, denoted by $\boldsymbol{c}_u^i$, are not known a priori, and must be determined as part of the solution process. Apart from the evolution of the dependent variables throughout the module, symbolically given by Ω^i, the module also

delivers a group of parameters $\boldsymbol{c}_c^i$, based on Ω^i, that are used as input for the neighbouring module M^{i+1}. The unknown parameters for the whole assembly of modules can be put together in a vector $\boldsymbol{c}_u = (\boldsymbol{c}_u^1, \ldots, \boldsymbol{c}_u^n)$. Assume that we guess $\boldsymbol{c}_u$ and calculate the dependent variables throughout all modules. Most likely we did not manage to give the correct values for the components of $\boldsymbol{c}_u$, and the evolution of the dependent variables throughout the whole model will be unphysical. The real solution must fulfil certain matching criteria that ensures that the solution obtained in one module fits in a physically correct manner with the solutions from the neighbouring modules. For a well-posed problem, the number of such criteria equals the total number of unknown parameters. Let Δ_j be a quantitative measure of how well criterion j is fulfilled ($j = 1, \ldots, r$), the value zero corresponding to exact compliance. An outline of the trial procedure, from specifying the components of $\boldsymbol{c}_u$ to obtaining quantitative values for the degree of fulfilment of the different Δ_j, is given in figure 3.2. In the figure, Ω symbolises the evolution of the process variables obtained by combining the output of all the modules.

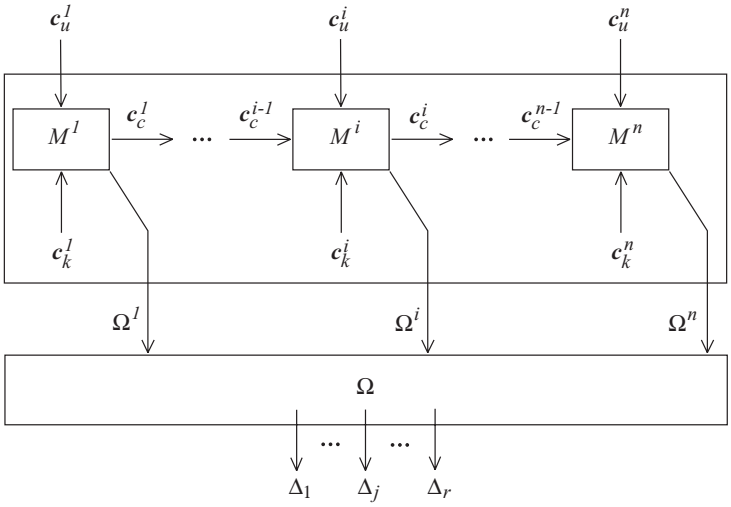

FIGURE 3.2. Outline of how the known and guessed parameters (the $\boldsymbol{c}_k^i$ and $\boldsymbol{c}_u^i$, respectively) result in a description Ω of how the process variables varies along the machine direction. Ω is then used to give quantitative values Δ_j of how well the solutions from the different modules complies with the matching criteria.

Now, assume that the Δ_j are continuous functions of the components of $\boldsymbol{c}_u$. The procedure described above can then be considered a continuous function Z, taking the vector $\boldsymbol{c}_u$ as input and yielding a vector $(\Delta_1, \ldots, \Delta_r)$ as output.

Solving for the dependent variables in the blade forming section, modelled by the assembly of modules, then turns into finding the roots of Z. Any algorithm for non-linear root-finding that does not demand explicit knowledge of the function is a candidate to perform this task. In the present study, both the Gauss-Newton and the (more robust) Levenberg-Marquardt methods have been used, neither showing any advantage over the other for the model at hand. Both of these methods are traditionally applied to non-linear least-squares problems. However, by using them to minimise the sum

$$S_\Delta = \sum_{j=1}^{r} \left[\Delta_j(\boldsymbol{c}_u)\right]^2 \ ,$$

they can also be employed to find the roots of Z. The main difference between the least-squares problem and the root-finding problem is that, for the former, the model-functions and hence also the function to minimise are known, whereas in our case we cannot give Z explicitly. Information about the components of the gradient of Z, which are necessary to implement the above methods, must therefore be generated numerically. Routines for employing these methods in the fashion described is conveniently provided in MATLAB, which is also the reason why they were chosen. Details about the methods can be found in e.g. Press *et al.* (1986). In each iteration, the Gauss-Newton method minimises a local quadratic approximation of S_Δ, in which the contributions of the second derivatives to the Hessian of S_Δ are neglected[1]. The Levenberg-Marquardt method is a blend of the steepest descent method and the Gauss-Newton method. The former is used far from the minimum, but as the extremum is approached, the Levenberg-Marquardt method turns into the latter in a continuous fashion.

3.2. The modules

By using the three basic types of modules schematically illustrated in figure 3.3, we can model any blade forming section of interest to us, including the application of suction. Since the system of equations required to analyse these 'fundamental modules' are different from each other, they constitute a suitable division of the full problem. In the following sections, we shall in turn consider each kind of fundamental module. In figure 3.3, we have also indicated what parameters are necessary to solve the systems of equations, i.e. the components of the vectors $\boldsymbol{c}_k$ and $\boldsymbol{c}_u$. Inside the i^{th} module, a local co-ordinate system $\tilde{x}$ is used, whose origin is located at the inlet. $\tilde{x}^i_{out}$ is the position of the outlet. The subscripts *in* and *out* refer to the inlet and the outlet respectively. Consequently, f^i_{in} means the position of the upper wire at the inlet, etc.

[1] It is hence an inverse-Hessian method, which is also how it is referred to in Press *et al.* (1986).

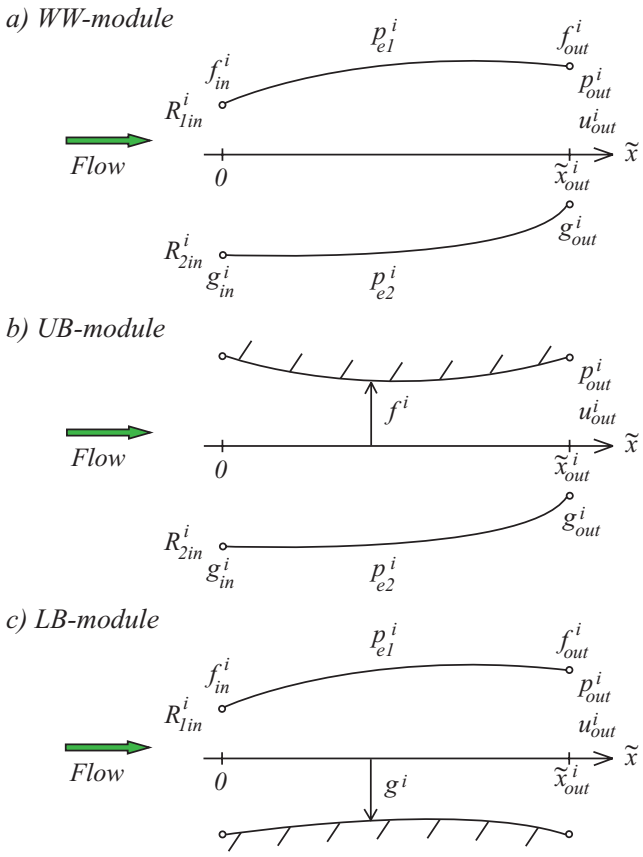

FIGURE 3.3. The fundamental modules, and the information that needs to be specified in order to calculate the dependent variables throughout the modules. $\tilde{x}$ is a local co-ordinate system. The subscripts *in* and *out* refer to the inlet and the outlet, respectively. Confer the text for an explanation of the rest of the notation.

In order to reduce the size of the vector $\boldsymbol{c}_u$ containing the unknown parameters, we shall in section 3.5 build 'composite modules' based on the fundamental modules. These will then be used in the model of the forming section.

3.2.1. *Modules of type WW – An upper and a lower wire*

Modules of type WW, outlined in figure 3.3(a), are used for parts of the forming section where no blades are present. Consequently, it consists of two permeable

wires between which the suspension flows, and it is described by equations 2.63 to 2.68.

Due to the non-linear nature of the governing equations, we have little hope that the dependent variables can be obtained by an analytical solution procedure, and we have to resort to numerical methods. Nevertheless, it is possible to partly integrate our system of equations analytically in order to reduce the number of equations. In what follows, C_l^i denote integration constants ($l = 1, \dots$). Equation 2.66 is easily integrated into

$$p + \frac{u^2}{2} = C_1^i \,. \tag{3.1}$$

Subtracting equation 2.68 from equation 2.67, one finds

$$\varepsilon_1 f_{xx} + \varepsilon_2 g_{xx} = p_{e1}^i - p_{e2}^i \,. \tag{3.2}$$

Introducing

$$k = \frac{\varepsilon_1 f + \varepsilon_2 g}{\varepsilon_1 + \varepsilon_2} \,, \tag{3.3}$$

and integrating equation 3.2 twice, it follows that

$$k = \int_0^{\tilde{x}} \int_0^{\tilde{x}'} \frac{p_{e1}^i(\tilde{x}'') - p_{e2}^i(\tilde{x}'')}{\varepsilon_1 + \varepsilon_2} \, \mathrm{d}\tilde{x}'' \, \mathrm{d}\tilde{x}' + C_2^i \tilde{x} + C_3^i \,. \tag{3.4}$$

Note that, if $\varepsilon_1 = \varepsilon_2$, then k is the position of the centreline between the two wires. We shall let $F^i(\tilde{x})$ denote the known function defined by the double integral in equation 3.4. Now, by combining equation 2.67 and 2.68, we obtain the following equation for the distance between the fabrics,

$$h_{xx} + \frac{\varepsilon_1 + \varepsilon_2}{\varepsilon_1 \varepsilon_2} p = \frac{p_{e1}^i}{\varepsilon_1} + \frac{p_{e2}^i}{\varepsilon_2} \,, \tag{3.5}$$

where $h = f - g$. By combining equations 2.63, 2.64 and 2.65, and integrating once, it is found that

$$uh = -\frac{R_1 + R_2}{\kappa} + C_4^i \,. \tag{3.6}$$

Using equation 2.63 to eliminate p in equation 3.5, and then integrating, yields

$$\frac{R_1^2}{2} + \kappa \frac{\varepsilon_1 \varepsilon_2}{\varepsilon_1 + \varepsilon_2} h_x = -\kappa \frac{\varepsilon_1}{\varepsilon_1 + \varepsilon_2} \int_0^{\tilde{x}} \left(p_{e1}^i(\tilde{x'}) - p_{e2}^i(\tilde{x'}) \right) \mathrm{d}\tilde{x}' + C_5^i \,. \tag{3.7}$$

Let $G^i(\tilde{x})$ denote the known function defined by the integral on the right hand side of equation 3.7. The same procedure, but using equation 2.64 instead of 2.63 to eliminate the pressure, yields

$$\frac{R_2^2}{2} + \kappa \frac{\varepsilon_1 \varepsilon_2}{\varepsilon_1 + \varepsilon_2} h_x = \kappa \frac{\varepsilon_2}{\varepsilon_1 + \varepsilon_2} G^i(\tilde{x}) + C_6^i \,. \tag{3.8}$$

By adding equation 3.7 and equation 3.8, it follows that

$$R_1^2 + R_2^2 = 2\left(\frac{\kappa}{\varepsilon_1+\varepsilon_2}\Big((\varepsilon_2-\varepsilon_1)G^i(\tilde{x}) - 2\varepsilon_1\varepsilon_2 h_x\Big) + C_5^i + C_6^i\right). \tag{3.9}$$

From the difference between the equations 3.7 and 3.8, one finds

$$R_1 - R_2 = \frac{2}{R_1+R_2}\Big(C_5^i - C_6^i - \kappa G^i(\tilde{x})\Big). \tag{3.10}$$

If the denominator on the right hand side of equation 3.10 were to take the value zero somewhere in the solution domain, the analysis would no longer be valid. However, as physical drainage resistances are always finite and positive, this is of little concern to us. Noting that

$$R_1^2 + R_2^2 = \frac{(R_1+R_2)^2}{2} + \frac{(R_1-R_2)^2}{2},$$

we can combine the equations 3.6, 3.9 and 3.10 into an expression relating h and u,

$$\kappa^2(C_4^i - uh)^2\Bigg(\kappa^2(C_4^i-uh)^2 + 8\kappa\frac{\varepsilon_1\varepsilon_2}{\varepsilon_1+\varepsilon_2}h_x + \\ +4\Big(\kappa\frac{\varepsilon_1-\varepsilon_2}{\varepsilon_1+\varepsilon_2}G^i(\tilde{x}) - C_5^i - C_6^i\Big)\Bigg) + 4\Big(\kappa G^i(\tilde{x}) + C_5^i - C_6^i\Big)^2 = 0. \tag{3.11}$$

Another equation containing only h and u is readily obtained by using equation 3.1 to eliminate p from equation 3.5,

$$h_{xx} + \frac{\varepsilon_1+\varepsilon_2}{\varepsilon_1\varepsilon_2}\left(C_1^i - \frac{u^2}{2}\right) - \frac{p_{e1}^i}{\varepsilon_1} - \frac{p_{e2}^i}{\varepsilon_2} = 0. \tag{3.12}$$

It would be easy to use this equation to eliminate the velocity from equation 3.11, hence obtaining one single differential equation for h. Nevertheless, we shall refrain from doing so. Albeit a rather complex appearance, the system consisting of equations 3.11 and 3.12 has the nice feature that the highest derivative, i.e. h_{xx}, appears linearly. This would be lost if we were to eliminate u. The other dependent variables are easily expressed in terms of u, h and k. For the positions of the wires, we have

$$f = k + \frac{\varepsilon_2}{\varepsilon_1+\varepsilon_2}h \quad \text{and} \quad g = k - \frac{\varepsilon_1}{\varepsilon_1+\varepsilon_2}h. \tag{3.13}$$

The pressure is directly given by equation 3.1, and the drainage resistances are obtained by combining equations 3.6 and 3.10,

$$R_{1,2} = \frac{\kappa}{2}(C_4^i - uh) \pm \frac{C_5^i - C_6^i - \kappa G^i(\tilde{x})}{\kappa(C_4^i - uh)}. \tag{3.14}$$

The following boundary conditions are specified in order to determine the integration constants C_1^i–C_6^i:

- The position of the upper wire at the inlet and the outlet, f^i_{in} and f^i_{out}, respectively.
- The position of the lower wire at the inlet and the outlet, g^i_{in} and g^i_{out}, respectively.
- The drainage resistances at the inlet for the upper and the lower wire, R^i_{1in} and R^i_{2in}, respectively.
- The pressure at the outlet, p^i_{out}.
- The velocity at the outlet, u^i_{out}.

Other choices of conditions are possible. To reduce the size of the vector of unknown parameters, $\boldsymbol{c}_u$, it would be preferable to specify the conditions on R_1 and R_2 at the same position as the conditions on p and u. Therefore, it was considered to specify all these variables at the inlet. It turns out, however, that if the module extends towards infinity in the upstream direction, p always tends asymptotically to the pressure of the surrounding atmosphere when the upstream end is approached, regardless of what is specified at the outlet of the module. The atmospheric pressure will subsequently be set to zero, without loss of generality. In the same way, u always tends to 1 at the far upstream end. Consequently, specifying the physically correct conditions $p = 0$ and $u = 1$ at the upstream end of an infinitely long module does not introduce any information into the problem. As infinity cannot be represented numerically, it is replaced by a very large value. Due to this, the numerical algorithm will find a solution anyway, albeit erroneous. This can be seen by comparing the numerical solution with an analytical solution to a linearised version of the equations (such a comparison is done in order to verify the algorithm in section 3.7). As one sometimes needs an infinitely long WW-module (e.g. at the upstream end of the model domain), the boundary conditions on R_1, R_2, p and u were moved to the downstream end to avoid this problem. This yield correct solutions. However, when several modules were used together to form a larger problem, it turned out that the overall solution algorithm managed to find the unknown parameters in $\boldsymbol{c}_u$ with less iterations if the drainage resistances were specified at the upstream end. This advantage was found to outweigh the larger size of $\boldsymbol{c}_u$.

From the conditions above follows that

$$C^i_1 = p^i_{out} + \frac{{u^i_{out}}^2}{2}\,, \tag{3.15}$$

$$C^i_2 = \frac{1}{\tilde{x}^i_{out}} \left(\frac{\varepsilon_1(f^i_{out} - f^i_{in}) + \varepsilon_2(g^i_{out} - g^i_{in})}{\varepsilon_1 + \varepsilon_2} - F^i(\tilde{x}^i_{out}) \right), \tag{3.16}$$

$$C^i_3 = \frac{\varepsilon_1 f^i_{in} + \varepsilon_2 g^i_{in}}{\varepsilon_1 + \varepsilon_2}\,. \tag{3.17}$$

The constants C^i_4, C^i_5 and C^i_6 must be determined as part of the solution process. As h and u are known at the outlet, the discretised versions of the

equations 3.11 and 3.12 need not be applied at $\tilde{x}^i_{out}$. Instead, the discretisation of equation 3.11 at the outlet is used to determine C^i_4. Discretisations of the equations 3.7 and 3.8 at the inlet are used, together with R^i_{1in} and R^i_{2in}, to determine C^i_5 and C^i_6, respectively. The details are given in section 3.4.

3.2.2. *Modules of type UB and LB – A blade and a wire*

Modules of type UB (see figure 3.3(b)) consist of an upper fabric to which a blade is applied, and an opposing permeable free wire. Correspondingly, in a module of type LB (illustrated in figure 3.3(c)) the blade is applied to the lower fabric, whereas the upper fabric is free. As explained in chapter 2, when a blade is applied, the fabric is assumed to follow the surface of the blade, which corresponds to $f = f^i(\tilde{x})$ or $g = g^i(\tilde{x})$ being given. If the wire is in perfect contact with the blade, no drainage occurs. Consequently, the drainage resistance of a wire will not change as long as it is in contact with a blade, but remain at the same level it was at the leading edge of the blade.

For an UB-module, the equations 2.63–2.68 reduce to

$$R_{2x} = \kappa \frac{p - p^i_{e2}}{R_2}\,, \tag{3.18}$$

$$[uh]_x = -\frac{p - p^i_{e2}}{R_2}\,, \tag{3.19}$$

$$uu_x + p_x = 0\,, \tag{3.20}$$

$$p - p^i_{e2} - \varepsilon_2 g_{xx} = 0\,. \tag{3.21}$$

Like the equations governing the WW-module, the equations 3.18–3.21 can be integrated into a system for h and u,

$$\kappa^2(C^i_4 - uh)^2 + 2\kappa\varepsilon_2(h_x - f^i_x) - C^i_6 = 0\,, \tag{3.22}$$

$$h_{xx} + \frac{1}{\varepsilon_2}\left(C^i_1 - \frac{u^2}{2}\right) - \frac{p^i_{e2}}{\varepsilon_2} - f^i_{xx} = 0\,, \tag{3.23}$$

whose solution is then used to obtain the other dependent variables through $p = C^i_1 - u^2/2$, $g = f^i - h$ and $R_2 = \kappa(C^i_4 - uh)$. In order to solve equation 3.22 and 3.23, and to determine the integration constants, one must specify the following:

- The position of the blade surface, f^i.
- The position of the free fabric at the inlet and the outlet, g^i_{in} and g^i_{out}.
- The drainage resistance of the free wire at the inlet, R^i_{2in}.
- The pressure at the outlet, p^i_{out}.
- The velocity at the outlet, u^i_{out}.

Having done this, C_1^i can be determined directly. C_4^i and C_6^i must be determined together with the dependent variables in the same way as for a WW-module.

A module of type LB is treated in a completely analogous fashion.

3.3. The matching criteria

We shall now define the criteria Δ_j, introduced in section 3.1, that will enable us to match the solutions from different modules with each other. Apart from criteria of the kind derived in this section, modelling considerations might demand that special Δ_j are introduced in order to deal with particular features such as e.g. loadable blades. Examples of this can be found among the criteria introduced in section 3.6 for the forming zone considered in this study.

Assume that an interface between two modules is located at x_b. For obvious reasons, the position of the wires must be continuous across the interface, but what about the other variables? Let x_b^- and x_b^+ denote the upstream and downstream side of the interface, respectively. By integrating equation 2.66 across the interface, we find

$$\left[\frac{u^2}{2}\right]_{x_b^-}^{x_b^+} + [p]_{x_b^-}^{x_b^+} = 0\,. \tag{3.24}$$

Hence, if there is a discontinuity in e.g. p, then there must be one in u as well, and vice versa. Let us assume a discontinuity in the pressure. The consequent discontinuity in the velocity, and the fact that the suspension is incompressible, would demand either a discontinuity in h, or that a finite volume of liquid is expelled from, or sucked into, the gap between the wires at the position x_b. The former alternative has already been ruled out, and the latter would require infinite dewatering velocities (positive or negative). The conclusion is that both the pressure and the velocity are continuous across the interface. From the necessity that the dewatering velocities are finite also follows that the drainage resistances are continuous.

Our choice of modules implies that x_b corresponds to the position of a blade edge. Without loss of generality we assume that it is the edge of a blade applied to the lower wire. Equation 2.67 is then valid across the interface, and an integration like the one above yields

$$[f_x]_{x_b^-}^{x_b^+} = 0\,, \tag{3.25}$$

which tells us that the derivative of the position of a free wire must be continuous. The equation for the lower fabric is however not valid at the point x_b. This is due to the edge acting as a point force Q_b on the fabric, a possibility that was not included in the derivation of equation 2.68. In the following form,

however, it is valid,

$$p - p_{e2} - \varepsilon_2 g_{xx} - Q_b \delta(x_b) = 0\,, \tag{3.26}$$

where $\delta(x)$ is a Dirac-function. Integration across the interface yields

$$[g_x]_{x_b^-}^{x_b^+} = -\frac{Q_b}{\varepsilon_2}\,, \tag{3.27}$$

and a discontinuity is hence permissible as a result of us having neglected the bending stiffness of the wires.

The requirements of continuity of the dependent variables, and of the derivative of the position of a free fabric, are all candidates for matching criteria Δ_j at an interface. Nevertheless, not all of them will be needed at each interface. For example, at each iteration performed by the algorithm that is employed to find the root to Z, the module furthest downstream will be solved first (see section 3.6). The solution obtained for this module will, owing to the continuity of the variables, give the boundary conditions on p and u at the outlet of the next module upstream. Hence there is no need to formulate criteria Δ_j in order to match these variables at the interface. Other criteria may, depending on the circumstances, also be naturally fulfilled.

It is easy to quantify the degree of compliance of the different criteria. If some quantity ϕ must be continuous across the interface at x_b, a natural measure of the discrepancy is $\phi(x_b^+) - \phi(x_b^-)$.

Continuity criteria on the dependent variables themselves are straightforward to employ. When derivatives are involved, as in e.g. the criterion 3.25, the derivatives on both sides of the interface must be calculated numerically from values of the variable at the mesh points introduced in section 3.4. This is done by using finite difference approximations of the derivative. Downstream of the interface, a discretisation analogous to 3.37 is used, upstream a discretisation analogous to 3.38.

3.4. A finite difference solver for the modules

In this section, we discuss how to numerically solve the equations for the WW-module. The procedures for the other module types are analogous.

Let us discretise the $\tilde{x}$-axis of the module by replacing it by a set of discrete mesh points $\tilde{x}_l$ $(l = 1, \ldots, N)$, where $\tilde{x}_1$ corresponds to the inlet and $\tilde{x}_N$ to the outlet. The discretisation, which is illustrated in figure 3.4, is such that the distance between the points equals the constant $\Delta\tilde{x}$. At the mesh point $\tilde{x}_l$, h and u take the values h_l and u_l, respectively, and our ambition is to determine those values as well as the constants C_4^i, C_5^i and C_6^i. The unknowns can be grouped together in a column vector $\boldsymbol{q}$,

$$\boldsymbol{q} = (h_1, u_1, \ldots, h_l, u_l, \ldots, h_N, u_N, C_4^i, C_5^i, C_6^i)^T\,. \tag{3.28}$$

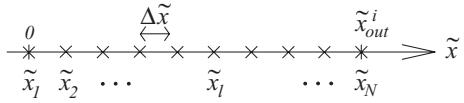

FIGURE 3.4. The discretisation of the $\tilde{x}$-axis in the i^{th} module. The positions of the mesh points $\tilde{x}_l$ $(l = 1, \ldots, N)$ are indicated by $\times$.

The boundary conditions immediately yield the trivial equations

$$h_1 = f^i_{in} - g^i_{in}\,, \tag{3.29}$$

$$h_N = f^i_{out} - g^i_{out}\,, \tag{3.30}$$

$$u_N = u^i_{out}\,. \tag{3.31}$$

To obtain algebraic equations for the other components in $\boldsymbol{q}$, we shall replace the equations 3.11 and 3.12 by second order finite difference approximations. At the mesh points $\tilde{x}_l$, $l = 2, \ldots, N-1$, this is done by making the following substitutions in the two equations,

$$\tilde{x} \;\rightarrow\; \tilde{x}_l\,, \tag{3.32}$$

$$u \;\rightarrow\; u_l\,, \tag{3.33}$$

$$h \;\rightarrow\; h_l\,, \tag{3.34}$$

$$h_x \;\rightarrow\; \frac{h_{l+1} - h_{l-1}}{2\Delta\tilde{x}}\,, \tag{3.35}$$

$$h_{xx} \;\rightarrow\; \frac{h_{l+1} - 2h_l + h_{l-1}}{\Delta\tilde{x}^2}\,. \tag{3.36}$$

The truncation errors in the discretisations of h_x and h_{xx} are $\Delta\tilde{x}^2 h_{xxx}/6$ and $\Delta\tilde{x}^2 h_{xxxx}/12$, respectively. The resulting algebraic equations can be considered related to h_l and u_l for $l = 2, \ldots, N-1$.

Equations for u_1 and C^i_4 are obtained by discretising equation 3.11 at the mesh points $\tilde{x}_1$ and $\tilde{x}_N$. The same substitutions as above are used, with the exception of the one for h_x. The derivative is at the inlet replaced by

$$h_x \;\rightarrow\; \frac{-3h_1 + 4h_2 - h_3}{2\Delta\tilde{x}}\,, \tag{3.37}$$

and at the outlet by

$$h_x \;\rightarrow\; \frac{3h_N - 4h_{N-1} + h_{N-2}}{2\Delta\tilde{x}}\,. \tag{3.38}$$

The truncation error is in both cases $-\Delta\tilde{x}^2 h_{xxx}/3$.

The equations used to determine C^i_5 and C^i_6 are the discretised versions of the equations 3.7 and 3.8 at the inlet. They are obtained through the following

substitutions,

$$\tilde{x} \rightarrow \tilde{x}_1\,, \tag{3.39}$$

$$R_1 \rightarrow R^i_{1in}\,, \tag{3.40}$$

$$R_2 \rightarrow R^i_{2in}\,, \tag{3.41}$$

$$h_x \rightarrow \frac{-3h_1 + 4h_2 - h_3}{2\Delta\tilde{x}}\,. \tag{3.42}$$

We now have as many equations as unknowns, and together they form a non-linear algebraic equation system $\boldsymbol{\sigma}(\boldsymbol{q}) = 0$. Since it is straightforward to explicitly form the (sparse) Jacobian matrix $\boldsymbol{J}_{\boldsymbol{\sigma}}$ of $\boldsymbol{\sigma}(\boldsymbol{q})$, we solve the system by the damped Newton method. The algorithm can be outlined in the following way:

i) $\boldsymbol{q}_0$ = initial guess
ii) until stopping criterion fulfilled
Solve $\boldsymbol{J}_{\boldsymbol{\sigma}}(\boldsymbol{q}_k)\boldsymbol{s}_k = -\boldsymbol{\sigma}(\boldsymbol{q}_k) \;\Rightarrow\; \boldsymbol{s}_k$
$\boldsymbol{q}_{k+1} = \boldsymbol{q}_k + \beta\boldsymbol{s}_k$
end

We are interested in finding a good approximation to the root of $\boldsymbol{\sigma}(\boldsymbol{q})$, rather than to minimise the residual. For this reason, the iterations are carried out as long as the ratio between the norm of the correction and the norm of the old approximate solution, i.e. $\Delta q_{rel} = \|\boldsymbol{s}_k\|/\|\boldsymbol{q}_k\|$, is larger than a chosen tolerance. β is the damping factor. At the first iteration it is set to 1, and it is kept at that value as long as Δq_{rel} decreases monotonously. If, however, this quantity increases at some point, β is reduced by some factor (typically 10). The algorithm then returns to the approximate solution obtained before the faulty update, and performs iterations with the lower β. If this is done successfully a certain number of iterations, then β is augmented by the same factor again. If not, β is further reduced, until the monotonously decreasing behaviour of Δq_{rel} is re-established. At each damping level, a certain number of successive iterations must be succesful before β is augmented. The upper limit of β is 1. Naturally, the algorithm may fail to converge when started too far from the solution. Nevertheless it has proved robust when employed to find the roots of the different $\boldsymbol{\sigma}(\boldsymbol{q})$ encountered so far. Even when quite naive choices of $\boldsymbol{q}_0$ are made, a solution is obtained.

The linear equation system appearing in step *ii* of the algorithm is solved through LU-factorisation with partial pivoting, by a method that takes into account the sparse structure of the coefficient matrix. Prior to the factorisation, the columns of $\boldsymbol{J}_{\boldsymbol{\sigma}}$ is permuted through minimum degree ordering, in order to yield sparser factors. The algorithms employed by MATLAB to perform these tasks are described by Gilbert *et al.* (1992).

3.5. Composite modules

The more modules that are involved in the complete model of the forming section, the larger the size of the vector $\boldsymbol{c}_u$ that contains the parameters that are a priori unknown to us. At each interface between modules, new unknown parameters are introduced. Although causing no problems so far, this might potentially be a problem for models involving many modules, due to the increased demand on the algorithm in charge of determining the root of Z.

We note that a UB-module, or a LB-module, is always preceded on the upstream side by a WW-module. Consequently, we can reduce the total number of interfaces between modules, without loss of flexibility, by constructing modules which consist of an upstream part with an upper and a lower fabric, and a downstream part with a fabric on one side and a blade on the opposing side. This is easily done by employing the fundamental modules already developed. A module obtained by combining an upstream WW-module with a downstream UB-module will be termed a WUB-module. The corresponding composite module obtained by using a LB-module instead of the UB-module will be referred to as a WLB-module. In what follows, we present only the WUB-module, as the WLB-module is derived in the same way.

Let the i^{th} module be a downstream UB-module, and the $(i+1)^{\text{th}}$ module be an upstream WW-module[2]. Denote the vectors containing the unknowns in the two modules $\boldsymbol{q}^i$ and $\boldsymbol{q}^{i+1}$, respectively (see section 3.4 for their components). At the outlet of the WW-module, we should specify f_{out}^{i+1}, g_{out}^{i+1}, p_{out}^{i+1} and u_{out}^{i+1}, whereas, at the inlet of the UB-module, we should give g_{in}^{i} and R_{2in}^{i}. When the modules are combined into a WUB-module, these become "internal" parameters, and should no longer be part of the input to the composite module. Instead, they have become new unknowns. The purpose of specifying p_{out}^{i+1} is to introduce information to determine the constant C_1^{i+1}. However, as p and u are continuous across the interface between the modules, it follows that $C_1^{i+1} = C_1^i$. Thus we can remove p_{out}^{i+1} from the list of unknown internal parameters that has to be determined iteratively. The vector $\boldsymbol{q}_c$ containing all the unknowns for the WUB-module hence becomes

$$\boldsymbol{q}_c = (\boldsymbol{q}^{i+1}, f_N^{i+1}, g_N^{i+1}, u_N^{i+1}, g_1^i, {R_2}_1^i, \boldsymbol{q}^i)^T \,,$$

where integer subscripts on dependent variables refer to mesh points in the module indicated by the superscript.

By formulating equations through which the new unknowns can be obtained, we can form a system $\boldsymbol{\sigma}_c(\boldsymbol{q}_c) = 0$ consisting of these equations, together with the algebraic equations for the i^{th} and the $(i+1)^{\text{th}}$ module. Solving the system by the algorithm introduced in section 3.4 yields $\boldsymbol{q}_c$.

[2]The module numbering starts at the downstream end of the full model, since this is the order in which they are solved for the dependent variables. See section 3.6.

The equations below follow immediately from continuity,

$$f_N^{i+1} = f^i(0)\,, \tag{3.43}$$

$$g_N^{i+1} = g_1^i\,, \tag{3.44}$$

$$u_N^{i+1} = u_1^i\,, \tag{3.45}$$

where $f^i(\tilde{x})$ is the position of the surface of the blade. It remains to derive equations for g_1^i and ${R_2}_1^i$. Recalling the relation between g, k and h given by equation 3.13, the condition that g_x should be continuous across the interface between the modules turns into

$$\left[k_x - \frac{\varepsilon_1}{\varepsilon_1+\varepsilon_2}h_x\right]_{x_b^-}^{x_b^+} = 0\,. \tag{3.46}$$

Here, like in section 3.3, it has been assumed that the interface is located at x_b, and that $-$ and $+$ refer to the upstream and downstream side, respectively. Since

$$k_x = \frac{G^i(\tilde{x})}{\varepsilon_1+\varepsilon_2} + C_2^i\,, \tag{3.47}$$

the condition 3.46 can be rewritten as

$$-\varepsilon_1\Big(h_x(x_b^+) - h_x(x_b^-)\Big) + (\varepsilon_1+\varepsilon_2)(C_2^i - C_2^{i+1}) + \\ +G^i(0) - G^{i+1}(\tilde{x}_{out}^{i+1}) = 0\,. \tag{3.48}$$

An equation for g_1^i is obtained by discretising the equation above and inserting $h_1^i = f^i(0) - g_1^i$. By discretising equation 3.8 at x_b^-, and inserting ${R_2}_N^{i+1} = {R_2}_1^i$, the result will serve as an equation for ${R_2}_1^i$. To discretise $h_x(x_b^+)$, the substitution 3.37 is used, and, to discretise $h_x(x_b^-)$, the substitution 3.38.

If necessary, one could of course construct composite modules containing more than two fundamental modules in exactly the same way as above. Even a single algebraic equation system for the full problem can be obtained, making the root-finding algorithm discussed in section 3.1 redundant.

3.6. The considered forming section

Using the modules developed in this chapter, the forming section in figure 1.6 can be divided into four modules, as illustrated in figure 3.5. Note that the problem domain extends an infinite distance upstream and downstream of the blades. Infinity must, of course, numerically be replaced by a (sufficiently) large number. In the figure are also indicated what parameters are specified at the outset of the solution procedure, including the force per unit width Q by which the middle blade is applied to the fabric. Q is non-dimensionalised by the wire tension in the lower fabric. The numbering of the modules (the encircled integers) starts at the downstream end of the section. The position of

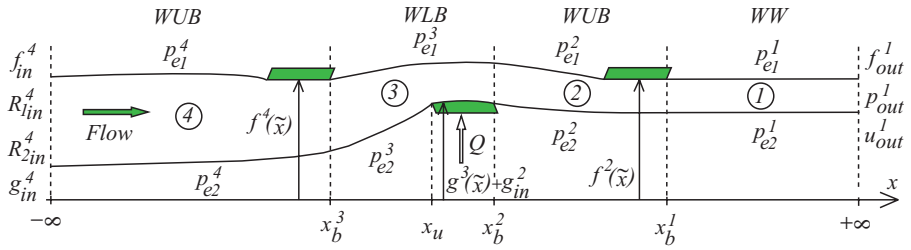

FIGURE 3.5. The division of the forming section into modules. Confer the text for an explanation of the notation.

the three internal interfaces between modules are denoted x_b^1, x_b^2 and x_b^3. The upstream edge of the middle blade is denoted x_u. The only external pressure functions not identically zero (corresponding to pressures different from that of the atmosphere) are p_{e1}^2 and p_{e1}^3. For them, we have $p_{e1}^2 = p_{e1}^3 = p_v$, where p_v is the pressure in the vacuum box between the upper blades (p_v is a a negative constant).

The parameters that are not known a priori, and that are not supplied by a neighbouring module during the calculations following the choice of a trial $\boldsymbol{c}_u$, are the following (note that they constitute the components of $\boldsymbol{c}_u$):

Module 1:	R_{1in}^1, R_{2in}^1 g_{in}^1, g_{out}^1
Module 2:	R_{1in}^2, R_{2in}^2 f_{in}^2, g_{in}^2
Module 3:	R_{1in}^3, R_{2in}^3 g_{in}^3

They are determined by requiring that the quantities Δ_j below, which are functions of $\boldsymbol{c}_u$, are zero:

$$\Delta_1 = [R_1]_{x_b^{1-}}^{x_b^{1+}} \qquad \Delta_2 = [R_2]_{x_b^{1-}}^{x_b^{1+}}$$

$$\Delta_3 = [g_x]_{x_b^{1-}}^{x_b^{1+}} \qquad \Delta_4 = h_x(+\infty)$$

$$\Delta_5 = [R_1]_{x_b^{2-}}^{x_b^{2+}} \qquad \Delta_6 = [R_2]_{x_b^{2-}}^{x_b^{2+}}$$

$$\Delta_7 = [f_x]_{x_b^{2-}}^{x_b^{2+}} \qquad \Delta_8 = g_x(x_u^-) - g_x(x_b^{2+}) - \tfrac{QD}{h_0}$$

$$\Delta_9 = [R_1]_{x_b^{3-}}^{x_b^{3+}} \qquad \Delta_{10} = [R_2]_{x_b^{3-}}^{x_b^{3+}}$$

$$\Delta_{11} = [g_x]_{x_b^{3-}}^{x_b^{3+}}$$

We recall that $-$ and $+$ refer to the upstream and downstream side, respectively. Criterion Δ_4 corresponds to the condition that the fabrics are parallel at downstream infinity, and the quantity Δ_8 is necessary to determine the position of the loadable blade. It is derived by assuming that the blade force is balanced

by the tension in the fabric. The pressure takes no part in the balance, since there is no pressure drop across the wire when no dewatering takes place.

The middle blade in figure 3.5 has a slightly curved shape, hence symbolically indicating that the present study has not been limited to flat blades. If blades of large curvatures are employed, the wires do not necessarily stay in contact with the blades along their full length, which was one of the assumptions made in chapter 2. In situations where the contact between the wire and the "physical" blade is unnatural, the extent of the "model" blade in the upstream or downstream direction (or both) is introduced as an additional unknown parameter in the vector $\boldsymbol{c}_u$. The new parameter(s) is then determined by requiring that the slope of the wire is tangential to the blade surface at the leading or trailing edge of the blade (or both). Thus, in a way, the algorithm determines how much of the "physical" blade would have to be cut off, if the slope of the wire was to equal that of the blade at the leading and/or trailing edge. The need to introduce the extension of the blade in the upstream or downstream direction as an unknown is easily recognised by considering the change in the slope of the contacting wire at the upstream or downstream edge of the blade. Physically, the wire must either be tangential to the blade surface at the point of contact, or be wrapped over the edge of the blade. Consequently, at a blade edge x_b, the slope of the wires must fulfil the following conditions in order for the contact with the blade not to be abnormal:

$$[f_x]_{x_b^-}^{x_b^+} \geq 0$$

$$[g_x]_{x_b^-}^{x_b^+} \leq 0$$

If these criteria are violated, the wire will first (or last) contact the blade at some point downstream (or upstream) of the edge, and the position of the edge of the "model" blade must be introduced as an unknown.

The first step of the solution process is to provide the algorithm in charge of determining the root of Z (see section 3.1) with an initial guess for $\boldsymbol{c}_u$. This guess is then iteratively improved till all $|\Delta_j|$ are smaller than a chosen tolerance. During the solution process, the algorithm calculates $Z(\boldsymbol{c}_u)$ several times. Each time, all the modules are solved, starting with the module at the downstream end of the section, i.e. module 1 in figure 3.5. The necessary parameters that are not a priori known are taken from the input $\boldsymbol{c}_u$. The solution obtained for module 1 then supplies the pressure and the velocity at the downstream end of module 2, which is calculated next, again taking the unknown parameters from $\boldsymbol{c}_u$. The modules 3 and 4 are subsequently calculated in the same way. Once all the modules have been solved, the quantities Δ_1–Δ_{11} are calculated, which constitute the output from Z. The evolution of the dependent variables throughout the forming section obtained during the final iteration constitutes the solution.

Although finding the solution implies calculating each module several times, the time required to obtain a converged solution when the above algorithm is implemented in MATLAB on an ordinary desktop computer, is of the order 1 minute for a reasonably good initial guess. Apart from increased flexibility, an advantage of the module approach is that solving only one module at a time requires less computer memory. If speed, and not computer memory, is an issue, all four modules can be solved simultaneously as described in section 3.5.

3.7. Verification

Prior to employing the algorithm presented in this chapter, we shall verify that it behaves in a correct manner, and that it has been correctly implemented. This includes both checking numerical characteristics, such as grid independence and convergence rate, as well as certifying that the output is in reasonable accordance with physical reality. When considering numerical properties, we can limit our attention to the variables h and u, as they are the ones we calculate numerically.

In order to confirm that grid independence can be achieved, the dependent variables were calculated throughout a forming section like the one in figure 3.5. Several different calculations were carried out, each with a different number of mesh points. The results, as well as the details of the input parameters, are presented in figure 3.6. The positions of the blade edges are indicated by $\triangle$ in the figure. Clearly grid independence has been achieved when Δx (non-dimensionalised with the length of the blade in the machine direction, which is also called the blade 'width') is 0.025, which corresponds to 40 mesh points along each blade. This is a better indication of the coarseness of the mesh than the total number of points, as the pressure pulses, which is driving the changes in the other variables, usually extends a couple of blade widths upstream of the blade. Apparently, grid independence is achieved earlier for h than for u, which is to be expected since h is in a way an integrated quantity (its value is related to the integral of the dewatering velocities along the machine direction), and as such rather insensitive. Indeed, one cannot see the individual curves in figure 3.6(a).

Calculations with different number of mesh points were also used to calculate the convergence rate of the implemented algorithm. The results are presented in figure 3.7. The input parameters were those given in the caption of figure 3.6. A calculation on a very fine grid, for which Δx divided by the blade width was 0.003125, was taken as an estimate of the exact solution. The quantities considered were the distance between the wires far downstream of the blades, and the minimum value of the velocity in the forming section. The latter was determined by fitting a 4^{th} order polynomial to the data around the node yielding the lowest u, and then determining the minimum of that polynomial. By inspection of figure 3.7, we conclude that the convergence rate

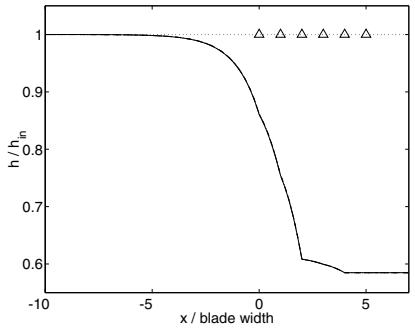

(a) Gap size.

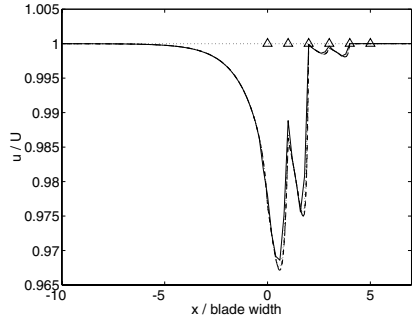

(b) Velocity.

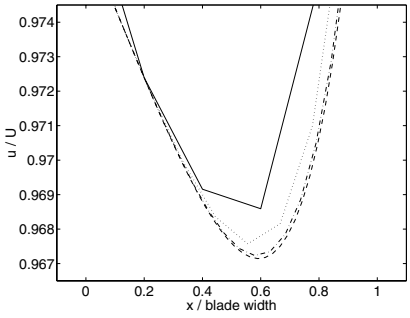

(c) Velocity, close up.

FIGURE 3.6. Grid independence. In all the figures: (—) Δx/blade width = 0.2. (· · ·) Δx/blade width = 0.1. (- · -) Δx/blade width = 0.05. (- - -) Δx/blade width = 0.025. Flat blades, width 10 mm. Blade spacing 10 mm. Blade force 450 N/m. Suction pressure -1 kPa. Wire speed 25 m/s. Wire tensions 11 kN/m. Initial drainage resistances 34 kNs/m^3. Drainage coefficient 9.0×10^6 kg/(m^3 s). Density 1000 kg/m^3.

is quadratic, as it should be given the second order discretisation introduced previously in this chapter.

Zhao & Kerekes (1995) undertook a one-dimensional linear analysis of two wires that were wrapped over a thin blade (see section 1.2). According to their analytical solution, the wires downstream of the blade are moving parallelly along straight paths, hence implying zero pressure and a constant velocity

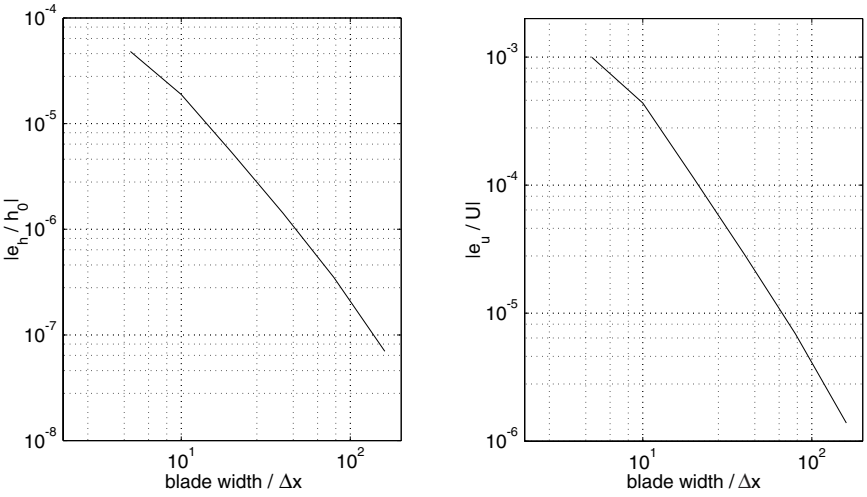

(a) Error e_h in the downstream gap size as a function of Δx.

(b) Error e_u in the minimum value of the velocity as a function of Δx.

FIGURE 3.7. Convergence rates for the dependent variables. The results from a simulation where Δx/blade width = 0.003125 were taken as estimates of the exact values. The parameter set is the same as in figure 3.6.

(equal to that far upstream of the blade) in that region. As it is only the solution upstream of the blade that is non-trivial, the same problem can hence be studied by employing a single WW-module, and the obtained (non-linear) solution should agree well with the results of Zhao & Kerekes (1995), provided that the wrap of the wires over the blade is small enough not to seriously violate their linearity assumption. In figure 3.8, such a comparison is presented. The boundary conditions needed to solve the WW-module were obtained from the linear solution. 2000 uniformly spaced mesh points were used to discretise the WW-module, whose length (non-dimensionalised with h_0) was 150. The analysis by Zhao & Kerekes (1995) assumes that the drainage resistance is constant. In order to mimic this, the drainage coefficient K was set to a very low value in order to prevent significant changes of the resistance along the module. The value chosen was roughly 1 % of the value which should have been used if a fibre suspension of normal consistency (about 0.5 %) was simulated. As can be seen in figure 3.8, the agreement between the linear and the non-linear pressure predictions is excellent. This is an important observation as Zhao & Kerekes (1995) found good agreement between their results and measurements of the

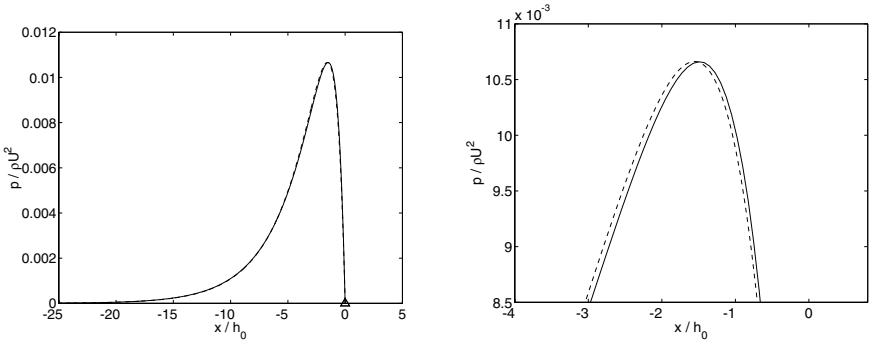

(a) The complete pressure pulse.

(b) A close up.

FIGURE 3.8. (- - -) The linear solution by Zhao & Kerekes (1995) for the pressure distribution in front of a thin blade at $x = 0$. (—) The non-linear solution from a WW-module. Total wrap angle 0.01 rad (corresponding to a blade force of 70 N/m). Wire speed 25 m/s. Wire tensions 7 kN/m. Initial gap size 2 mm. Initial drainage resistances 34 kNs/m^3. Drainage coefficient in the non-linear calculation 9.0×10^4 kg/(m^{3}s). Density 1000 kg/m^3.

pressure pulse generated by the deflection of two wires over the downstream edge of a flat blade. The pressure was measured through pressure holes drilled through the blade, and one of their result plots have been reproduced in figure 3.9. The pressure pulse obtained through a non-linear calculation (using a LB-module), for the set of parameters corresponding to the solid line in figure 3.9, is plotted in figure 3.10. The linear solution, which was used to obtain the necessary geometrical input parameters for the LB-module, is also plotted. The agreement between the linear and the non-linear solution in figure 3.10 is not as good as in figure 3.8, which is not surprising as the deflection of the wires is several times larger in the former case. Nevertheless, both the linear and the non-linear results are supported by the pressure measurements.

Zahrai *et al.* (1997) performed a two dimensional simulation of a single flat blade applied to a pair of fabrics, and made a comparison with experimental results. The pressure distribution next to the wire in contact with the blade is reproduced in figure 3.11. The pressure measurements were performed with the same technique employed by Zhao & Kerekes (1995). Applying the model developed in this study to the same problem yields the results presented in figure 3.12. From the study by Zahrai *et al.* (1997), it is clear that the pressure

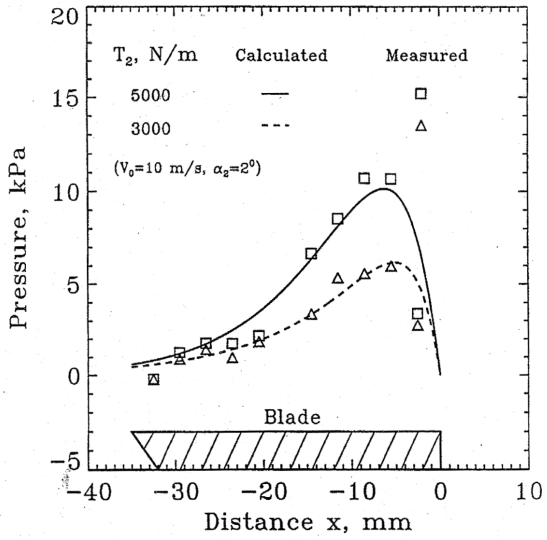

FIGURE 3.9. A reproduction of one of the comparisons between the linear theory and the experimental measurements presented by Zhao & Kerekes (1995). No deflection of the wires at the leading edge. The wrap over the trailing edge is 2°. Wire speed 10 m/s. (—) and (□): Wire tensions 5 kN/m. Initial gap size 0.8 mm. Estimated drainage resistance 39.5 kNs/m^3. (- - -) and (△): Wire tensions 3 kN/m. Initial gap size 1.0 mm. Estimated drainage resistance 23 kNs/m^3. Density 1000 kg/m^3.

gradients in the z-direction are very small over the blade[3]. Hence, it is justifiable to compare the pressure distribution in figure 3.12, which is an average over the gap between the wires, and the one in figure 3.11. Considering that we are comparing a one-dimensional and a two-dimensional simulation, the agreement is fairly good. The pressure pulses, and especially the downstream one, are slightly overestimated. This is in accordance with the results presented in figure 1.5, where a comparison is made between a linear one-dimensional and a linear two-dimensional analysis of the pressure distribution caused by a thin blade deflecting a pair of wires. In both figure 3.11 and figure 3.12, one can see that the pressure is locally negative, which means that the pressure in the gap is predicted to be lower than that of the surroundings. The negative peaks in the pressure distribution from the two-dimensional simulation, located immediately downstream of the blade edges, are due to strong acceleration of

[3]Note that this supports the conclusion in chapter 2 that the pressure gradients in the z-direction are of negligible magnitude.

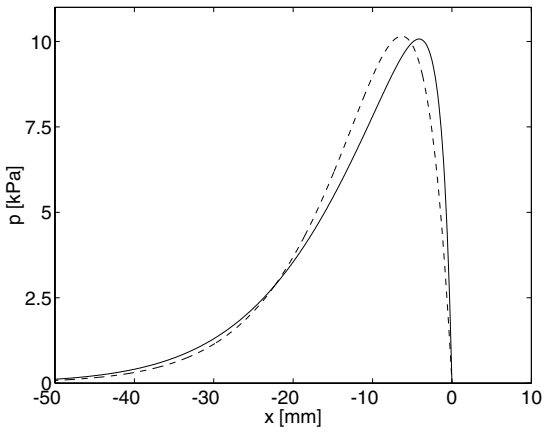

FIGURE 3.10. (—) Non-linear calculation of the pressure over a flat blade for the parameter set that corresponds to the solid line in figure 3.9. (- - -) The corresponding linear analytical solution. $\Delta x = 0.15$ mm.

the fluid around the sharp corners caused by the edges. The negative pressure observed in other regions are due to stationary waves forming on the wires under conditions of high drainage resistances. Criteria for determining when this is expected to occur have been given by Zhao & Kerekes (1995) and, in a more accurate form, by Zahrai & Bark (1995). Indeed, waves should appear for the parameter set given in the caption of figure 3.11. However, there are good reasons to believe that the pressure in the gap cannot become significantly lower than that of the surroundings, an issue which we will comment on in the subsequent chapters. For now we content ourselves with the observation that the present model yields roughly the same output as the one by Zahrai *et al.* (1997) for a single blade.

In view of the outcome of the different tests and comparisons made in this section, we conclude that the algorithm seem to be correctly implemented, and that the model will most likely serve well as a tool for obtaining at least qualitatively correct results.

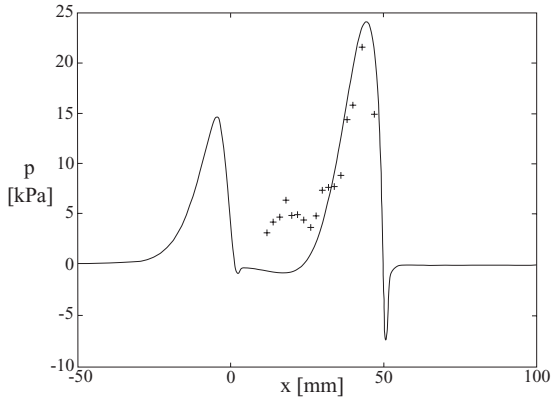

FIGURE 3.11. The pressure distribution next to the contacting wire when a flat blade is applied to a pair of fabrics (Zahrai *et al.* 1997). (—) 2D simulation. (+) Experimental measurements. The leading and trailing edges of the blade are located at $x = 0$ mm and $x = 50$ mm, respectively. Fabric tensions 5 kN/m. Wire speed 20 m/s. Initial gap size 3 mm. Constant drainage resistances 31 kNs/m^3. The slopes of the wires upstream and downstream of the blades were 0.035 and -0.07, respectively.

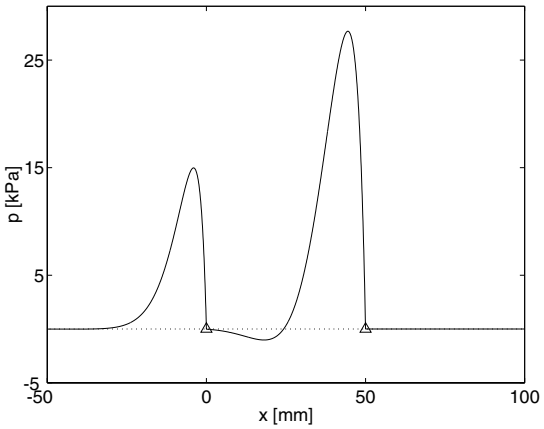

FIGURE 3.12. The pressure distribution when the model developed in this study is employed to solve the same problem as in figure 3.11. $\Delta x = 0.15$ mm. The edges of the blade are indicated by $\triangle$.

CHAPTER 4

Results

This chapter contains the results obtained from a number of different numerical simulations. The focus will be on the pressure distribution in the forming section for different sets of parameters. Given the nature of our model, and our ambition to obtain qualitative rather than quantitative results, the numerical details concerning the calculations are not given, unless they are found to be of special interest. The number of mesh points have been chosen well above the limit for grid independence. Typically the mesh is such that a blade is resolved with 100 points or more. The tolerances for the Newton iterations, and the algorithm that determines the root to the system function Z, have been set low enough not to yield errors larger than the discretisation errors.

In chapter 2 it was seen that the equations governing the model are defined by the three non-dimensional numbers ε_1, ε_2 and κ, together with the non-dimensional suction pressures. However, instead of giving these parameters for each simulation, we will specify the set of input parameters used in each calculation in dimensional form. Hence we hope to make the results more intuitively accessible to readers having practical experience of papermaking.

According to Zhao & Kerekes (1995), the drainage resistance of a newsprint stock, dewatered to a fibre mat of basis weight 10 g/m^2, is about 20 kNs/m^3. Assuming that the mat has a fibre mass concentration of 4 % and that the density of the fibres is 1.5 times that of water, the permeability k_ζ of the mat can be estimated to 1.25×10^{-11} m^2. Employing this permeability, and taking the fibre mass concentration in the free suspension to be 0.5 %, the drainage coefficient K is 9.0×10^6 kg/(m^{3}s). This value is used for the simulations unless otherwise specified. The density was always taken to 1000 kg/m^3. If a suction pressure is applied in between the two upper blades, this is explicitly stated. The default is that no such pressure is used.

The geometry of the model is, unless something else is specified, such that the locations in the z-direction of the upper wire at the inlet of the model domain, of the two blades in contact with that wire, and of the upper wire at the outlet of the model, are the same. In other words, they are positioned at the same level. If curved blades are used, the lowest points of the surfaces of the blades are located at the same position as the wire at the inlet and outlet. The position of the lower blade and the lower wire (apart from at the

inlet far upstream) is determined as part of the solution process. The term 'blade spacing' refers to the distance between the trailing edge of one blade, and the leading edge of the next blade downstream, which is normally applied to the opposing wire. When the wire is not able to remain in contact with the blade along its full length, the numerical algorithm reduces the extension of the blade–wire contact length in the machine direction until the wire attaches smoothly to the blade (see chapter 3). Nevertheless, the 'blade spacing' is the distance between the true trailing edge of one blade and the true leading edge of the next. The 'blade force' specified in connection with the simulations is the force by which the lower blade is applied to the lower wire.

When applicable, the symbols $\triangle$ indicate the positions of blade edges in the figures.

4.1. The magnitude of non-linear effects

A non-linear solution is more demanding to obtain than a linear solution. It is interesting to see how large the differences are between a linear and a non-linear solution for the forming section in figure 3.5. Therefore, a linear solver was developed. Due to the presence of the blades, the same system of equations cannot be used throughout the whole model domain. Hence, like in chapter 3, the forming section was divided into WW-, LB- and UB-parts, and a separate linear solution was obtained in each part. The different solutions were then matched with each other. Although the matching procedure could in principle be carried out analytically, thus yielding a fully analytical solution, the same iterative procedure as in the non-linear case was performed for practical reasons.

Figure 4.1 contains a comparison between the two kinds of solutions. The compared quantity is the amplitude of the pressure in front of the first blade. The relative difference between the two solutions is seen in figure 4.1(a). When we are approaching industrially relevant magnitudes of the blade force, the relative difference is larger than 15 %, which is not insignificant if quantitative values are of interest. Naturally, if other quantities are considered, the difference might be either larger or smaller. Figure 4.1(b) is a logarithmic plot of the absolute difference. The result is a straight line with slope 2, which confirms that the linear solution has been correctly calculated.

4.2. The position of the blades

In figure 4.2, a series of calculations are presented in which the blade spacing is increased successively, starting from a very low value. Note that the scales in the different subfigures are not the same.

In figure 4.3 are seen the paths of the wires in the simulation giving rise to the pressure distribution in figure 4.2(c). It is qualitatively representative of all the simulations presented in figure 4.2.

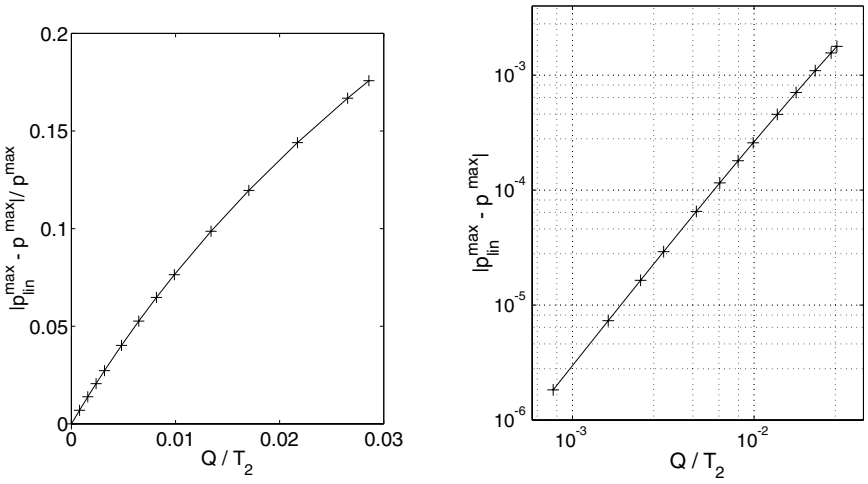

(a) Relative difference.

(b) Absolute difference.

FIGURE 4.1. The difference between the amplitude of the pressure peak in front of the first blade. p_{max}^{lin} and p_{max} are the linear and non-linear values, respectively. Flat blades, width 14 mm. Blade spacing 25 mm. Initial gap size 2 mm. Wire speed 25 m/s. Wire tensions 7 kN/m. Initial drainage resistances 20 kNs/m^3. Drainage coefficient 3.0×10^7 kg/(m^{3}s). (+) Calculated values.

It was found by Zhao & Kerekes (1995) that a linear solution yields zero pressure downstream of a deflection of the wires, if no further deflections occur. This result carries over to the non-linear case, which is seen if one attempts to find the non-linear solution through an infinite series of subsequent linearisations in the region downstream of the deflection. As there is no deflection of the wires at the trailing edge of the third blade (which is flat), the pressure is zero downstream of the leading edge of the third blade in the figures 4.2(a)–(f). Although the first blade is flat, there is a deflection of the wires at the leading edge, caused by the pressure pulse in front of the trailing edge. This pulse extends in the upstream direction past the leading edge of the blade, hence causing a deflection at that edge. However, the interaction between the corresponding pulse and the one causing the deflection is such that the influence on the total pressure distribution can only bee seen as a change in the gradient of the pressure at the blade edge.

When the blades are positioned close together, the pressure pulses merge, and the resulting pressure distribution is of larger magnitude. The pressure pulses in front of the trailing edge of the first blade, and the leading edge of the second blade, are the ones of largest magnitude, even in figure 4.2(f) where the blades are located so far apart that the pulses no longer merge. It is interesting to see that the two last pulses almost disappears when the distance between the blades is very small.

Figure 4.4 contains the pressure pulses obtained in two situations of very large blade spacing. In both cases, the distance between the inlet of the model domain and the first blade (expressed in terms of blade widths) was 14.3. It is clear that the blade distance continues to have an influence on the pressure pulses, albeit a small one, even when the pressure pulses do not merge. This is of course due to the influence of the blade distance on the angles with which the wires approach and leave the blades. For example, by inspection of figure 4.4 it is clear that positioning the blades further apart has increased the wrap over the leading edge of the third blade. Intuitively, one would expect the wrap over the trailing edge of the first blade to increase as well, when the distance between the blades is larger. Nevertheless, the results presented in figure 4.4 indicates that this is not the case here.

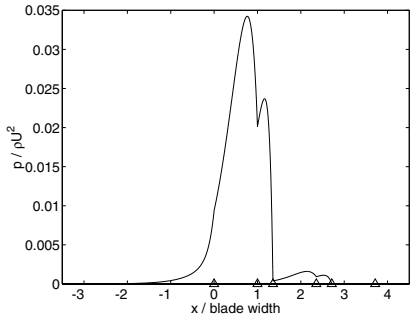

(a) Blade spacing 5 mm.

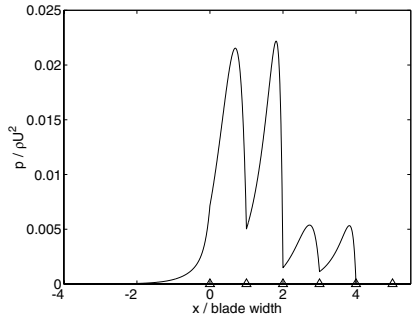

(b) Blade spacing 14 mm.

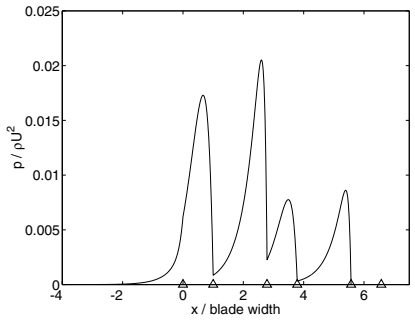

(c) Blade spacing 25 mm.

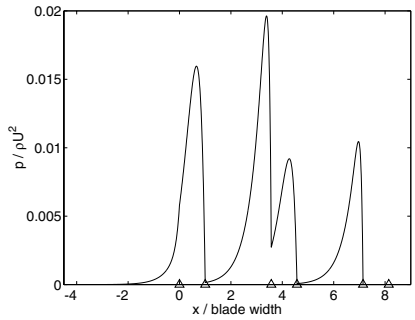

(d) Blade spacing 36 mm.

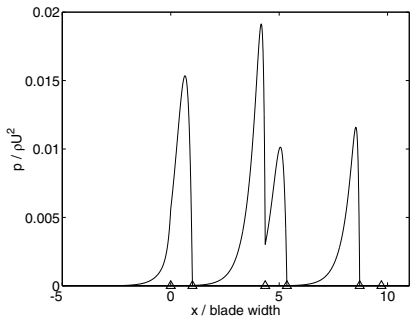

(e) Blade spacing 47 mm.

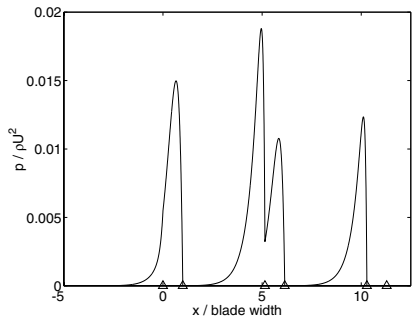

(f) Blade spacing 58 mm.

FIGURE 4.2. The influence of the blade spacing on the pressure pulses. Flat blades, width 14 mm. Blade force 300 N/m. Wire tensions 7 kN/m. Initial gap size 2 mm. Wire speed 25 m/s. Initial drainage resistances 34 kNs/m^3.

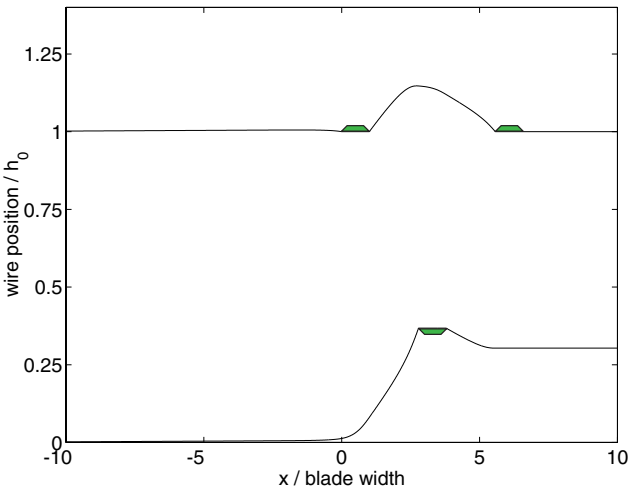

FIGURE 4.3. The paths of the wires corresponding to the pressure distribution in figure 4.2(c). The filled areas indicate the positions of the blades.

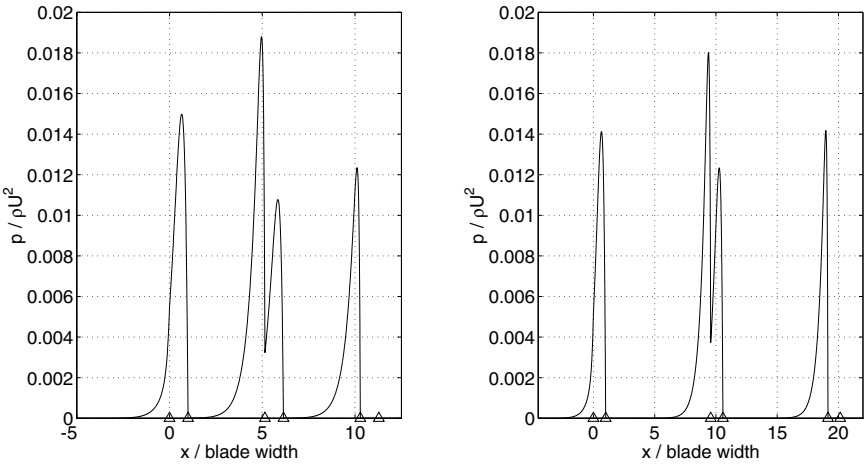

(a) Blade spacing 58 mm.

(b) Blade spacing 120 mm.

FIGURE 4.4. The pressure pulses in two cases of large blade spacing. The parameters are the same as for the calculations presented in figure 4.2.

4.3. The curvature of the blades

Figure 4.5 shows the difference between the pressure distributions in the forming section when flat blades, and blades with constant radius of curvature, are used. The curved blades are such that the blades are symmetric with respect to an axis normal to the blade surface at the midpoint of the blade. In other words, they extend the same distance upstream and downstream of the top of the blade. Blades of this kind will be referred to as (symmetrical) 'circular' blades. Although the blades are short, the pressure distribution is influenced

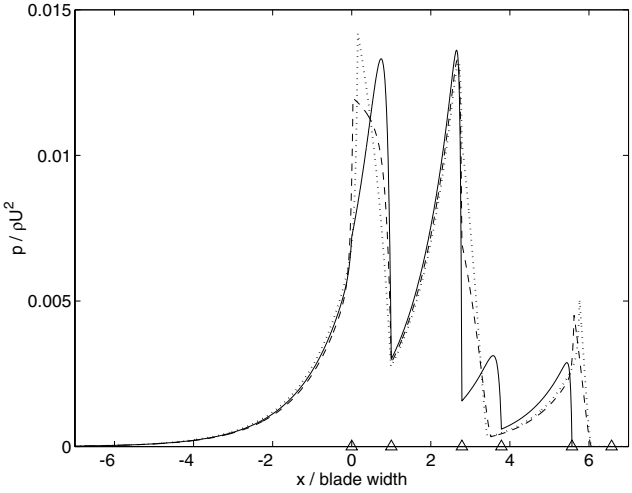

FIGURE 4.5. The pressure distribution when blades of different curvature are used. (—) Flat blades. (- - -) Circular blades, radius 1 m. (· · ·) Circular blades, radius 0.6 m. Initial gap size 2 mm. Blade width 14 mm. Blade spacing 25 mm. Blade force 300 N/m. Wire speed 25 m/s. Wire tensions 9 kN/m. Initial drainage resistances 20 kNs/m^3.

already when the blades have the rather modest radius of 1 m. This corresponds to the blade surface protruding a distance equivalent to 1.2 % of h_0 with respect to the level at the edges of the blade. For the blade of radius 0.6 m, the corresponding value is 2.0 % of h_0. Due to their curvature, the circular blades are not necessarily in contact with the wires along their full width. An example of this is seen in figure 4.6, which illustrates how the fabric leaves the circular middle blade of radius 0.6 m tangentially, before it reaches the trailing edge. Table 4.1 presents the fraction of the blades, upstream and downstream of the middle, that has contact with the fabric in the simulations. The early departure of the wire from the middle blade, when it is circular, explains the disappearance of the pulse in front of the trailing edge, which is

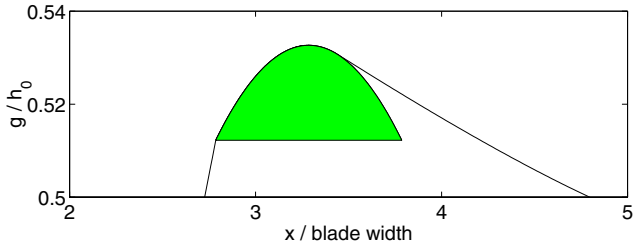

FIGURE 4.6. The path of the lower wire, g, as it wraps the middle circular blade of radius 0.6 m. Parameters as given in the caption of figure 4.5.

	Radius 1 m	Radius 0.6 m
Blade 1, upstream	94 %	69 %
Blade 1, downstream	100 %	98 %
Blade 2, upstream	100 %	100 %
Blade 2, downstream	46 %	31 %
Blade 3, upstream	90 %	62 %
Blade 3, downstream	0 %	0 %

TABLE 4.1. The fraction of the blades, upstream and downstream of the middle, that is in contact with the fabric. The values correspond to the calculations presented in figure 4.5. The radii in the column headers refer to the curvature of the blades.

present when flat blades are used. As the blade surface at the middle of the third blade is at the same level as the upper wire at the outlet of the model domain, it is inevitable that the fabric leaves the blade at the middle when it has a finite radius of curvature.

In figure 4.7, the pressure gradients in the machine direction are plotted for the distributions in figure 4.5. When flat blades are used, the negative gradients are clearly dominant, corresponding to large accelerating forces on the suspension when the pressure decreases at the end of the pulse. The build up of the pressure at the beginning of the pulse is a much more gradual process. Circular blades yield less severe negative gradients, but, as is discussed below, sometimes also positive gradients of larger amplitude.

Consider the pressure distribution for the flat blades in figure 4.5. The first blade generates a single pressure pulse. The reason is that, for the present parameter set, the wrap of the wires over the leading edge is only about half of the wrap over the trailing edge. A suspension particle approaching the

first blade will therefore feel the presence of the leading edge as an increase in the pressure, but where the pressure would start to decrease if there were no further deflections of the fabrics, the pressure instead continues to increase due to the large pulse generated by the trailing edge. However, the pressure gradient right before the leading edge is that seen at the late stages of a pulse (due to the leading edge), whereas the gradient right downstream of the leading edge is that at an earlier stage of another pulse (that generated by the trailing edge). This explains the change of the slope in the pressure distribution at the leading edge of the flat blade in figure 4.5, and also the positive peak seen at the leading edge of the first blade in figure 4.7(a). At the middle blade, the situation is different. The wrap of the fabrics is larger over the leading edge than over the trailing edge, and a decrease in the pressure is observed at the end of the pulse generated by the leading edge, albeit interrupted at a very late stage by the pulse from the trailing edge. At the third blade, there is a single pulse generated by the deflection of the wires at the upstream edge. At the downstream end there is no fabric wrap, and hence no pressure pulse. The features of the pressure distribution that we just discussed can be seen whenever three flat blades are used in the configuration employed so far. The same comments therefore applies to the pressure distribution seen in figure 4.4(b), where the blades are positioned very far apart. Consequently, the pulses at the three blades can be looked upon from right to left as a series, describing the situation around a single blade, when the wrap over the leading edge is finite and the wrap of the fabrics over the trailing edge is first zero, then finite but less than at the upstream edge, and last finite and of larger magnitude than at the leading edge.

Now, let us consider the pressure gradients in the case of circular blades, seen in the figures 4.7(b)–(c). We note in table 4.1 that the fabrics are not in full contact with the upstream side of the first and the third blade. The large positive gradients in front of these blades are a consequence of the formation of a high pressure that deflects the wire, so that it can make contact with the blades tangentially. This also explains why their is no such peak at the middle blade, where the wires are wrapped over the blade edge and hence do not need to adjust to the inclination of the surface of the blade. At the positions where the fabrics first make contact with the blade, the pressure gradient changes discontinuously to modest negative values and remains there for a short distance downstream. This corresponds to the relatively (with respect to flat blades) gradual decrease of the pressure over the circular blades that can be seen in the corresponding pressure distributions in figure 4.5.

Figure 4.8 contains the pressure distributions in five simulations where the first and the third blades are flat, whereas the radius of curvature of the middle blade is varied. By positioning the blades far apart, the effects of the curvature on the pressure distribution at the middle blade can be studied with minimal interference from the pulses at neighbouring blades. As the distance between

the blades is very large, it is easier for the wires to wrap the middle blade along its full width than was the case in figure 4.5. Only on the downstream side of the blade of radius 0.4 m is the fabric forced to leave the blade surface before reaching the trailing edge. In that case 69 % of the downstream side remains in contact with the wire. At the trailing edge of the blade of radius 0.6 m, the wire leaves very near tangentially to the blade surface. In figure 4.8 it is very clear how the second pulse disappears as the magnitude of the deflection of the wires over the trailing edge is made smaller by decreasing the radius of curvature of the blade. At the same time the maximum value of the pressure increases. It is also interesting to see that even the blade of radius 3 m exhibits a small but noticeable difference with respect to the flat blade. The pressure distributions in figure 4.8 are consistent with the linear results by Roshanzamir (2000) for a single curved blade applied to a pair of fabrics. In that study, the blade surface was given by a second order polynomial. The pressure gradients corresponding to the simulations in figure 4.8 are plotted in figure 4.9. The magnitude of the gradients in the regions where the pressure is building up is about the same for the different radii. This is a consequence of the fabrics being wrapped over the upstream edge of the blade. If the situation was such that the lower fabric made contact with the blade downstream of the leading edge, a pressure would have to be built up to adjust the slope of the wire to that of the blade surface, hence generating large positive gradients as seen in front of the points of first contact in figure 4.7(b)–(c). In figure 4.9 the magnitude of the negative gradients are reduced as the radius of curvature is decreased. This is a result of the pressure immediately downstream of the leading edge becoming of larger magnitude. Note especially, in figure 4.8, how the gradual decrease of the pressure over the surface of the blade with radius 0.4 m starts without the pressure from the pulse at the leading edge having fallen at all.

Figure 4.10 illustrates the influence of the radius of curvature on the pressure distribution around the middle blade for a different set of parameters than in figure 4.8. The main differences are that the width of the blades and the initial gap size are several times larger, 50 mm and 8 mm, respectively, and that the wire speed is only 10 m/s. In the simulations where the radius of the middle blade was 1 m and 0.6 m, the fabric only wraps 53 % and 34 % of the downstream half of the blade, respectively. The pressure events in figure 4.10 and figure 4.8 clearly show similarities. The effects of the curvature is however stronger in figure 4.10, which is not surprising since the middle blade is more than three times wider than in figure 4.8.

An interesting question is whether the decrease in the pressure distributions, after the wire has made contact with the circular blade, bear any resemblance with the pressure distributions generated during roll forming, right before the fabrics are taken off the roll. Especially when the fabrics leave tangentially to the blade surface, there might be some similarities. In the experimental study of roll forming by Holm (2002), it was observed that a

suction pressure is generated where the wires are taken off the roll. Such a suction should occur also during blade forming using curved blades, if the fabric leave the blade surface before the trailing edge[1]. Although the ratio between the wire tension and the radius of the roll is a far to simplistic description of the pressure distribution during roll forming, it is tempting to calculate the corresponding ratios for the circular blade with radius 1 m in figure 4.8, and the circular blade with radius 3 m in figure 4.10. The corresponding pressure distributions seem to have a plateau right downstream of the leading edge, and it is imaginable that this plateau corresponds to the pressure level that would prevail at the last part of the pressure pulse during forming with a roll of the same radius as the blade. The ratio (non-dimensionalised with ρU^2) is 0.01 for the blade of radius 1 m, and 0.02 for the blade of radius 3 m. This is in fairly good agreement with the magnitude of the pressure at the flat part of the distributions, and does at least not contradict that similarities might exist.

[1] The same phenomena was made use of in the past when table rolls and foils were employed to drain fibre suspensions (see e.g. Norman, 1989).

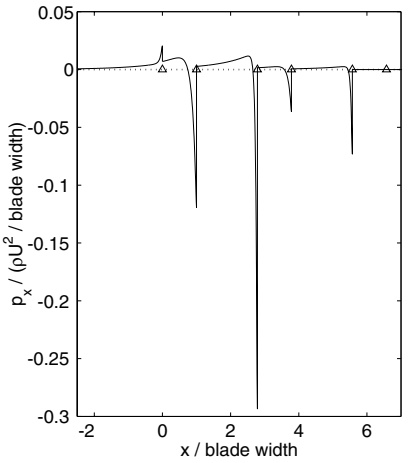

(a) Flat blade.

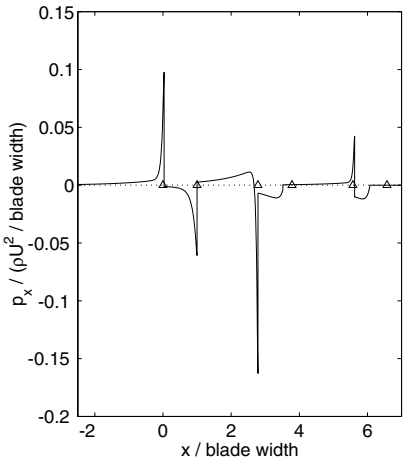

(b) Circular blade, radius of curvature 1 m.

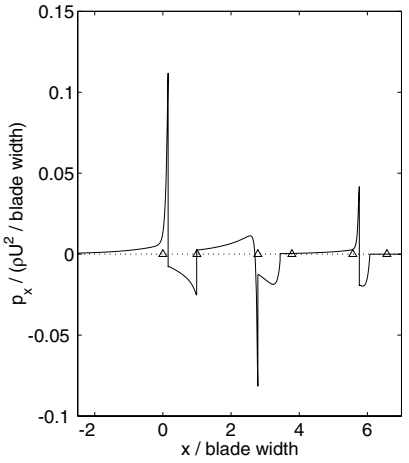

(c) Circular blade, radius of curvature 0.6 m.

FIGURE 4.7. The dependence of the pressure gradient in the machine direction on the curvature of the blades. The parameters are the same as in the caption of figure 4.5. Note that the scales on the vertical axes of the subfigures are not the same.

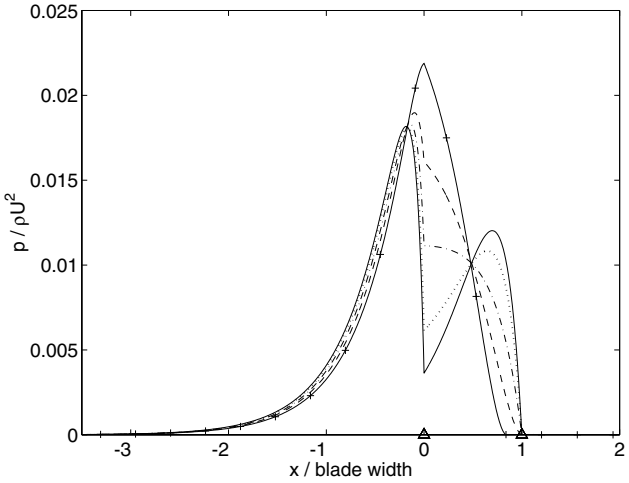

FIGURE 4.8. The effect of blade curvature on the pressure pulses. Enlargement of the situation at the middle blade. (—) Flat middle blade. (· · ·) Middle blade radius 3 m. (- · -) Middle blade radius 1 m. (- - -) Middle blade radius 0.6 m. (+) Middle blade radius 0.4 m. The first and the third blades are flat. Blade width 14 mm. Blade spacing 100 mm. Blade force 300 N/m. The tension in the wires are 7 kN/m. The initial drainage resistances are 34 kNs/m^3. Initial gap size 2 mm. Wire speed 25 m/s.

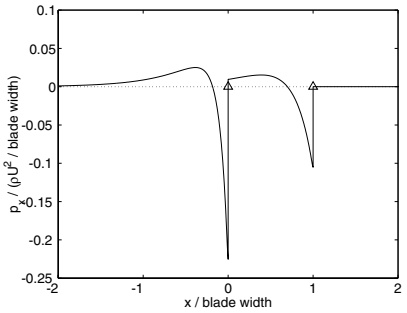

(a) Flat middle blade.

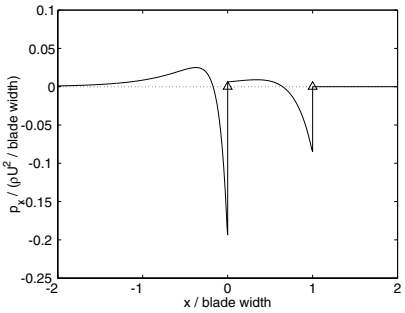

(b) Middle blade radius 3 m.

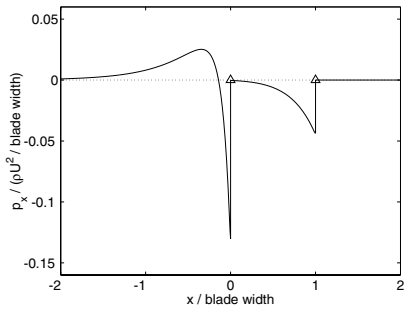

(c) Middle blade radius 1 m.

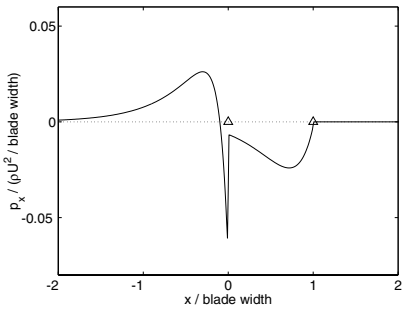

(d) Middle blade radius 0.6 m.

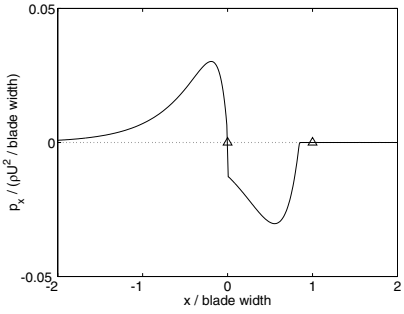

(e) Middle blade radius 0.4 m.

FIGURE 4.9. The gradients in the machine direction corresponding to the pressure distributions in figure 4.8. Note that the scales on the vertical axes of the subfigures are not the same.

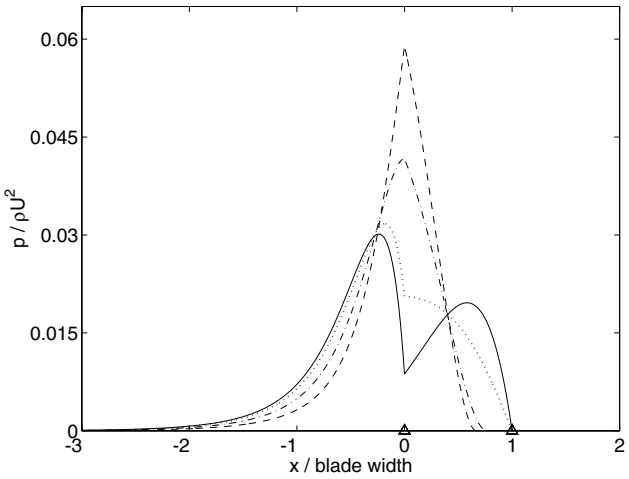

FIGURE 4.10. The effect of blade curvature on the pressure pulses. Enlargement of the situation at the middle blade. (—) Flat middle blade. (· · ·) Middle blade radius 3 m. (- · -) Middle blade radius 1 m. (- - -) Middle blade radius 0.6 m. The first and the third blades are flat. Blade width 50 mm. Blade spacing 280 mm. Blade force 300 N/m. The tension in the wires are 6 kN/m. The initial drainage resistances are 15 kNs/m^3. Initial gap size 8 mm. Wire speed 10 m/s.

4.4. The blade load

Figure 4.11 illustrates how the force by which the middle blade is applied to the lower wire influences the pressure distributions for one case involving flat blades, and one case involving circular blades of radius 0.6 m. Like we have seen in section 4.3, employing curved blades sometimes means that the fabrics are not in contact with the blades along their full length. Table 4.2 contains the fractions of the upstream and downstream halves of the blades in figure 4.11(b) that are in contact with the wire. Naturally, a higher blade load implies that the portions of the blades wrapped by the fabrics increase. From figure

	200 N/m	275 N/m	350 N/m
Blade 1, upstream	48 %	53 %	58 %
Blade 1, downstream	98 %	100 %	100 %
Blade 2, upstream	100 %	100 %	100 %
Blade 2, downstream	47 %	63 %	78 %
Blade 3, upstream	81 %	100 %	100 %
Blade 3, downstream	0 %	0 %	0 %

TABLE 4.2. The fraction of the blades in figure 4.11(b), upstream and downstream of the middle, that is in contact with the fabric for the different blade forces.

4.11(a) it is clear that a higher force in the case of flat blades does little more than increase the amplitude of the pressure pulses. This increase is of course due to larger wrap angles at the blade edges. Very little happens to the overall shape of the pressure distribution. However, the situation is slightly more complex when circular blades are considered. In figure 4.11(b) we note that the magnitude of the pressure over the middle blade is affected only slightly by the increased load, in comparison with the pulse in front of the blade. The explanation is that the wrap angle of the fabrics at the leading edge is changed quite a lot when a higher blade load is employed, whereas, at the trailing edge, the effect is that the position where the wire separates from the blade surface is moved downstream along the blade, which does not correspond to a large change in the slope of the wires. Instead, it merely yields a small additional distance for the pressure to develop along the blade. As a consequence, the pressure distribution over the middle blade seizes to be of the same amplitude as the pressure pulse generated in front of the leading edge, when the load is increased. The same thing does not happen at the first blade, since the fabric regains contact with the trailing edge when the blade force is made larger.

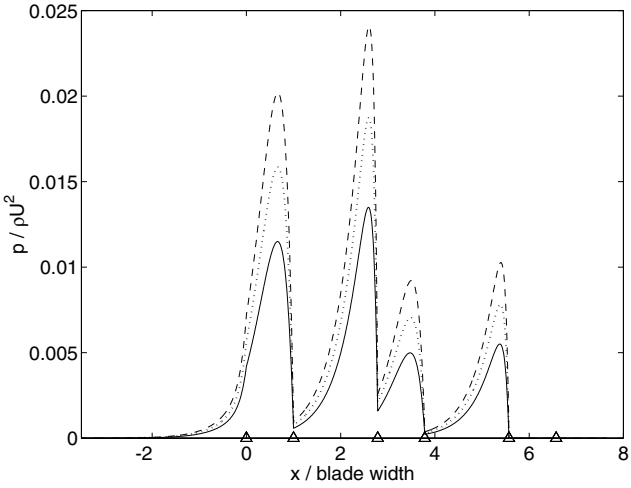

(a) Flat blades.

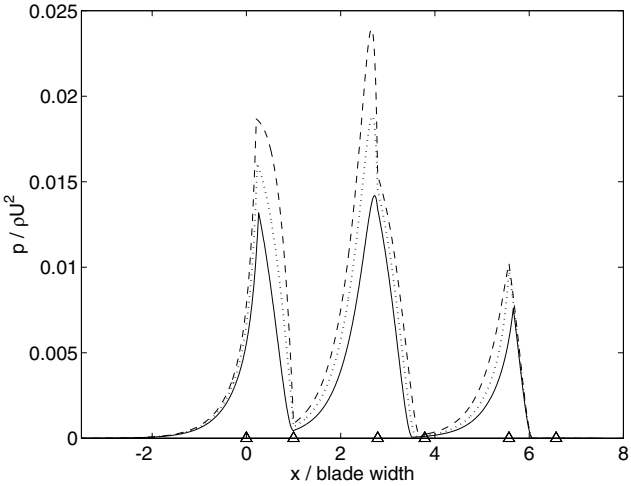

(b) Circular blades, radius 0.6 m.

FIGURE 4.11. The influence of the magnitude of the blade force for flat blades and circular blades of radius 0.6 m. (—) $F = 200$ N/m, $(\cdots)$ $F = 275$ N/m, (- - -) $F = 350$ N/m. Blade spacing 25 mm. Blade width 14 mm. Wire tensions 7 kN/m. Initial gap size 2 mm. Wire speed 25 m/s. Initial drainage resistances 34 kNs/m^3.

4.5. The wire tension

Changing the tension in the fabrics naturally has an effect on the pressure distribution. An example of this is seen in figure 4.12, where the distributions are given for a case of high wire tensions, a case of low wire tensions, and two cases where different tensions are used in the two wires.

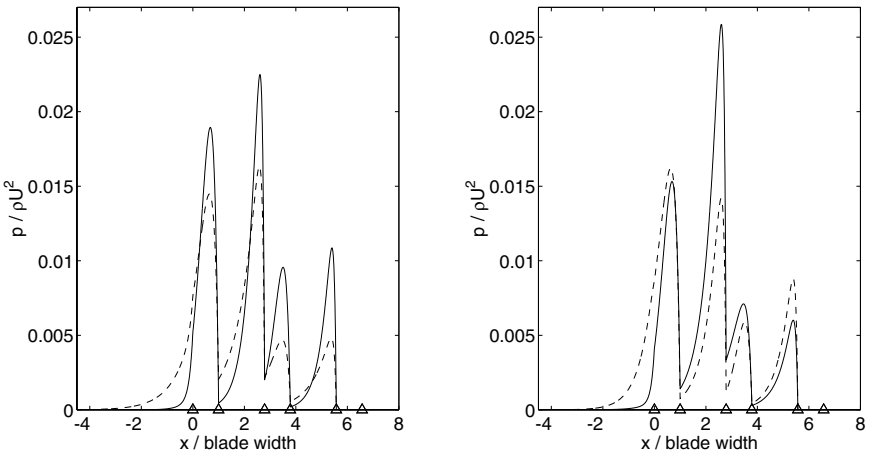

(a) (—) $T_1 = T_2 = 6$ kN/m, (- - -) $T_1 = T_2 = 10$ kN/m

(b) (—) $T_1 = 10$ kN/m $T_2 = 6$ kN/m, (- - -) $T_1 = 6$ kN/m $T_2 = 10$ kN/m

FIGURE 4.12. The influence of the wire tension on the pressure distributions. Flat blades, width 14 mm. Blade spacing 25 mm. Blade force 300 N/m. Initial gap size 2 mm. Wire speed 25 m/s. Initial drainage resistances 34 kNs/m^3.

In the linear solution by Zhao & Kerekes (1995) for the deflection of a pair of fabrics over a thin blade, the length scale of the term that determines the extent of the (single) pressure pulse is reduced when the wire tension is decreased. This agrees with the results seen in figure 4.12(a), where a smaller tension clearly yields pressures pulses that extend a shorter distance in the upstream direction. A vertical force balance tells us that the blade load must be balanced by the vertical components of the wire tension immediately upstream and downstream of the edges of the middle blade. As the blade load is the same in the simulations, a lower wire tension hence implies a larger deflection of the wires, and consequently a pulse of larger amplitude. This is also seen in figure 4.12(a). As the wires are horisontal far downstream of the blades, and almost horizontal far upstream, the sum of the forces from the first and the

third blade approximately equals the load from the middle blade. Although there is probably some redistribution of the force between the upper blades when the parameters are changed, the blade forces are likely to be roughly the same in the two simulations presented in figure 4.12(a). The same reasoning that was applied for the middle blade is therefore also valid for the first and the third blade.

Let us now consider figure 4.12(b), and comment on what is seen by comparing with the case of equal wire tensions of 6 kN/m in figure 4.12(a). The tension in the wire in contact with the middle blade is the same as the tension in the wire opposing the first and the third blade, and vice versa. When discussing the results we shall therefore limit our discussion to the middle blade, and merely note that the inverse reasoning applies to the other blades. As the forces by which the first and the third blade pushes against the upper wire is smaller than the load at the middle blade, the effects are however less clearly seen at the upper blades.

Using a higher tension in the upper wire enhances the amplitude of the pressure pulses upstream of the edges of the middle blade. Green (1997) noted that the integrated pressure distribution at a blade equals the product of the total wrap angle and the tension in the wire opposing the blade. Although the integrated pressure can change either as a result of a different width of the distribution, or a different amplitude, the result highlights the importance of the tension in the opposing wire for the pressure pulses. It is hence not surprising that the amplitude of the pulses at the middle blade increases when the tension in the upper wire is given the value 10 kN/m, instead of 6 kN/m. This is what is seen when comparing the solid curves in the figures 4.12(b) and 4.12(a). On the other hand, when the lower wire has a tension of 10 kN/m, instead of 6 kN/m, the middle blade does not have to displace the lower fabric as much before a balance is reached between the wire tensions and the load. Consequently, the wrap decreases, and according to the result by Green (1997), the integrated pressure as well. This is seen as pulses of reduced magnitude when the solid curve in figure 4.12(a) is compared with the dashed curve in figure 4.12(b).

4.6. The drainage resistance

The thickness and characteristics of the fibre mat when it arrives at the blade forming section determines the initial resistance to dewatering. This resistance influences the rate of thickening of the fibre mat (a process which of course changes the drainage resistance), and the pressure distribution throughout the blade forming zone. Results from some calculations demonstrating the influence of the initial resistance on the development of the pressure can be seen in figure 4.14. An example of how the resistances varies during the forming process is seen in figure 4.13. It corresponds to the dash-dotted curve in figure 4.14(a). Note how the resistances remain constant when the corresponding wire passes

over a blade surface, where, by assumption, no dewatering takes place. At the end of the model domain, the resistance of the lower wire has increased more than that of the upper wire. The presence of the first blade prevents the drainage through the upper wire that would otherwise result from the large pressure at that blade. In the same way, the middle blade prevents drainage through the lower wire. However, as the pressure at the middle blade is considerably lower than at the first blade, the resistance of the upper wire remains lower even after the middle blade.

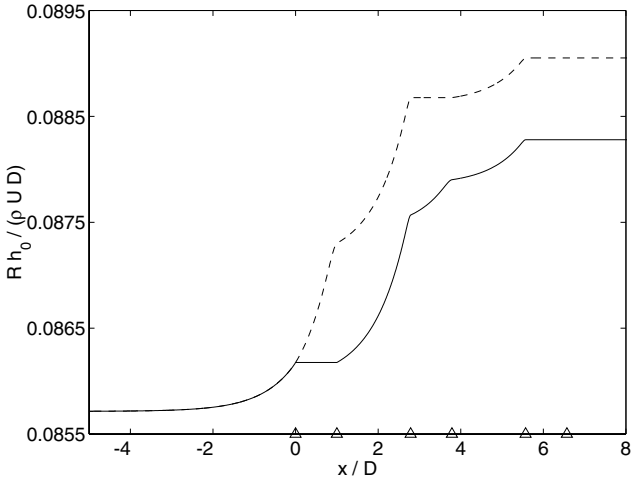

FIGURE 4.13. The evolution of the drainage resistances throughout the forming section. D is the blade width. (—) Resistance of the upper wire. (- - -) Resistance of the lower wire. The initial drainage resistances are 30 kNs/m^3. Flat blades, width 14 mm. Blade spacing 25 mm. Blade force 100 N/m. Wire tensions 9 kN/m. Initial gap size 1 mm. Wire speed 25 m/s.

We observe in figure 4.14 that the pressure pulses become more narrow, and of larger amplitude, for higher values of the drainage resistance. This is in accordance with the study by Zhao & Kerekes (1996). The narrowing of the pulses can also be predicted by considering the linear theory by Zhao & Kerekes (1995), which we have already made use of to explain the results in section 4.5. In their solution for the pressure pulse upstream of a thin blade, the length scale of the dominating term is reduced when the dewatering resistance increases. It is also reasonable that the pressure pulses should be of less amplitude for low drainage resistances, since a low resistance makes it more difficult to create a large pressure drop across the fabric.

The two pressure distributions in figure 4.14(b) correspond to very high values of the initial drainage resistance. In such situations, damped waves might appear on the fabrics upstream of the blades, as was found in the one-dimensional analysis by Zhao & Kerekes (1995), and the two-dimensional analysis by Zahrai & Bark (1995). In these (linear) studies, the authors assume a constant drainage resistance, and in both of them are given a criterion for when oscillating solutions occur. The critical value of the drainage resistance for the parameters in the caption of figure 4.14 is 67 kNs/m^3 according to the criterion by Zhao & Kerekes, and 66 kNs/m^3 if calculated with the criterion by Zahrai & Bark. Although the drainage resistance varies along the machine direction during our simulations, which is exemplified in figure 4.13, these values are likely to serve well as estimates of the limit which must not be surpassed if oscillating solutions are to be avoided. The oscillations seen in figure 4.14(b) are a result of the initial drainage resistances being above the critical value.

From the point of view of the model, the regions of negative pressure in figure 4.14(b) correspond to positions where the pressure is locally lower in the gap between the wires than outside of the fabrics. In chapter 5 we will discuss whether such regions actually exist in the forming zone. The issue is related to what would happen if a pressure drop across the wire was to generate a flow from the outside into the suspension between the fabrics, an event which could be termed 'reversed drainage'.

In figure 4.15 the pressure gradients in the machine direction are plotted for the distributions in figure 4.14(a). It is evident that the negative gradients can be of quite large magnitude when the dewatering resistances are low. As the corresponding fibre mats are thin, and most likely fragile, this could perhaps inflict damage on the fibre web.

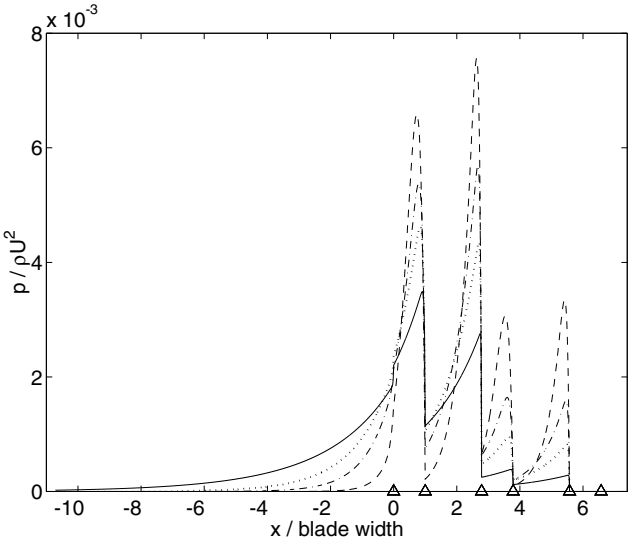

(a) (—) $R_0 = 10$ kNs/m^3, $(\cdots)$ $R_0 = 20$ kNs/m^3, $(-\cdot-)$ $R_0 = 30$ kNs/m^3, $(---)$ $R_0 = 50$ kNs/m^3.

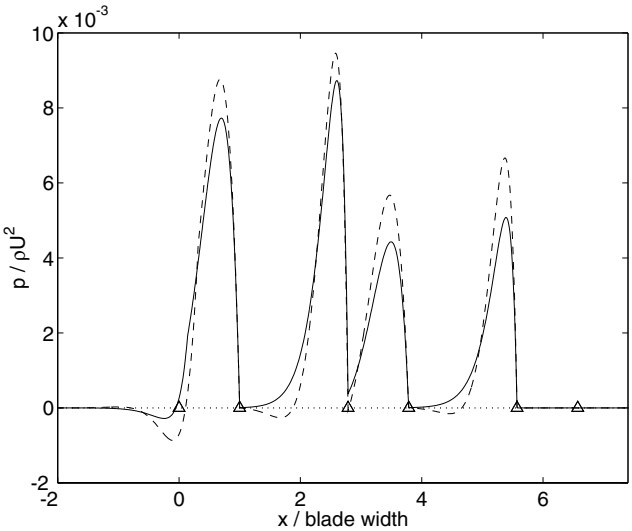

(b) (—) $R_0 = 70$ kNs/m^3, $(---)$ $R_0 = 90$ kNs/m^3.

FIGURE 4.14. The influence of the initial drainage resistance. In the graphs, $R_{10} = R_{20} = R_0$. Flat blades, width 14 mm. Blade spacing 25 mm. Blade force 100 N/m. Wire tensions 9 kN/m. Initial gap size 1 mm. Wire speed 25 m/s.

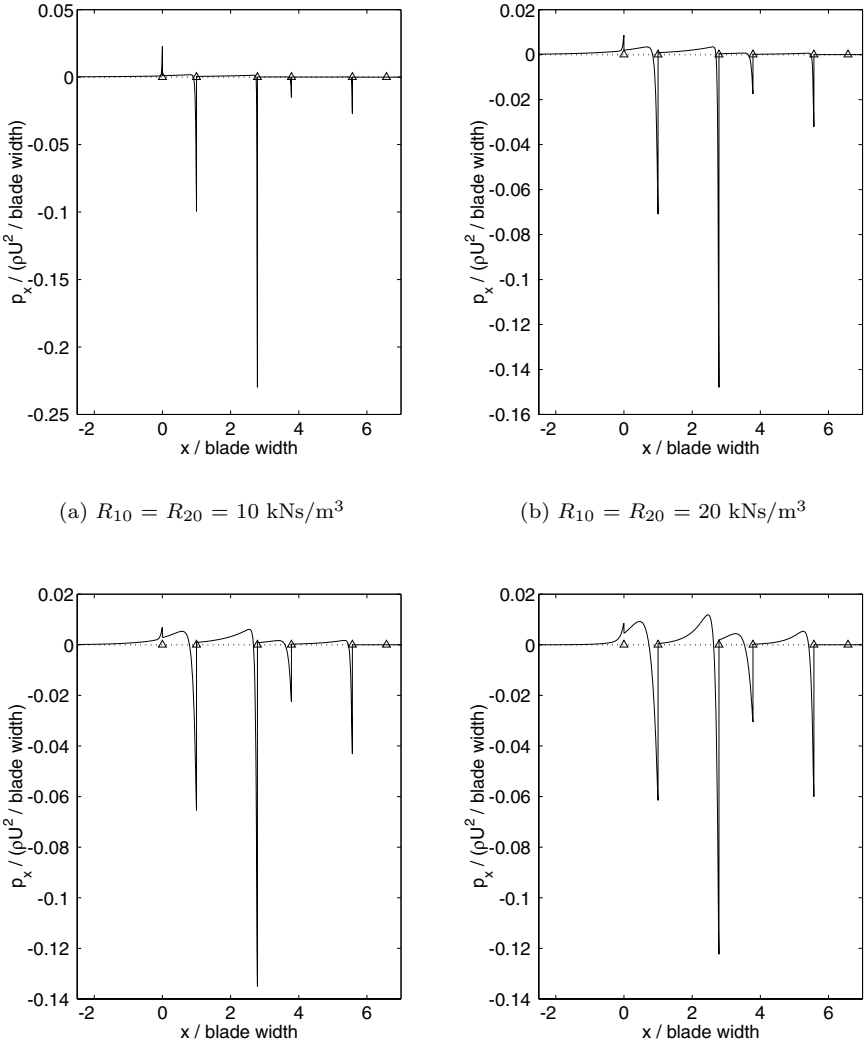

(a) $R_{10} = R_{20} = 10$ kNs/m^3

(b) $R_{10} = R_{20} = 20$ kNs/m^3

(c) $R_{10} = R_{30} = 30$ kNs/m^3

(d) $R_{10} = R_{50} = 50$ kNs/m^3

FIGURE 4.15. The influence of the initial drainage resistance on the pressure gradients. The graphs correspond to those seen in figure 4.14(a). Note that the scales on the vertical axes of the different subfigures are not the same.

4.7. The gap size far upstream

Different paper grades correspond to different distances between the wires when they reach the blade forming section. In order to illustrate the influence of the gap size far upstream of the blades on the pressure distribution, a series of calculations were undertaken with different values of h_0. The results from four such simulations are found in figure 4.16. As the wire speed is the same

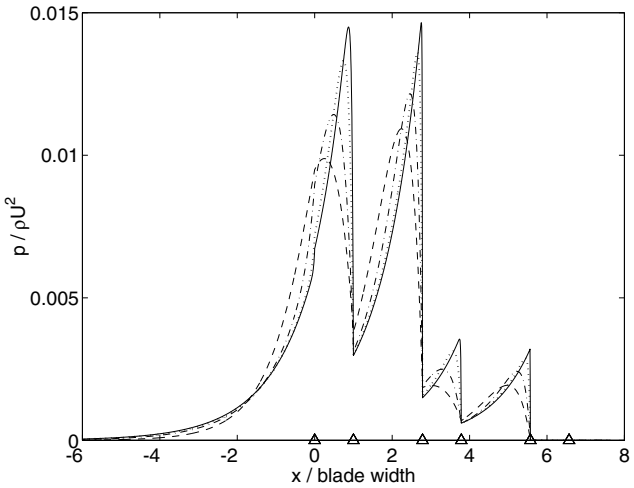

FIGURE 4.16. The influence of the initial wire distance h_0 on the pressure pulses. (—) $h_0 = 1$ mm, $(\cdots)$ $h_0 = 2$ mm, $(- \cdot -)$ $h_0 = 5$ mm, $(- - -)$ $h_0 = 10$ mm. Flat blades, width 14 mm. Blade spacing 25 mm. Blade force 300 N/m. Wire speed 25 m/s. Wire tensions 9 kN/m. Initial drainage resistances 20 kNs/m^3.

in all calculations, an increase in h_0 means that the amount of momentum flowing between the fabrics is augmented. The blade force, which has the value 300 N/m in all cases, must hence have less influence on the flow at large gap sizes, which explains the decrease in the amplitude of the pressure. We also note that the pressure pulses have a more rounded shape for the larger values of h_0, and the gradients in the machine direction are consequently smaller in these cases. A word of caution should be raised against the calculation were $h_0 = 10$ mm, and perhaps also against the case where $h_0 = 5$ mm. We recall that our model depends upon the assumption that the characteristic length scale in the machine direction is much larger than the characteristic scale in the z-direction (see chapter 2). The two largest values of h_0 are not small in comparison with the width of the blades, here 14 mm, which can often be taken

as an indication of the order of the reach of the pressure pulses in the machine direction.

Simulations were also undertaken with circular blades of radius 1 m and 0.6 m. The same trends were observed as in figure 4.16.

4.8. The drainage coefficient

The drainage coefficient K, defined by the relation 2.8, depends on the concentration of fibres in the suspension, the viscosity of the liquid phase of the suspension, and the characteristics of the fibre mat. Figure 4.17 illustrates the effect of changing K from the value 9.0×10^6 kg/(m^{3}s) to 1.9×10^7 kg/(m^{3}s). The former value have been used for the major part of the calculations in this thesis, and at the beginning of this chapter it is explained how we came to this value. Among other things, we assumed the mass concentration of fibres in the suspension to be 0.5 %. The latter value is obtained if one instead assumes the mass concentration to be 1 %. Obviously, changing the value of K does not

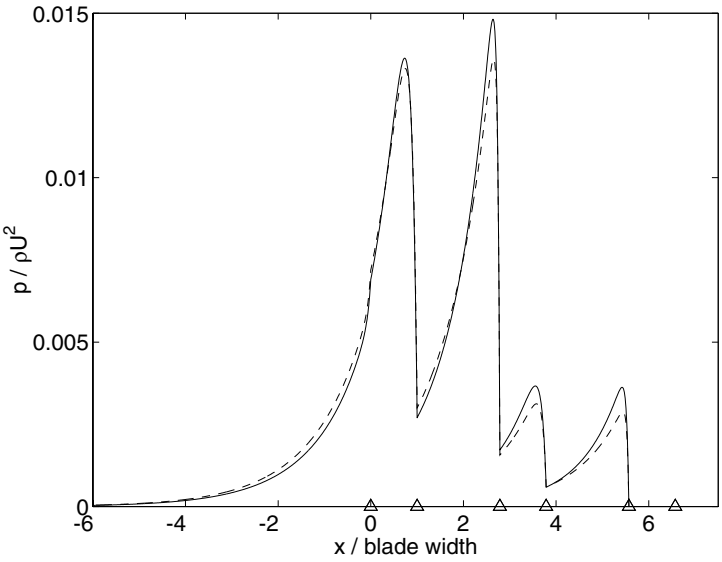

FIGURE 4.17. The influence of the drainage coefficient. (—) $K = 1.9\times10^7$ kg/(m^{3}s), (– – –) $K = 9.0\times10^6$ kg/(m^{3}s). Flat blades, width 14 mm. Initial gap size 2 mm. Blade spacing 25 mm. Blade force 300 N/m. Wire speed 25 m/s. Wire tensions 9 kN/m. Initial drainage resistances 20 kNs/m^3.

have a great effect on the calculated pressure distribution. Looking at the two upstream pulses, we note that the higher value of K yields pressure pulses that

extend slightly less in the upstream machine direction, and that are of somewhat larger amplitude. As for the downstream pulses, the slope of the dashed curve compared to the slope of the solid curve suggests that the same trend would have been observed if the pulses had been allowed to extend further in the upstream direction. As the higher value of K results in a faster increase in the drainage resistances, the mechanisms behind the trend are probably the same that causes the pressure pulses to be more narrow and of larger magnitude when the initial drainage resistance is higher (see section 4.6).

4.9. Applying a suction pressure

In this section are presented some results from calculations where the effects of applying a suction box were simulated. This was done by specifying a low pressure outside of the upper wire between the first and the third blade. Using the notation introduced in section 3.6, this corresponds to setting $p_v < 0$.

We mentioned in connection with figure 4.14(b) in section 4.6, that results yielding reversed drainage are dubious, and referred the discussion of this to chapter 5. In most simulations presented in this chapter, there are regions between the first and the third blade where the pressure is quite low. Applying realistic suction in these situations results in pressures substantially below the atmospheric pressure, i.e. where $p < 0$. If this happens at positions where the wire opposing the suction box is not in contact with a blade, reversed drainage will take place. In order not to obtain corrupt data when realistic amounts of suction is applied, a slightly different configuration of the blades were used for the simulations in this section than was described at the beginning of the chapter. It is illustrated in figure 4.18. The difference with respect to the original configuration is that the third blade is no longer positioned at the same level as the first blade. Instead it has been given a position in the z-direction closer to the middle blade. The distance between the trailing edge of the third blade and the outlet, which in the earlier simulations was of no importance due to the trivial nature of the solution downstream of the last blade, is also taken to be quite short (2.14 when non-dimensionalised with the blade width). As the fabrics have the same vertical positions at the inlet and the outlet of the model domain as before, the combined effect is that the wrap of the wires over the leading edge of the third blade is increased, and, more important, that a large wrap is achieved at the trailing edge. The corresponding pressure pulses are of large magnitudes and merge with the pulses from the upstream blade, so that the minimum level of the pressure between the two upper blades is quite high when the suction pressure is zero (an example of this is the solid curve in figure 4.19). This leaves room for employing quite large amounts of suction before the validity of the corresponding solutions is questionable. Although the blade arrangement in figure 4.18 may seem quite strange, the corresponding pressure distribution in figure 4.19 is likely to be reasonably typical for the region around the first three blades in a forming section containing more blades than employed

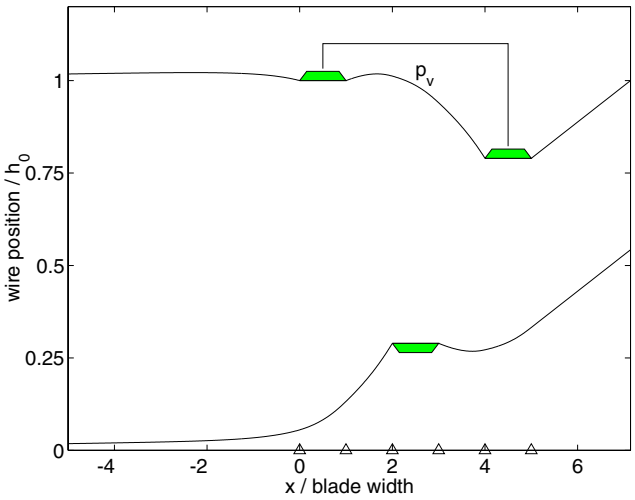

FIGURE 4.18. The blade configuration used to study the influence of the suction pressure. The filled areas indicate the blades. The suction box is outlined on top of the upper wire. The parameters yielding the wire positions in this figure are given in the caption of figure 4.19. $p_v = 0$. The computational domain extends upstream to x = -14.3, where f and g are 1 and 0, respectively. The vertical position of the third blade is 0.78.

here. In such a section the wrap at the downstream edge of the third blade would be caused by the deflection of the wires by the second loadable blade.

Figure 4.19 contains a comparison between one simulation where no suction is applied, and another where the suction pressure is -5 kPa. Note that there is no position where the pressure is less than zero. The pressure peak at the first blade is of larger amplitude for the case where a suction pressure is applied. This is a consequence of a larger wrap of the fabrics over the trailing edge. If the middle blade was not present, the model would still predict a large wrap over the downstream edge of the first blade, due to the lower wire being sucked up into the vacuum box together with the upper fabric. However, this would imply a considerable amount of reversed drainage through the lower wire, and is hence not likely to happen in a real paper machine (see chapter 5). Hence, the presence of a middle blade that applies a load to the lower wire is most probably crucial to obtaining the augmented wrap and the effects this implies. Since the pressure pulse upstream of the trailing edge of the first blade extends past the leading edge, the wrap of the fabrics over that edge will increase as well. The pressure pulses generated at the middle blade have decreased as a

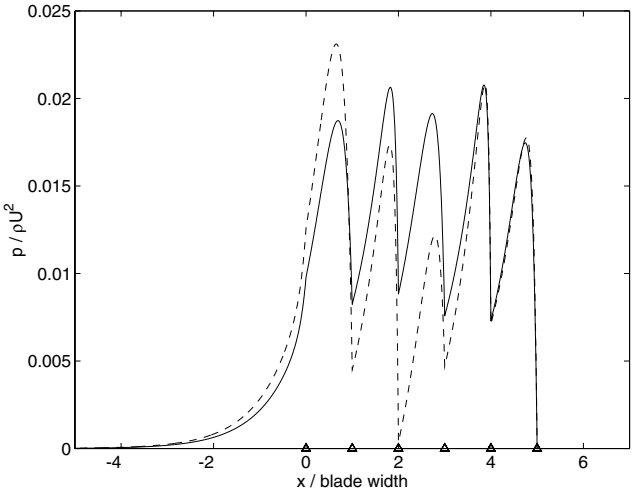

FIGURE 4.19. The influence of suction on the pressure distribution. (—) No suction. (- - -) Suction pressure -5 kPa. Flat blades, width 14 mm. Blade spacing 14 mm. Blade force 400 N/m. Initial gap size 2 mm. Wire speed 25 m/s. Wire tensions 11 kN/m. Initial drainage resistances 34 kNs/m^3.

result of the suction. This is natural. When the underlying mechanisms of blade dewatering were discussed in chapter 1, it was concluded that the high pressures observed in the forming section are a result of the necessity to reduce the amount of suspension that has to pass the constriction created by a blade when it is applied to the wire. The path of the suspension is slightly deflected by the blade, and the resulting pressure pushes the opposing fabric outwards and forces liquid through the wires. If a low pressure prevails outside one of the fabrics, the increased drainage through that wire will reduce the need to deflect the suspension, and the generated pressure will be lower. This will of course result in less drainage through the fabric in contact with the blade.

Figure 4.20 shows the effect of employing a suction pressure of -10 kPa, while the rest of the parameters are the same as in the simulations in figure 4.19. As can be seen, there is a region where p is significantly below zero. Nevertheless, since this occurs over the middle blade, no reversed drainage occurs. Actually, a careful inspection of figure 4.20 reveals that the region of negative values of p extends a very short distance upstream of the leading edge of the middle blade. This is a consequence of the need of a finite distance for the pressure pulse located upstream of the leading edge to re-establish a positive pressure. However, as the distance is extremely short, the implications of the reversed drainage are so local that they do not significantly affect the

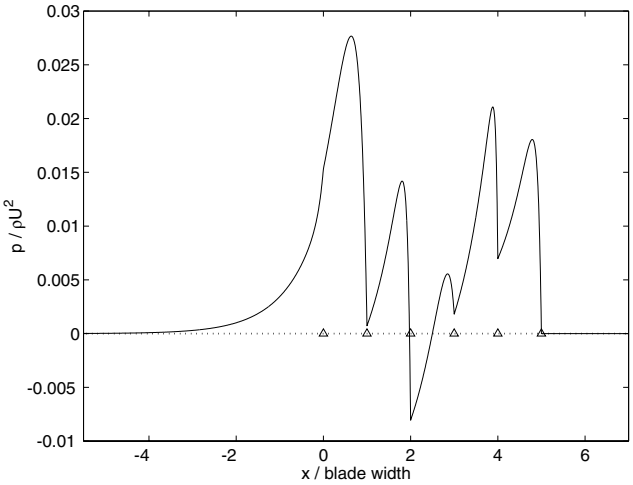

FIGURE 4.20. The pressure distribution for a suction pressure of -10 kPa. The other parameters are the same as in figure 4.19.

overall solution (see chapter 5). Thus the pressure distribution is reasonably trustworthy. The same conclusions can be drawn from figure 4.20 as from figure 4.19.

The purpose of suction boxes is to increase the drainage. We just concluded that employing them increases the drainage through the fabric on the side of the suction box, but at the same time reduces the amplitude of the pressure pulses generated by an opposing blade. A natural question to ask is how the total amount of drainage is affected. When no suction was used, the non-dimensional distance between the wires was 0.46 at the downstream end of the model domain. When the suction pressure was -5 kPa and -10 kPa, the corresponding value was 0.40 and 0.34, respectively. The total dewatering was thus augmented by 13 % and 26 %.

Another interesting issue is to what extent the asymmetry of the drainage changes when suction is employed. Let us consider the change in the drainage resistances between the inlet and the outlet. When no suction is applied, R_1 increases with 13 % and R_2 with 16 %. When the suction is -5 kPa, the corresponding values are 16 % and 16 %, respectively. And finally, when the suction is -10 kPa, the values are 19 % and 16 %, respectively. Hence, about the same amount of fibre mat growth takes place on the lower wire in all three cases. Apparently, the lower drainage through the fabric at the middle blade is compensated by the higher drainage at the first blade. Unsurprisingly, the growth is enhanced on the upper wire. However, due to the short length of the forming section, the changes are quite small.

The influence of the suction on the pressure gradients in the machine direction are presented in figure 4.21, where the case of zero suction pressure is compared with the situation when -10 kPa is used. Clearly, the suction enhances the magnitude of the negative gradients, whereas the positive gradients remain at about the same level.

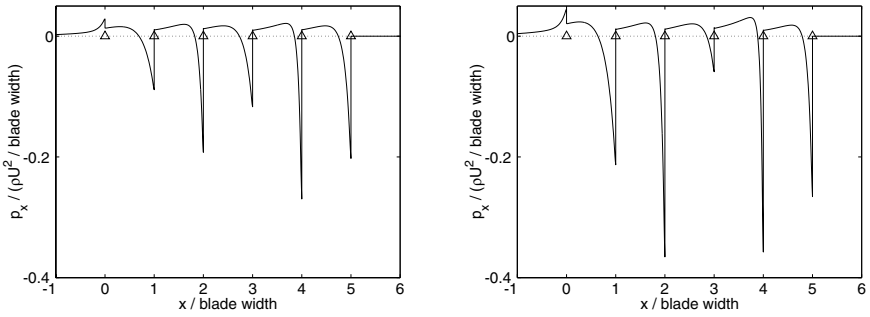

(a) No suction.

(b) Suction -10 kPa.

FIGURE 4.21. The influence of the suction on the pressure gradients. The cases presented here correspond to the pressure curves in figure 4.19.

CHAPTER 5

Discussion and summary

5.1. Discussion

The focus of this thesis is on the pressure distribution in the model domain, since this is truly a key quantity. The integral of the pressure along the machine direction is closely related to the total drainage achieved in the forming section, whereas the amplitude of the pressure is related to the retention of fibres, fines and fillers. A third very interesting characteristic of a pressure distribution is the magnitude of the gradients in the machine direction. It is believed that they play a principal part in the mechanisms underlying the positive effects that blade dewatering has on the formation in the paper sheet. Most likely, too large gradients can also inflict mechanical damage on the fibre web during its forming. Hence, it is extremely valuable to be able to predict the pressure.

5.1.1. *Limitations of the model*

Our model has one serious weakness. When considering the equations 2.63–2.71, we note that our model is not concerned with the direction of the flow through the wires. It follows from the equations that if, somewhere in the model domain, p falls below p_{e1} or/and p_{e2}, the curvature of the corresponding wire/wires changes signs, and the centre of curvature moves from the suspension side of the wire (the fabric is curved 'inwards') to the exterior side (the fabric is curved 'outwards'). At the same time, due to the flow through the fabric/fabrics being directed from the outside towards the suspension, the drainage resistance decreases. This is the process we have referred to as 'reversed drainage' in the previous chapters, and it is not likely to take place as described by our model in a real paper machine. One objection one can pose is that the drainage resistance would probably not decrease in the way predicted, if indeed there was a flow from the outside. This is however only a detail. The real issue is whether p actually can fall substantially below p_{e1} or p_{e2}, and whether the wires actually can have large curvatures directed outwards. To understand why this is probably not possible, we shall consider what would happen if, perhaps hypothetically, the pressure in the suspension was to become lower than the pressure prevailing outside one of the wires.

We assume for practical reasons that the region between the wires can be divided into two fibre mats of high fibre concentration, separated by a free

suspension of lower concentration (see figure 2.1). This is perhaps the case in the early part of the forming section. In the downstream part, the fibre mats completely occupy the available space between the wires, and the drainage is best described as a thickening process. The presence of a free fibre suspension is however not crucial for the discussion below, and the conclusions drawn apply to the latter case as well.

The hypothetical pressure drop across the wire and the corresponding fibre mat can only exist under two different circumstances. Firstly, there could be a flow through the wire and the fibre mat, i.e. reversed drainage. In that case the pressure difference would be maintained by the pressure loss created by viscous and inertial effects in the pores of the wire and the fibre mat (see chapter 2). Secondly, surface tension could create menisci in the pores of the wire or the fibre mat, across which the pressure drop would take place, in this case without the need for a flow. Let us start by pursuing the consequences of the first scenario.

Holm (2002) gave the value $2.6–3.6\times10^{-10}$ m^2 for the permeability of a triple layer wire. A typical thickness of a fabric is 0.7–0.8 mm. Assuming water, the corresponding drainage resistance for the fabric is about 2.4 kNs/m^3, according to the definition in chapter 2. This value is very low in comparison with the combined resistance of the fabric and the fibre mat during drainage of water (see chapter 4). We can thus conclude that the major part of the pressure drop occurs over the fibre mat. It is hence not the flow of water through the wire that generates the pressures necessary to deflect it when water is expelled from the gap during normal drainage. Instead, the fibre mat, which creates most of the pressure drop, push the fabric outwards. When fluid is moving in the other direction, from the exterior into the gap, as we have assumed for the sake of discussion, the fibres can no longer exercise a force on the wire by pushing it. In fact, if the wire was to be significantly curved outwards, the fibres would actually have to pull the fabric, since we cannot count on the pressure drop over the fabric to do the work. However, it is highly unlikely that the fibres are attached to the wire in such a way that a distributed force of the order of 1–10 kPa could be transmitted to the fabric. Instead, what would happen, if the flow velocity is not very small, is that the fibre mat lets go of the wire, and fluid enters the region between the fabric and the fibre mat. This fluid would not generate a significant pressure drop across the wire. Our conclusion must be that the pressure on the suspension side of the wire cannot be significantly lower than on the exterior side if there is a flow through the wire. Thus the fabric will never, to any large degree, be curved outwards due to a flow through the wire. One should also remember that we have assumed water to be the fluid passing through the wire. Since at least part of the drained water remains as a liquid layer on the outside of the fabric, this might be a valid assumption in many regions. However, the liquid film is doctored off at the upstream edges of the blades, and downstream we cannot count on

the presence of water that can be sucked back through the wire, and neither, probably, outside the wire opposing a vacuum box after a long distance of applied suction. In those situations, the fluid passing through the wire, and also perhaps the fibre mat, would have to be air. Due to its lower viscosity, the viscous resistance air makes when passing through a permeable material is only about 1/50 of that of water. The ratio between the inertial effects is even smaller. Hence, if air is involved in the reversed drainage process, the pressure drop across the wire would surely not be enough to give it a curvature directed outwards. Instead, air would enter into the gap between the fabrics.

We now turn to the surface tension scenario. First we note that if previously expelled water is present on the exterior of the wire, this water must be pulled back through the wire in a process like the one described above, before menisci can form in the pores of the fabric. In a study of the effects of doctoring on the pressure pulse generated by a blade, Roshanzamir *et al.* (2001) calculated the thickness of the adhering water layer upstream of the blade to about 0.5 mm, which should be put in relation to the initial distance between the wires, in that case 3.5 mm. Hence, the process of reversed drainage can probably in some situations take place over a considerable distance along the machine direction before the menisci appears, during which we would not see any significant deflection of the wire. The wire usually consists of strands of polyester and polyamide, which are both hydrophilic materials. The wetting angles for water are 43° and 46°, respectively (Holm 2002). When the menisci have formed, they can consequently maintain a certain pressure difference and prevent a flow of air into the gap region. As a typical pore size in the wire is about 0.2 mm, the pressure drop across the menisci must not exceed about 1 kPa. Above that value, the menisci cannot withstand the pressure, the pores open, and air enters into the gap. Possibly, menisci yielding large pressure differences could form in the small pores of the fibre mat. However, for the same reasons as when a flow occurs through the wire and the mat, the capillary pressures corresponding to the menisci cannot be transmitted to the wire.

Having considered these two scenarios, we conclude that the maximum pressure drop available across a fabric to give it a curvature outwards is about 1 kPa. This pressure difference is only created after reversed drainage has made the liquid adhering to the exterior surface of the wire return into the gap. If, even only briefly, the pressure exceeds the limit of the capillary pressure, the menisci disappears and no pressure drop remains. In a real paper machine, the fabrics are hence never substantially sucked towards the suspension, not even the fabric on the opposite side of a suction box.

The issues discussed above limit the applicability of all models for the forming section developed up to date, including the one presented in this thesis. Any solution yielding pressures in the suspension region more than about 1 kPa lower than on the outside of either fabric must be considered unrealistic. Solutions not violating this general criteria could arguably be correct, provided

that it is clear that there is no water adhering to the fabric causing reversed drainage. If this condition cannot be fulfilled, the pressure difference across the fabric and the fibre mat must be of such small magnitude that the reversed drainage does not cause the fibre mat to separate from the fabric. One should also pay attention to the development of the drainage resistance. If menisci have formed in the pores of the wire, it should remain constant as there is no change in the thickness or porosity of the fibre mat. In situations yielding reversed drainage of small magnitude, the resistance might perhaps decrease somewhat due to fibres breaking lose from the suspension side of the fibre mat, or due to an increase of the permeability. However, most likely the mat is separated from the wire before such phenomena come into effect. Although it would be easy to implement using our concept of modules, the model in the thesis does not include a feature that prevents the drainage resistance from decreasing when reversed drainage occurs.

It is not sure that reversed drainage (causing the fibre sheet to separate from the wire), or even air breaking into the gap between the fabrics, is a source of problems in the industrial process. Given the large suction pressures often employed in the forming section (of the order -10 kPa), these situations perhaps occur frequently. The significance of the phenomena stems from our desire to predict the pressure distribution in the forming section. Without appropriate models for reversed drainage and for the breakthrough of air, many important situations cannot be simulated. These include the production of grades of large basis weights (as the current models yield oscillating solutions, see section 4.6 of chapter 4), and many forming section designs involving suction shoes.

5.1.2. *Modelling reversed drainage*

The rigorous modelling of reversed drainage, and the breakthrough of air, is a complex task. However, it is possible that the module concept introduced in this thesis in some situations can be employed to simplisticly incorporate the effects of these phenomena on the pressure distribution. We shall give an outline of how this might be done for the forming section in figure 1.6 in one special case.

Assume that the pressure in the vacuum box is of such magnitude that present models would predict a pressure in the suspension region upstream and downstream of the middle blade that is lower than the atmospheric pressure outside the bottom fabric, despite the load applied by the middle blade. Assume further that there are no menisci in the pores of the fabric that can maintain a pressure drop of that kind across the bottom wire. Hence, either the capillary pressure is of inadequate magnitude, or there is a layer of water adhering to the outside of the fabric. The intruding fluid[1] which then enters

[1] We shall use this label for the fluid entering from the outside, since it is not clear whether we are dealing with water or air.

from the exterior of the bottom wire into the region between the fabrics is assumed to cause the fibre mat to separate from the wire, and the mat will be considered to function as a delimiter between the intruding fluid and the suspension. We shall consider the new fluid as inertialess and, as it makes only very small resistance when passing through the wire, it will easily return to the outside of the bottom wire when it is forced to do so for geometrical reasons. We also count on the load from the middle blade to ensure that the pocket of intruding fluid is limited to a region beginning downstream of the trailing edge of the first blade, and ending upstream of the leading edge of the third blade. The situation is illustrated in figure 5.1, where we have also divided the forming section into modules. The pocket of intruding fluid is illustrated (unrealistically) by the dashed line. The WW-module and the WUB-module were

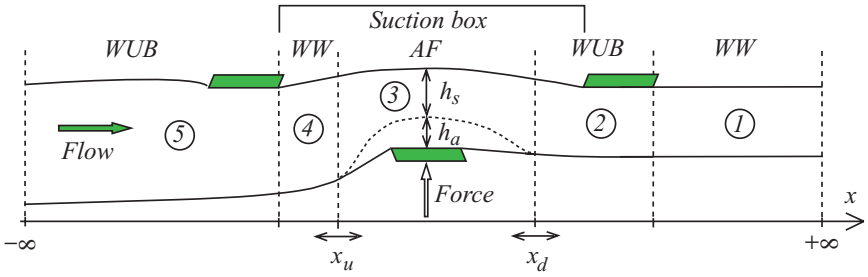

FIGURE 5.1. The division of the forming section into modules in a situation where fluid has passed through the bottom wire into the region between the fabrics. The intruding fluid is contained in the pocket illustrated (unrealistically) by the dashed line. In addition to the module types developed in chapter 3, a new AF-module is introduced. Confer the text for an explanation of the notation.

thoroughly discussed in chapter 3. In addition to these we have introduced the AF-module, the extension of which exactly coincides with the pocket of intruding fluid. It is schematically illustrated in figure 5.2. We need a description of the new module, and for this we turn to the equations 2.63–2.71, that describe the WW-module.

We start by observing that, as the intruding fluid only generates small pressure drops when passing through the fabric, the pressure in the AF-module does not significantly differ from the atmospheric pressure. This allows us to make the approximation $p \equiv 0$ for the module. We get a system of equations for the AF-module if we insert this in the equations 2.63–2.71, and replace $f - g$ in equation 2.65 by the distance between the upper wire and the pocket of intruding fluid, denoted h_s. Note that for the AF-module in figure 5.1, p_{e1} equals the suction pressure, and p_{e2} is zero. The height of the pocket, h_a, can

of course be obtained from the relation $h_s + h_a = f - g$. The resulting system of equations is easily solved analytically, and the integration constants can be determined provided that the parameters in figure 5.2 are known. As $p \equiv 0$, the lower wire moves along linear paths. The upper wire is curved as a result of the suction. The velocity and the drainage resistance of the lower wire will be constant throughout the module. An important difference with respect to

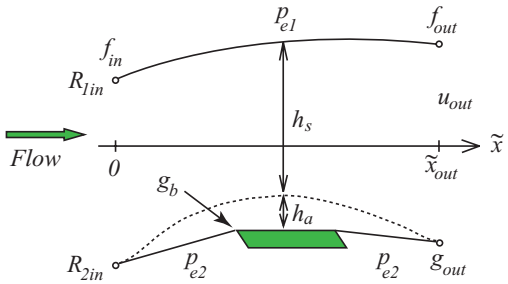

FIGURE 5.2. An illustration of the AF-module together with the information that needs to be specified in order to calculate the dependent variables throughout the module. g_b is the vertical position of the blade. The rest of the notation is equivalent to that of figure 3.3.

the modules introduced previously, is that the position of the lower wire at the inlet does not need to be specified – it is determined by requiring that h_a is zero at $\tilde{x} = 0$.

The evolution of the dependent variables throughout the forming section in figure 5.1 can now be obtained by employing the algorithm presented in chapter 3. The position of the inlet and the outlet of the AF-module, denoted x_u and x_d in figure 5.1, are not known apriori. Instead, they are included in the vector $\boldsymbol{c}_u$ and determined as part of the solution process. The corresponding matching conditions are that there should be no discontinuity in the pressure at the interface between the modules 2 and 3 in figure 5.1, and that g_x should be continuous across the interface between the modules 3 and 4. Of course, p should be continuous across the latter interface, and g_x across the former, as well. However, this is naturally taken care of by the algorithm when the modules in the section are solved, and need not be enforced by the matching process.

There are many similarities between the procedure outlined above for treating the intrusion of fluid in the forming section in figure 5.1, and how we have already handled situations where the fabric does not stay in contact with a blade along its full width (see chapters 3 and 4). Neither in that case are the positions of all the interfaces between the modules known a priori.

The reason for choosing the forming section in figure 5.1 to illustrate the possibilities of the module-based algorithm was motivated by the fact that we could predict the approximate location of the pocket, and hence include an appropriate module in the model. Before the algorithm can be extended to more general situations, a careful analysis must be undertaken of when intrusion of fluid occurs, and where the pockets are located.

5.1.3. *A comment on future research*

Detailed models have been developed for the application of a single blade to a pair of fabrics, exemplified by e.g. the studies by Zahrai *et al.* (1997) and Roshanzamir *et al.* (1998). The present work has resulted in a simple and flexible tool by which the interaction between different components in the blade forming section can be investigated at low computational cost. Nevertheless, before we can say that we have a good idea about the pressure distributions in general blade forming sections, future research must solve the issues discussed in section 5.1.1 that impose restrictions on which configurations of the dewatering devices and which parameter combinations that we can simulate. In parallel with this work, we must fill the large gaps that exist in our knowledge of the coupling between the pressure distributions and their effect on fibre flocs and the fibre web. Before this is done, we will not be able to benefit from accurate simulations of the pressure.

5.2. Summary

In chapter 2 and 4 of this thesis we have presented a model for quite general blade forming sections, allowing us to study the interaction between the pressure pulses generated by several blades positioned alternately to the two fabrics and one sided suction. The model has been employed to study the particular generic section illustrated in figure 1.6. In chapter 3 we performed tests to verify the implementation of the model, and made comparisons with some previously published simulations of a single blade applied to a pair of fabrics. The agreement was found to be good, which is very important as the numerical results used as reference have been found to be in reasonable accordance with experimental measurements. Our conclusion is that we can probably employ the model in order to obtain at least qualitatively correct results under many circumstances. The exceptions have been discussed in section 5.1.1.

In chapter 4, results are presented which illustrate the potential of the model to be used as a tool in the design of blade forming sections, and for troubleshooting in the industrial process. Some not previously documented observations connected to the pressure distributions in blade formers are made. Among them, the following deserve particular attention:

- Reducing the distance between the blades leads to non-trivial interaction between the pressure pulses. Some pulses are amplified, some are reduced.
- A suction box positioned opposite a blade reduces the amplitude of the pressure pulse generated by the blade.
- Curved blades do not necessarily stay in contact with the fabrics along their full width, even when the degree of curvature is modest.
- If the fabric establish contact with the blade downstream of the leading edge, a large positive pressure gradient occurs in the machine direction. The negative pressure gradients are reduced when curved blades are employed.

Acknowledgments

I would like to thank Docent Anders Dahlkild and Professor Bo Norman for their assistance during my work on this thesis, and Dr. Galina Shugai for some valuable discussions. Most of all I thank Caroline – I am sorry I ruined the summer.

This project has been financially supported by VINNOVA and the participating industrial partners within the FaxénLaboratoriet.

References

Acheson, D. 1990 *Elementary Fluid Dynamics*. Oxford University Press.

Bando, T., Iwata, H. & Nagano, A. 1994 Drainage mechanism on a twin-wire former. part 1: Factors affecting on the drainage phenomena. *Japan Tappi* **48** (7), 1493–1498.

Baumann, W.-D. 1989 Duoformer-D – a new approach to top wire forming. In *TAPPI Twin Wire Seminar*, pp. 115–120.

Brauns, R. 1986 Wet end developments. In *CPPA Technical Section Annual Meeting*, vol. A, pp. 275–282.

Chen, E., Schultz, W. & Perkins, N. 1998 A two-dimensional viscous model of a wet paper forming process. In *TAPPI Engineering Conference*, pp. 53–61.

Gilbert, J. R., Moler, C. & Schreiber, R. 1992 Sparse matrices in MATLAB: Design and implementation. *SIAM Journal on Matrix Analysis and Applications* **13** (1), 333–356.

Green, S. 1997 Analytical and computational modeling of twin-wire blade forming. *Journal of Pulp and Paper Science* **23** (7), 353–357.

Green, S. 2000 Modeling suction shoes in twin-wire blade forming: Results. *Journal of Pulp and Paper Science* **26** (2), 53–58.

Green, S. & Kerekes, R. 1998 Numerical analysis of pressure pulses induced by blades in gap formers. In *TAPPI Engineering Conference*, pp. 185–192.

Green, S. & Roshanzamir, A. 1997 The effect of blade wear on twin wire blade forming. In *TAPPI Engineering & Papermakers Conference*, pp. 889–896.

Green, S., Zhao, R. & Kerekes, R. 1997 Pressure distribution between forming fabrics in blade gap formers: Blades of finite width and fabrics of finite stiffness. In 83$^{\text{rd}}$ *Annual Meeting, Technical Section CPPA*, pp. 89–95.

Green, S. I. 1999 Modeling suction shoes in twin-wire blade forming: Theory. *TAPPI Journal* **82** (9), 136–142.

Holm, R. 2002 On the fluid mechanics of partial dewatering during roll forming in paper making. Licentiate thesis, Royal Institute of Technology (KTH), Stockholm.

James, D. F. & Davis, A. M. 2001 Flow at the interface of a model fibrous porous medium. *Journal of Fluid Mechanics* **426**, 47–72.

Malashenko, A. & Karlsson, M. 2000 Twin wire forming – an overview. In 86$^{\text{th}}$ *Annual Meeting, PAPTAC*, pp. 189–201.

Mantar, E., Co, A. & Genco, J. 1995 Drainage characteristics of pulp slurries under dynamic conditions. *Journal of Pulp and Paper Science* **21** (2), 44–50.

Meyer, H. 1971 Hydrodynamics of the sheet-forming process. *TAPPI Journal* **54** (9), 1426–1450.

Moch, N. 1995 On variable permeability during the dewatering process in paper machines. Master's thesis, Royal Institute of Technology (KTH), Stockholm.

Nigam, M. & Bark, F. 1997 An analytical method to calculate the flow past a blade in twin-wire formers. *Tech. Rep.*. Department of Mechanics, Royal Institute of Technology (KTH), Stockholm.

Nordström, B. 1995 Effects of headbox design and dewatering conditions on twin-wire forming of TMP. PhD thesis, Royal Institute of Technology (KTH), Stockholm.

Norman, B. 1979 Principles of twin-wire forming. *Svensk Papperstidning* **82** (11), 330–336.

Norman, B. 1989 Overview of the physics of forming. In *Fundamentals of Papermaking, Transactions of the Ninth Fundamental Research Symposium*, , vol. 3, pp. 73–149.

Norman, B. & Söderberg, D. 2001 Overview of forming literature 1990–2000. In *Transactions of the* 12^{th} *Fundamental Research Symposium*. Oxford.

Paradis, M. A., Genco, J. M., Bousfield, D. W., Hassler, J. C. & Wildfong, V. 2002 Determination of drainage resistance coefficients under known shear rate. *TAPPI Journal* **1** (6), 12–18.

Parsheh, M. 2001 Flow in contractions with application to headboxes. PhD thesis, Royal Institute of Technology (KTH), Stockholm.

Press, W. H., Flannery, B. P., Teukolsky, S. A. & Vetterling, W. T. 1986 *Numerical Recipes – The Art of Scientific Computing*. Cambridge University Press.

Roshanzamir, A. 2000 Hydrodynamics of blade gap forming. PhD thesis, University of British Columbia (UBC), Vancouver.

Roshanzamir, A., Green, S. & Kerekes, R. 1998 Two-dimensional simulation of pressure pulses in blade gap formers. *Journal of Pulp and Paper Science* **24** (11), 364–368.

Roshanzamir, A., Green, S. & Kerekes, R. 2000*a* Two-dimensional simulation of suction shoes in gap formers. *Journal of Pulp and Paper Science* **26** (4), 158–162.

Roshanzamir, A., Green, S. & Krekes, R. 2000*b* The effect of non-darcy's law drainage on the hydrodynamics of blade gap formers. In *TAPPI Papermakers Conference and Trade Fair*, pp. 701–708.

Roshanzamir, A., Kerekes, R., Green, S. & Ollivier-Gooch, C. 1999 Hydrodynamic pressure generated by doctoring in blade gap formers. In *TAPPI Engineering/Process and Product Quality Conference & Trade Fair*, pp. 1181–1189.

Roshanzamir, A., Ollivier-Gooch, C., Kerekes, R. J. & Green, S. I. 2001 Hydrodynamic pressure generated by doctoring in blade gap formers. *TAPPI Journal* **84** (7).

Sims, D. 1985 Twin wire forming developments. In *TAPPI Twin Wire Seminar*, pp. 43–51.

Söderberg, D. 1999 Hydrodynamics of plane liquid jets aimed at applications in paper manufacturing. PhD thesis, Royal Institute of Technology (KTH), Stockholm.

Taylor, G. 1971 A model for the bondary condition of a porous material. part 1. *Journal of Fluid Mechanics* **49** (2), 319–326.

Turnbull, P. F., Perkins, N. C., Schultz, W. W. & Beuther, P. D. 1997 One-dimensional dynamic model of a paper forming process. *TAPPI Journal* **80** (1), 245–253.

Wildfong, V., Genco, J., Shands, J. & Bousfield, D. 2000 Filtration mechanics of sheet forming. part II: Influence of fine material and compression. *Journal of Pulp and Paper Science* **26** (8), 280–283.

Zahrai, S. & Bark, F. 1995 On the fluid mechanics of twin wire blade forming in paper machines. *Nordic Pulp and Paper Research Journal* **10** (4), 245–252.

Zahrai, S. & Bark, F. 1996 Analytical and numerical approaches to solve the model equations for the flow of pulp in blade forming process. *AIChE Symposium Series* **92** (311), 68–73.

Zahrai, S., Bark, F. & Norman, B. 1997 An analysis of blade dewatering in a twin-wire paper machine. *Journal of Pulp and Paper Science* **23** (9), 452–459.

Zahrai, S., Martinez, M. D. & Dahlkild, A. A. 1998 Estimating the thickness of the web during twin-wire forming. *Journal of Pulp and Paper Science* **24** (2), 67–72.

Zhao, R. & Kerekes, R. 1995 Pressure distribution between forming fabrics in blade gap formers: Thin blades. *Journal of Pulp and Paper Science* **21** (3), 97–103.

Zhao, R. & Kerekes, R. 1996 The effect of consistency on pressure pulses in blade gap formers. *Paperi Ja Puu – Paper and Timber* **78** (1–2), 36–38.